

Reduction of nitrogen oxides over zeolite supported Ni catalysts

B.I. Mosqueda Jiménez

2002

Ph.D. thesis
University of Twente



Twente University Press

Also available in print:

<http://www.tup.utwente.nl/catalogue/book/index.jsp?isbn=9036518180>

*Reduction of nitrogen oxides over
zeolite supported Ni catalysts*

Promotie commissie

Voorzitter/Sekretaris:	Prof. dr. J. Feijen	(U Twente)
Promotor:	Prof. dr. J. A. Lercher	(T U München)
Assistent-promotor:	Dr. K. Seshan	(U Twente)
Leden:	Prof. dr. ir. L. Lefferts	(U Twente)
	Prof. dr. ir. J.A.M. Kuipers	(U Twente)
	Prof. dr. F. Kapteijn	(T U Delft)
	Prof. dr. B. Weckhuysen	(U Utrecht)
Deskundige	Dr. A. Jentys	(T U München)

The research described in this thesis was funded by the Dutch Technology Foundation (STW/NWO) project 326-710



Twente University **Press**

Twente University Press, P.O. Box 217, 7500 AE Enschede, www.tup.utwente.nl

Print: Océ Facility Services, Enschede

© Bertha I. Mosqueda Jiménez, Enschede, The Netherlands 2002

ISBN 90 365 1818 0

REDUCTION OF NITROGEN OXIDES
OVER ZEOLITE SUPPORTED Ni CATALYSTS

PROEFSCHRIFT

ter verkrijging van
de graad van doctor aan de Universiteit Twente,
op gezag van de rector magnificus,
Prof. Dr. F. A. van Vught,
volgens besluit van het College voor Promoties
in het openbaar te verdedigen
op vrijdag 15 november 2002 te 13:15 uur

door
Bertha Isabel Mosqueda Jiménez
geboren op 16 august 1973
te Valle de Santiago, Mexico

Dit Proefschrift is goedgekeurd door de promotor

Prof. Dr. J. A. Lercher

en assistent-promotor

Dr. K. Seshan

"The whole world steps aside for those
who know where they are going."

(Anonymous)

To my parents,
to Dany and Laurent

Acknowledgements

In four years I have met so many people that in one or another way have contributed to the culmination of this work, I do not have words to express all my gratitude.

I cannot forget to thank my professors at the department of Chemical Engineering in San Luis Potosí, Dr. Lupita Cárdenas, Dr. Brent E. Handy, Dr. Jorge Toro, Dr. Francisco Medellín, Dr. Roberto Leyva, among others, for encouraging me to go a bit farther and do my PhD studies in the other side of the Atlantic.

I would like to thank Prof. Johannes A. Lercher for giving me the opportunity of joining his research group. I thank Andy (Dr. A. Jentys) for his supervision and invaluable help during the correction of this thesis. I thank Seshan (Dr. K. Seshan), and Leon (Prof. Leon Lefferts) for the interesting discussions. I thank Jan (Dr. J.G. van Ommen) for being there to help when there was nobody else.

To the former crew in Twente, Sergio, Marco, Gerhard, J.P., Victor, Sheila, Martyn, Cristina, Gautam, László D., László L., Olivier, Manja, Isaac, I would like to thank for being there at my arrival to Enschede and making easier to get used to my “new world”, to Marta and David for experiencing together the arrival to a new place. I have to mention some other nice people that I met in Enschede, Monse, Tomas, Mercedes, Edu, and Chris. I appreciate the help of Bert and Cis, who respond always very efficiently to all my requests. I thank also the hospitality of the new members of the catalytic processes and materials group in Enschede.

To my colleagues in Munich, Alex H., Maria, Stefan G., Jochen, Sven, Xuebing, Shourong, Qing, Van Nhu, Hendrik, Linda, Krishna, Anil, Fred M., Jenö, Thomas, Stefan F., Gabriela, Jan K., I thank for all the moments we shared inside the lab during long stays. Christian W., Wolfgang and Florencia, I really appreciate your help during the measuring campaign in Hamburg. I thank Christian S. and Josef for all the help with experimental and non-experimental problems. Andreas F., Hilton, Adam, Florencia, Jan Olaf, Toshi, Hiroaki, Iker, Alex G., Oriol, it was always nice to go out with you for a drink or gathering to celebrate someone’s birthday. Martin and Renate, I have so many things to thank you, but here I have to limit it to some lines. Martin, thank you for introducing me to the experimental world of deNO_x and for being always there to help with all kind of troubles. Renate, thank you for opening your home’s door to me, for being always there when I need somebody. Deine Familie ist immer so nett und warm zu mir und ich muss sagen daß die Kuchen von deiner Mutter sind köstlich. I would like to thank also the help of Frau Schüler and Frau Hermann and the technicians in Munich, Xaver, Andreas M. and Martin N.

And now it is the turn of the members of the Spanish-speaking community at the TUM. Eva, Fermín, Gergana, Sofia, Horacio, Kike, Mauricio, Niki, Norge, thank you for the good moments we spent during lunchtime. Paula and Lidia, thank you for being always there willing to listen to my long stories and to help.

Laurent, I thank you for all your love and understanding, without you being by my side it would have been very difficult to finish. À mes beaux-parents, mon beau-frère et sa famille, je vous remercie votre chaleureuse reception. À ma belle-mamie je vous remercie votre introduction a la cuisine française, toujours une surprise.

A mis padres les agradezco todo su amor, respaldo, y los ánimos que siempre me infunden. A toda mi familia, gracias por el apoyo y comprensión. Dany, I thank you for being such a great sister; I wish our relation can stay as close as it has always being.

Agradezco el apoyo recibido por parte del CONACyT a lo largo de los 3 últimos años del desarrollo de este trabajo.

Bertha Mosqueda
November 2002

Table of contents

1. Introduction.....	1
1.1. Emissions of NO_x	2
1.2. Noxious effects	3
1.3. Legislation	3
1.3.1. Stationary sources.....	3
1.3.2. Mobile sources.....	4
1.4. Methods for NO_x control.....	6
1.4.1. Stationary sources.....	6
1.4.2. Mobile sources.....	10
1.5. Reduction of NO_x with hydrocarbons.....	14
1.5.1. Zeolite catalysts	15
1.5.2. Oxide-based catalysts	18
1.6. Scope and structure of the thesis.....	19
2. Reduction of nitric oxide by propene and propane on Ni-exchanged mordenite.....	27
2.1. Introduction	28
2.2. Experimental.....	29
2.2.1. Catalyst preparation	29
2.2.2. Physicochemical characterization.....	30
2.2.3. Catalytic measurements	31
2.3. Results.....	32
2.3.1. Influence of Nickel concentration.....	32
2.3.2. Influence of the acid site concentration	38
2.3.3. Effect of conversion on selectivity	42
2.4. Discussion	42
2.4.1. The acid-base properties of Ni ²⁺ exchanged MOR.....	42
2.4.2. Catalytic conversion of NO with propene/propane	44
2.5. Conclusions	48
References	49
3. Structure-activity relations for Ni-containing zeolites during NO reduction Part 1 - Influence of acid sites.....	53
3.1. Introduction	54

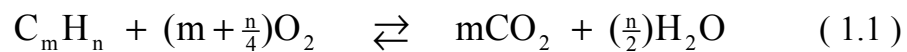
3.2. Experimental.....	55
3.2.1. Catalyst preparation	55
3.2.2. Physicochemical characterization.....	56
3.2.3. Catalytic measurements	57
3.3. Results.....	57
3.3.1. Physicochemical characterization.....	57
3.3.2. Kinetic measurements.....	66
3.4. Discussion	70
3.4.1. Acid sites	70
3.4.2. Catalytic activity.....	73
3.5. Conclusions	75
References	76
4. Structure-activity relations for Ni-containing zeolites during NO reduction	
<i>Part 2 - Influence of metal.....</i>	81
4.1. Introduction	82
4.2. Experimental.....	83
4.2.1. Preparation of samples.....	83
4.2.2. Characterization	84
4.2.3. Catalytic measurements	85
4.3. Results.....	85
4.3.1. Changes in activity after NO reduction	85
4.3.2. Characterization	91
4.4. Discussion	100
4.5. Conclusions	106
5. On the surface reactions during NO reduction with propene and propane	
<i>on Ni-exchanged mordenite.....</i>	111
5.1. Introduction	112
5.2. Experimental.....	113
5.2.1. Catalyst preparation	113
5.2.2. In situ infrared spectroscopy.....	114
5.2.3. Catalytic measurements	114
5.3. Results.....	115
5.3.1. Kinetics of the reduction of NO in the absence of oxygen	115
5.3.2. In situ infrared studies.....	116

5.3.3.	Reactivity of adsorbed nitrogen oxygen species with hydrocarbons	117
5.4.	Discussion	129
5.4.1.	Importance of the presence of oxygen	129
5.4.2.	Stability and reactivity of adsorbed NO _x species.....	130
5.4.3.	Reaction intermediates.....	131
5.5.	Conclusions	135
6.	Summary.....	141
6.1.	Summary	142
6.2.	Samenvatting	146
6.3.	Resumen	150
6.4.	Zusammenfassung.....	154
6.5.	Résumé	158
	Curriculum vitae.....	163
	List of publications.....	164

1. Introduction

1.1. Emissions of NO_x

Nowadays, fossil fuels represent the most important source of the energy required worldwide. The energy stored in fossil fuels is released by their combustion, according to the reaction



In addition to carbon dioxide and water, unburned hydrocarbons from incomplete combustion and products of partial oxidation e.g., carbon monoxide, alcohols, aldehydes, among others, are present in small amounts in flue gas. Generally, fossil fuels contain small amounts of sulfur and nitrogen. During combustion nitrogen oxides, commonly denoted as NO_x, are formed. Although, seven different nitrogen oxides are known to exist, NO, NO₂, NO₃, N₂O, N₂O₃, N₂O₄, N₂O₅, the constituents of the gas of combustions are mainly, NO, NO₂ and small amounts of N₂O. NO contributes with more than 90% of the total NO_x. Road and air traffic and combustion from stationary sources as thermal power plants are the main sources of the air pollution. Other sources are central and individual heating installations, industrial boilers and domestic waste incinerators

Three different types of NO_x are distinguished in flue gas, thermal, fuel and prompt NO_x. Thermal NO_x is formed by the reaction of oxygen with atmospheric nitrogen. Fuel NO_x is formed in the flame by the oxidation of the nitrogen-containing compounds in the fuel. Prompt NO_x is formed through the oxidation of HCN, produced from the reaction of nitrogen radicals and hydrocarbons (1).

1.2. Noxious effects

NO is rapidly oxidized to NO₂ by atmospheric oxidants such as ozone. NO₂ is a precursor of nitric acid that contributes substantially to the so-called acid rain. The acidification is the result of the reaction of NO₂ with water, involving hydroxyl groups (OH) and gives rise to nitric and nitrous acid. These acids return to earth's surface by dry and wet deposition.

The presence of high amounts of NO_x causes respiratory problems by irritation of the lung function. Long-term exposures to low levels of NO_x can destroy lung tissue, leading to emphysema. Susceptible subgroups include asthmatics, children, the elderly and people with existing respiratory disease.

1.3. Legislation

1.3.1. Stationary sources

Stationary sources are coal-, oil- and gas-fired power plants including gas turbines, engines, waste incinerators, refineries and gasifiers. The emissions of NO_x from stationary sources are regulated differently depending on the country (2). In Japan, national emission limits prescribe 60, 130 and 200 ppm for new large gas-, oil-, and coal-fired power plants. The local governments restrict these limits to values below 15, 30 and 60 ppm for power plants and below 5 ppm for gas turbines. In Europe, representative NO_x emission limits are 30-50, 55-75 and 50-100 ppm for new large gas-, oil- and coal-fired power plants and 25 ppm (15% O₂, dry) for gas turbines. In the United States there are two different NO_x limits depending on the ozone level in the area. The areas where the federal ozone standard is violated are called ozone non-attainment areas, and those with less

serious ozone problems are the ozone attainment areas. For the former the best available current technology (BACT) approach applies, while for the latter the lowest achievable emissions rate (LAER) approach applies. The Environmental Protection Agency establishes that utility generation stations must achieve by 2003 limits of 100 ppm in the “ozone seasons” (May-September). For gas turbines the BACT results in 9-25 ppm (15% O₂) of NO_x and the LAER is 3-15 ppm (15% O₂) of NO_x.

1.3.2. Mobile sources

Effects of air pollution leading to environment and health problems were recognized in California in the 1950s (3). Legislation was introduced to limit the emissions of carbon monoxide, hydrocarbons, nitrogen oxides and particulates caused by traffic. In 1966, regulations for the emissions from passenger cars equipped with spark ignition engines were introduced in California. In 1970, the US Clean Air Act was formulated, introducing drastic reduction in the limits of the emissions of exhaust gas from passenger cars (4). Table 1.1 summarizes a historical overview of the limits for exhaust gas emissions. Later, some other countries, as Japan, Australia and Switzerland adopted similar measures.

In the United States the Clean Air Act Amendments define two sets of federal standards, Tier 1 and Tier 2. The Tier 1 regulations were finally implemented in 1997, while the Tier 2 standards were adopted in December 1999, to be phased-in between 2004 and 2009. For the latter the same emission standards apply to all vehicle weight categories, e.g., cars, minivans, light duty trucks and sport utility vehicles. Independently of the fuel, the same emission limits apply. The Tier 2 tailpipe standards are structured into 8 certification levels of different stringency, called “certification bins” (see Table 1.2). Vehicle manufacturers have the choice to certify particular vehicles to any of the 8 bins.

Table 1.1 Historical overview of the limits for CO, HC and NO_x emissions from passenger cars in the USA (4).

Year	Area	Pass levels (g/mile except where stated)		
		CO	HC	NO _x
1966-1967	California	1.5%	275 ppm	-
1968-1969	Federal & California	1.5%	275 ppm	-
1970	Federal & California	23	2.2	-
1972	California	39	3.2	3.2
	Federal	39	3.4	-
1975	California	9	0.9	2
	Federal	16	1.5	2
1980	California	8	0.41	1
	Federal	7	0.41	2
1981	Federal & California	3.4	0.41	1
1993	California	3.4	0.25	0.4

Table 1.2 Tier 2 full useful life tailpipe emission standards (g/mi) (5)

Bin #	NO _x	NMOG ^a	CO	HCHO ^b	PM
8	0.20	0.125/0.156	4.2	0.018	0.02
7	0.15	0.090	4.2	0.018	0.02
6	0.10	0.090	4.2	0.018	0.01
5	0.07	0.090	4.2	0.018	0.01
4	0.04	0.070	2.1	0.011	0.01
3	0.03	0.055	2.1	0.011	0.01
2	0.02	0.010	2.1	0.004	0.01
1	0.00	0.000	0.0	0.000	0.00

^a non-methane organic gas^b formaldehyde

In the European Community the first law defining limit values for the emissions from motor vehicles was the Directive 70/220/EEC, approved by the Council in 1970. In December 1998 the Directive 98/69/EC was published. It sets the emission limits applicable to passenger cars and light commercial vehicles from January 2000 (Euro III stage) and from January 2005 (Euro IV stage) (6). Table 1.3 summarizes the emission limits established by the Directive 98/69/EC.

Concern for environmental problems has caused the search and development of alternative propulsion systems, such as electrical engines in conjunction with batteries and/or fuel cells, and small turbines and hybrid engine systems that include both an electrical engine together with batteries as well as small internal combustion engine used to reload the battery (4).

1.4. Methods for NO_x control

1.4.1. Stationary sources

Technologies for the control of NO_x emissions from stationary sources can be classified in two main groups, reduction of NO_x formation and removal of emitted NO_x. The elimination of nitrogen contained in the fuel and modification of combustion belong to the former. Although combustion modifications are extensively applied to lower NO_x emissions, aftertreatment methods are required to meet the most severe emissions limits.

The first methods used for the removal of NO_x from stationary sources included wet processes and the non-selective catalytic reduction, which implies the use of reducing agents that react preferentially with oxygen. Later these methods were replaced by the selective catalytic reduction with NH₃, SCR. NO decomposition represents the ideal method for the removal of NO, since it does not imply the

Table 1.3 Mandatory tailpipe emission limits for passenger cars and light commercial vehicles in the European Community (6)

Category	Class	Reference mass (RW) (kg)	Limit values (g/km)									
			Mass of CO		Mass of HC		Mass of NO _x		Combined		Mass of	
			L1	L2	L1	L2	L3	L3	mass of HC and NO _x	L2 + L3	particulates ^a	L4
Petrol		Diesel		Petrol		Diesel		Petrol		Diesel		
A (2000)	M ^b	All	2.3	0.64	0.20	-	0.15	0.50	-	0.56	0.05	0.05
	N ₁ ^c	I	RW≤1305	2.3	0.64	0.20	-	0.15	0.50	-	0.56	0.05
		II	1305<RW≤1760	4.17	0.80	0.25	-	0.18	0.65	-	0.72	0.07
	III	1760<RW	5.22	0.95	0.29	-	0.21	0.78	-	0.86	0.10	
B (2005)	M ^b	All	1.0	0.50	0.10	-	0.08	0.25	-	0.30	0.025	
	N ₁ ^c	I	RW≤1305	1.0	0.50	0.10	-	0.08	0.25	-	0.30	0.025
		II	1305<RW≤1760	1.81	0.63	0.13	-	0.10	0.33	-	0.33	0.04
	III	1760<RW	2.27	0.74	0.16	-	0.11	0.39	-	0.39	0.06	

^a For compression ignition engines.^b Except vehicles the maximum mass of which exceeds 2500 kg.^c And those Category M vehicles which are specified in note ^b.

addition of external agents. However no suitable catalyst with high activity has been found.

1.4.1.1 NO decomposition

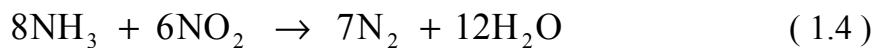
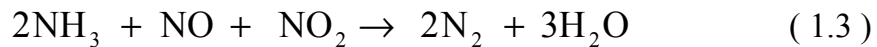
Nitric oxide is thermodynamically unstable in comparison to N_2 and O_2 and therefore its decomposition appears to be the simplest method for the removal of NO from exhaust streams. However, due to the high activation energy for the homogeneous decomposition of NO (~ 335 kJ/mol) temperatures as high as 1200°C are required to carry out this process (7). Therefore the use of a catalyst is required to perform the decomposition of NO at lower temperatures. In the 1960s catalysts based on noble metals and metal oxides were reported active for NO decomposition. In the early 80's Cu-containing zeolites were found highly active. The catalytic activities were strongly dependent of the zeolite structure, being CuMFI and CuFAU the most active. The catalytic activity increased with the Cu loading. However, CuMFI is not sufficiently active in practical conditions, e.g., very low NO concentration, high oxygen concentration and high space velocity. Intensive studies have been done in the search of improving these catalysts. Cu-MeAlPO-11s exhibited turnover frequency values comparable to those of CuMFI. Ni and Co were found to be positive promoters for NO decomposition over CuFAU. Samarium favorably modified the activity of CuMFI when present in small amounts (8).

1.4.1.2 NH₃ Selective Catalytic Reduction

The best-developed and most widely applied system for the control of NO_x emissions of flue gases from stationary sources is the selective catalytic reduction (SCR) (9). This reaction consists in the reduction of NO_x by NH_3 to form water and nitrogen. NH_3 is a very selective reducing agent even in the presence of oxygen (1). In the late 1970s the first SCR systems were installed in Japan on industrial and utility plants. Later in Europe and in the United States the SCR technology was

introduced. Nowadays SCR systems are not only used in coal-, oil- and gas-fired power stations, industrial heaters and cogeneration plants, but also in industrial and municipal waste incinerators, chemical plants and in the glass, steel and cement industries (2).

The reactions that can take place during the SCR processes are the following:



Three types of commercial catalysts have been developed for SCR systems: noble metals, metal oxides and zeolites. However noble metals are no longer used since they oxidize effectively NH_3 . The most widely employed catalysts are based in metal oxide mixtures, as vanadia supported on titania in the anatase form and promoted with tungsta or molybdena, $\text{V}_2\text{O}_5\text{-WO}_3$ (MoO_3)/ TiO_2 . This material has application in conventional SCR between 300 and 400°C. For higher temperatures application the use of zeolites in the acid form with transition metal ions has been found efficient. Recently, materials like V_2O_5 doped TiO_2 pillared clays have been found as active as commercial SCR catalysts (10).

The main problems occurring in the SCR systems are related to the formation of ammonium sulfates. These compounds are formed from the reaction of SO_3 , with water and ammonia. Ammonium sulfates can deposit and accumulate onto the catalyst causing catalyst deterioration, corrosion, emission of acidic particles and aerosols and pressure drop problems (1). Slip of NH_3 is present at ppm levels. The major causes of catalyst deactivation are: (i) loss of surface area by sintering and utilization of titania after long-term operation at high temperature in gas firing, (ii) poisoning of the catalyst active sites by alkali metals present in the flue gas in oil firing, (iii) plugging of catalyst pores by calcium compounds in coal firing, (iv)

poisoning by As in the case of wet bottom boiler, (v) accumulation of phosphorous components in lubricating oil in the case of diesel engines (11).

1.4.2. Mobile sources

The methods used for control of NO_x emissions in vehicles can be classified into three groups (4):

- a) Primary measures, include the introduction of speed limitations, fuel development and modification of engine design.
- b) Secondary measures, imply the aftertreatment control of engine exhaust mainly by the use of catalysts.
- c) A combination of the previous two.

The first drastic improvements in exhaust emissions from passenger cars with gasoline engines were achieved by modification of the engine design. In 1975 a further reduction in the admissible levels of exhaust emissions forced the development of heterogeneous catalysts for the aftertreatment control. Initially catalysts were focused in the conversion of carbon monoxide and hydrocarbons through oxidation reactions. In 1977, the emissions of nitrogen oxides started being regulated. Currently the best approach is the application of exhaust gas aftertreatment in combination of engine modification control. It is worth to mention that also the formulation of fuels plays a significant role in helping to achieve low vehicle emissions (12). Table 1.4 summarizes the specifications for gasoline and diesel fuels for the European Community.

The most common internal combustion engines are otto and diesel engines (13). Otto engines run on gasoline and are mainly used in passenger cars, whereas diesel engines are predominantly used in heavy-duty vehicles. One of the main differences between otto and diesel engines consists in the technique of introducing air and fuel into the cylinder. In the case of otto engines, air and fuel are mixed

before being introduced into the cylinder and the mixture is compressed in the cylinder and ignited by a spark plug. In diesel engines, only the air is compressed, and diesel is sprayed into the compressed air. The compression of the air in the cylinder results in a sharp increase temperature causing the self-ignition of the fuel. In addition, in otto engines the air/fuel ratio is maintained constant and very close to the stoichiometric value, while in diesel engines the amount of air in the cylinder is constant and the air/fuel ratio varies much more than in otto engines. Table 1.5 summarizes some characteristics of otto and diesel engines.

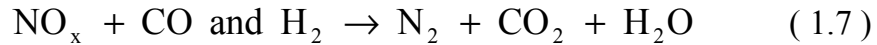
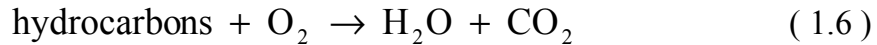
Table 1.4 Gasoline and diesel fuels specification for European Community (12)

	1996	2000	2005
Unleaded gasoline			
Sulfur, max. (mg/kg)	500	150	50
Total aromatics, max (vol%)	-	42	35
Benzene, max (vol%)	5	1	^a
Oxygen, max (wt%)	2.8	2.3	^a
Diesel			
Sulfur, max. (mg/kg)	500	350	50
Cetane number	49	51	^a
Polyaromatics, max. (wt%)	-	11	^a
Density 15 °C (kg/m ³)	860	845	^a
95% distillation point (°C)	370	360	^a

^a Currently undecided

1.4.2.1 Otto engine (Three-way catalyst)

The overall catalytic reactions promoted by the exhaust catalyst in a otto engine are the following (14):



The name “three-way catalyst” comes from the fact that the catalyst promotes the simultaneous removal of NO_x , hydrocarbons and carbon monoxide. Optimum conditions for NO_x reduction require composition conditions very close to stoichiometric ones, since excess of oxygen retards the reduction. While the oxidation of hydrocarbons and carbon monoxide is incomplete when the concentration of oxygen becomes limiting. Therefore, a careful control of the air/fuel ratio is required to work in the optimum conditions for the simultaneous removal of the three pollutants. Table 1.6 shows the composition of a typical three-way catalyst, its performance and some operating conditions.

Table 1.5 Characteristics of otto and diesel engines (13)

Engine type	Otto (gasoline)	Diesel
Vehicle type	mainly passenger cars	mainly heavy-duty vehicles
Ignition	spark ignition	compression ignition
Compression ratio ^a	7-10	16-24
λ	0.9-1.1	1.1-6
Effective efficiency	0.25-0.30	0.3-0.45
Cylinder pressure (bar)	5-10 (avg.)	~20 (avg.), 200 (max)

^a ratio of maximum (piston in lowest position) to minimum (piston in highest position) combustion chamber volume

^b $\lambda = (\text{air/fuel})_{\text{actual}} / (\text{air/fuel})_{\text{stoichiometric}}$

$\lambda < 1$ rich mixture, reducing atmosphere

$\lambda > 1$ lean mixture, oxidizing atmosphere

^c $\text{kW}_{\text{efficient mechanical energy}} \text{ per } \text{kW}_{\text{energy of fuel burned}}$

These catalysts are not efficient when the engine is operated out of the stoichiometric conditions, e.g., lean burn conditions.

Table 1.6 Composition, performance and operating conditions of a three-way catalyst (13)

Composition		
Carrier	Monolith:	cordierite (2MgO.2Al ₂ O ₃ .5SiO ₂)
	wall thickness	0.152 mm
	cells	62 / cm ²
	surface area	27 cm ² /cm ³
Wash-coat	alumina (γ -Al ₂ O ₃) + additives	
Active phase	Pt + Rh	1.24-1.41 g/l catalyst volume
	Mass ratio Pt:Rh	5-20:1
Performance		
Controlled	λ^a	0.99 ± 0.06 $X_{\text{HC}} > 80\%$, $X_{\text{NO\&CO}} > 70\%$
Uncontrolled	λ^a	1.05 ± 0.2 $X_{\text{HC}} > 50\%$, avg. 70% $X_{\text{CO}} > 20\%$, avg. 55% $X_{\text{NO}} > 10\%$, avg. 50%
Operating conditions		
Temperature	570-1170 K	
Space velocity	1 – 2 x 10 ⁵ m ³ _{gas} /m ³ _{reactor} /h	
Volume ratio	catalyst/cylinder	0.8 – 1.5 m ³ /m ³

$$^a \lambda = (\text{air/fuel})_{\text{actual}} / (\text{air/fuel})_{\text{stoichiometric}}$$

1.4.2.2 Diesel engine

Diesel passenger cars are popular in Europe because of the lower price of diesel compared to the gasoline. In the United States such a difference in price does not exist, for that reason diesel passenger cars are rare. Demand for diesel might increase due to the fuel economy advantage and lower carbon dioxide emissions (15).

Since 1980s secondary measures for emissions control in diesel engines have concentrated on the reduction of particulate matter. The emissions of harmful compounds, e.g., CO, hydrocarbons and NO_x were lower than the standards specified by legislation and their control was not necessary. Since 1991, oxidation catalysts have been implemented in passenger cars in the European Union and in some medium and heavy-duty trucks in the United States (4). In addition to converting CO and hydrocarbon emissions, these catalysts help to significantly reduce particulate emissions, as they oxidize high-boiling hydrocarbons which would otherwise condense in the exhaust system and increase the particle mass (16). Diesel oxidation catalysts consist of a ceramic or metallic monolithic support, on which special washcoat is deposited which is in contact with the precious metal component, being typically platinum or palladium (17).

Although oxidation catalysts are efficient for the control of particulate matter, carbon monoxide and hydrocarbons, the removal of NO_x from engines working under lean-burn conditions represents still a challenge. As it was mentioned above, the selective catalytic reduction is an efficient method for the removal of NO_x in the presence of excess of oxygen. However as this process requires ammonia or a compound that produces ammonia on the surface of the catalyst, the application of this method to on-road vehicles is not very feasible. The use of hydrocarbons as reducing agents under excess oxygen conditions has been studied as an approach for NO_x removal from emissions of diesel engines.

1.5. Reduction of NO_x with hydrocarbons

In 1990, the selective reduction of NO with hydrocarbons in an oxidizing atmosphere over CuMFI was first reported independently by Iwamoto and Held. In contrast to the direct NO decomposition where the presence of oxygen retards the

process, when hydrocarbons are used as reducing agents oxygen remarkably enhances the accomplishment of the reduction of NO (8).

1.5.1. Zeolite catalysts

In addition to Cu (18-38), a variety of ion-exchanged zeolites have been found to be active, Co (27, 29, 36, 39-49), Fe (50-55), Ni (36, 47, 48), Pt (56-61), Pd (62-65), Ga (36, 66, 67), Mn (36, 47, 48), Ce (68) and Ag (68), among others.

During the reduction of NO with hydrocarbons there is a maximum for NO conversion with respect to the temperature. At temperatures above that of the maximum NO conversion, the hydrocarbon experiences oxidation preferentially (48). For a given catalyst, the temperature of maximum NO conversion depends on the type of hydrocarbon (8). The zeolite morphology may affect the coordination of the cation, the relative diffusivities of the reactants (46, 47, 50) and/or the activation of the hydrocarbon molecule (22). An excellent review of the NO reduction with hydrocarbons on zeolite-based catalysts is (69).

1.5.1.1 *Cu-exchanged zeolites*

Many hydrocarbons have been tested as reducing agents. Most of the hydrocarbons are more or less active for the reduction of NO on Cu-zeolites, except for methane (8).

Isolated Cu ions in low-symmetry environments (22, 37) and intrazeolite copper oxide clusters provide active sites for the reduction of NO with propene (33). The change in oxidation of state of Cu has been reported to take place during the process of reduction of NO with propane (19).

CuMFI has a poor hydrothermal stability (70). There are two kinds of suppression/deactivation, fully reversible suppression by short exposure of the catalyst to water vapor and irreversible one after a long-term exposure of the catalyst to water vapor at high temperature (8). Another critical problem of Cu-

zeolite systems is the low thermal stability of the zeolite lattice, CuMFI deactivates when treated at or above 600°C even under dry conditions. Formation of CuO particles or clusters (20) and migration of Cu²⁺ ion into inert sites have been suggested as the causes (8). CuMFI was only slightly poisoned by SO₂, which is favorable for the practical application.

1.5.1.2 *Co-exchanged zeolites*

In contrast to Cu-exchanged zeolites, Co-exchanged zeolites are active for the reduction of NO with methane (40, 45, 49). Methane is a very desirable reducing agent since it is abundantly and readily available in many parts of the world. The activity of the Co-exchanged catalysts for the reduction of NO_x with hydrocarbons has been attributed to Co present as ions, while oxide-like Co species and protons contribute to the activity of the catalyst by enhancing the oxidation of NO (40, 71). It has been suggested that at high temperatures the reduction of NO with isobutane occurs without intermediate formation of NO₂ (71).

Water vapor decreases reversibly the activity of the NO reduction with methane due to the competitive adsorption of NO and water occurring on the surface of the catalyst (46, 47, 72).

1.5.1.3 *Fe zeolites*

FeZSM-5 catalysts are generally prepared by sublimation (50-52). Similarly than Cu zeolite catalysts, FeZSM-5 catalysts are not active for the reduction of NO with methane (52). Isobutane, butane and propane are active reducing agents when used over Fe zeolite catalysts. FeZSM-5 catalysts are characterized by a remarkable stability in the presence of large excess of water (52, 53, 73) and SO₂ (55, 73). The major problem with Fe-containing zeolites is that samples with a low iron content display their maximum at NO conversion sometimes at relative low temperatures, but the maximum NO conversion is unsatisfactory, while samples with a high Fe content show high activities at too high temperatures (69).

1.5.1.4 *Pt zeolites*

The temperature of maximum NO conversion of Pt zeolites is much lower than for the rest of metal exchanged zeolites catalysts (57, 70) and the activity was hardly affected by the addition of water vapor (56, 59). The major drawback of Pt-containing zeolites is the high selectivity to N₂O during the reduction of NO with hydrocarbons (57, 59).

1.5.1.5 *Pd zeolites*

The activity of Pd-containing zeolites has been related frequently with the required presence of acid sites (65, 74, 75). Metallic Pd particles are transformed in Pd²⁺ ion when supported on acidic materials resulting active and selective for the reduction of NO with methane. When supported on non-acidic materials, palladium is transformed into PdO clusters and is totally unselective for the conversion of NO and very active for the combustion of methane (63). PdHZSM-5 was observed to strongly dealuminate upon steaming losing its activity (65).

1.5.1.6 *Acidic zeolites*

Protonic zeolites were active for NO oxidation, being the Brønsted acid sites the active sites for this reaction (24, 76). For the reduction of NO with methane, NO conversions of ca. 40% were observed for a variety of H-zeolites. The selectivity of these materials was found to depend on the zeolite structure (77). For NO reduction with propene, the activity of H-zeolites is proportional to the amount of acid sites but independent of the strength (78). When exposed to water at high temperatures, the stability of H-zeolites is poor, since deactivation due to dealumination takes place (79).

1.5.1.7 *Bimetallic catalysts*

Bimetallic catalysts are frequently associated with the term bifunctional catalysts. The incorporation of Pt to Co-exchanged zeolites (80-82) causes an

increase in the NO conversion of N₂ of the catalysts in comparison with the values for the monometallic catalysts. Pt enhances the stability of the samples in the presence of water vapor (82). For an optimum performance of the catalysts Pt and Co should be in close vicinity in the zeolite framework (81).

In a Pd/CoHZSM-5 catalyst the role of Co is attributed to the acceleration of NO oxidation. The excess of Co loading leads to a decrease in activity for NO reduction with methane (83).

In an Ir/In/HZSM-5 catalyst, the function of NO oxidation has been associated to Ir and the reduction of NO₂ to N₂ to InO⁺ species (84).

1.5.2. Oxide-based catalysts

Many base oxides promoted by metals are active catalysts for the reduction of NO with hydrocarbons. Pt/Al₂O₃ (57, 85-90), Pt/SiO₂ (85, 88, 91, 92), Cu/Al₂O₃ (22, 89), Cu/SiO₂ (22), Ni/Al₂O₃ (89); Mn₂O₃ (93), CoO/Al₂O₃ (94); Pd/TiO₂ (95) are some of the catalysts that have been reported active.

Similarly that in the case of zeolitic materials, the effectiveness of base oxides/metals for the reduction of NO with hydrocarbons depends markedly on the nature of the reducing agent, the type of oxide/metal catalysts and its preparation method (96). Support plays an important role on the hydrocarbon activation (57).

When comparing metal-supported alumina, the maximum NO conversion of Ni/Al₂O₃ was found to be higher than that of Cu/Al₂O₃ and Pt/Al₂O₃. The presence of water caused a small reversible inhibition effect in the NO reduction over Pt/Al₂O₃, Cu/Al₂O₃ and Ni/Al₂O₃. In the other hand, SO₂ caused no effect on Pt/Al₂O₃, while Co/Al₂O₃ and Cu/Al₂O₃ deactivated. The activity of Rh/Al₂O₃ for the reduction of NO by propene was enhanced by the presence of SO₂ in the stream (89).

Transition metal-aluminum mixed oxide catalysts (Cu, Ni and Co-Al₂O₃) prepared by coprecipitation method showed high activity and selectivity for the

selective reduction of NO by propene and showed moderate activity even in the presence of 10% water. The high performance of the catalysts was attributed to the surface aluminate phase (97).

Pt-containing catalysts are inefficient at moderate and high temperatures, they catalyze the reduction of NO with hydrocarbons at temperatures below 300°C under lean-burn conditions (96). The activity of Pt-containing oxides is enhanced by a decrease in the metal dispersion (85, 91). N₂O is formed selectively from the reduction of NO with hydrocarbons over Pt catalysts and it may be suppressed by the addition of promoters (98).

1.6. Scope and structure of the thesis

At present the strict regulations regarding the emissions of NO_x from vehicles is still causing difficulties to meet the standard levels for NO_x emissions from the exhaust of diesel-engines automobiles. The approach of using hydrocarbons for the reduction of NO_x over transition metal exchanged zeolites is a promising route for the removal of NO_x under lean-burn conditions. In the design of new improved materials used as catalysts, understanding of how the complex process of the reduction of NO_x takes place is essential.

In this thesis Ni exchanged zeolites used as catalysts for the reduction of NO with hydrocarbons in the presence of excess of oxygen were studied. Propane and propene were used as reducing agents. In chapter 2 the effect of pretreatment methods, the effect of metal content and the influence of acid site concentration on the performance of Ni-exchanged mordenite were studied. In chapters 3 and 4 the influence of the pore geometry and channel diameter on the activity of Ni exchanged zeolite catalysts were studied. Chapter 3 focuses on the influence of the acid sites and in chapter 4 the role of metallic sites is emphasized. In chapter 5 a

mechanism for the reduction of NO with propane and propene on Ni-exchanged mordenite is proposed.

References

1. Janssen, F., and Meijer, R., *Catal. Today* **16**, 157 (1993).
2. Forzatti, P., *Appl. Catal. A* **222**, 221 (2001).
3. Webster, D. E., *Topics in Catal.* **16**, 33 (2001).
4. Lox, E. S. J., and Engler, B. H., in *Environmental Catalysis* (Eds.: G. Ertl, H. Knözinger, J. Weitkamp), Wiley-VCH Verlag GmbH, Weinheim, **1999**, p. 236.
5. Bertelsen, B. I., *Topics in Catal.* **16**, 15 (2001).
6. Greening, P., *Topics in Catal.* **16**, 5 (2001).
7. Garin, F., *Appl. Catal. A* **222**, 183 (2001).
8. Yahiro, H., and Iwamoto, M., *Appl. Catal. A* **222**, 163 (2001).
9. Hums, E., *Catal. Today* **42**, 25 (1998).
10. Long, R. Q., and Yang, R. T., *Appl. Catal. B* **24**, 13 (2000).
11. Nova, I., dall'Acqua, L., Lietti, L., Giamello, E., and Forzatti, P., *Appl. Catal. B* **35**, 31 (2001).
12. Booth, M., Buglass, J. G., and Unsworth, J. F., *Topics in Catal.* **16**, 39 (2001).
13. van Diepen, A. E., Makkee, M., and Moulijn, J. A., in *Environmental Catalysis, Vol. 1* (Eds.: F. J. J. G. Janssen, R. A. van Santen), Imperial College Press, London, **1999**, p. 369.
14. Taylor, K. C., *Catal. Rev.-Sci. Eng.* **35**, 457 (1993).
15. Adams, K. M., Cavataio, J. V., and Hammerle, R. H., *Appl. Catal. B* **10**, 157 (1996).

16. König, A., Herding, G., Hupfeld, B., Richter, T., and Weidmann, K., *Topics in Catal.* **16**, 23 (2001).
17. Farrauto, R. J., and Heck, R. M., *Catal. Today* **51**, 351 (1999).
18. Shichi, A., Satsuma, A., and Hattori, H., *Appl. Catal. B* **30**, 25 (2001).
19. Schay, Z., James, V. S., Pal-Borbely, G., Beck, A., Ramaswamy, A. V., and Guzzi, L., *J. Mol. Catal. A* **162**, 191 (2000).
20. Quincoces, C. E., Kikot, A., Basaldella, E. I., and Gonzalez, M. G., *Ind. Eng. Chem. Res.* **38**, 4236 (1999).
21. Liu, D. J., and Robota, H. J., *J. Phys. Chem. B* **103**, 2755 (1999).
22. Chajar, Z., Le Chanu, V., Primet, M., and Praliaud, H., *Catal. Lett.* **52**, 97 (1998).
23. Shimokawabe, M., Tadokoro, K., Sasaki, S., and Takezawa, N., *Appl. Catal. A* **166**, 215 (1998).
24. Halasz, I., and Brenner, A., *Catal. Lett.* **51**, 195 (1998).
25. Vergne, S., Berreghis, A., Tantet, J., Canaff, C., Magnoux, P., Guisnet, M., Davias, N., and Noirot, R., *Appl. Catal. B* **18**, 37 (1998).
26. Torre-Abreu, C., Ribeiro, M. F., Henriques, C., and Ribeiro, F. R., *Appl. Catal. B* **13**, 251 (1997).
27. Chang, Y. F., and McCarty, J. G., *J. Catal.* **165**, 1 (1997).
28. Rebrov, E. V., Simakov, A. V., Sazonova, N. N., Rogov, V. A., and Barannik, *Catal. Lett.* **51**, 27 (1998).
29. Bell, A. T., *Catal. Today* **38**, 151 (1997).
30. Cant, N. W., and Cowan, A. D., *Catal. Today* **35**, 89 (1997).
31. Corma, A., Palomares, A. E., and Fornes, V., *Res. Chem. Intermed.* **24**, 613 (1998).
32. Corma, A., Fornes, V., and Palomares, E., *Appl. Catal. B* **11**, 233 (1997).
33. Liese, T., and Grünert, W., *J. Catal.* **172**, 34 (1997).

34. Yan, J. Y., Lei, G.-D., Sachtler, W. M. H., and Kung, H. H., *J. Catal.* **161**, 43 (1996).
35. Petunchi, J. O., and Hall, W. K., *Appl. Catal. B* **3**, 239 (1994).
36. Witzel, F., Sill, G. A., and Hall, W. K., *J. Catal.* **149**, 229 (1994).
37. Grünert, W., Hayes, N. W., Joyner, R. W., Shpiro, E. S., Siddiqui, M. R. H., and Baeva, G. N., *J. Phys. Chem.* **98**, 10832 (1994).
38. d'Itri, J. L., and Sachtler, W. M. H., *Appl. Catal. B* **2**, L7 (1993).
39. Dedecek, J., Kaucký, D., and Wichterlová, B., *Topics in Catal.* **18**, 283 (2002).
40. Kaucký, D., Vondrová, A., Dedecek, J., and Wichterlová, B., *J. Catal.* **194**, 318 (2000).
41. Shichi, A., Satsuma, A., Iwase, M., Shimizu, K., Komai, S., and Hattori, T., *Appl. Catal. B* **17**, 107 (1998).
42. Tabata, T., and Ohtsuka, H., *Catal. Lett.* **48**, 203 (1997).
43. Ohtsuka, H., Tabata, T., Okada, O., Sabatino, L. M. F., and Bellussi, G., *Catal. Lett.* **44**, 265 (1997).
44. Tabata, T., Kokitsu, M., Ohtsuka, H., Okada, O., Sabatino, L. M. F., and Bellussi, G., *Catal. Today* **27**, 91 (1996).
45. Cowan, A. D., Dumpelmann, R., and Cant, N. W., *J. Catal.* **151**, 356 (1995).
46. Li, Y., and Armor, J. N., *J. Catal.* **150**, 376 (1994).
47. Li, Y., and Armor, J. N., *Appl. Catal. B* **3**, L1 (1993).
48. Li, Y., and Armor, J. N., *Appl. Catal. B* **2**, 239 (1993).
49. Li, Y., and Armor, J. N., *Appl. Catal. B* **1**, L31 (1992).
50. Chen, H. Y., Wang, X., and Sachtler, W. M. H., *Appl. Catal. A* **194-195**, 159 (2000).
51. Chen, H. Y., Voskoboinikov, T., and Sachtler, W. M. H., *Catal. Today* **54**, 483 (1999).

52. Chen, H. Y., Voskoboinikov, T., and Sachtler, W. M. H., *J. Catal.* **180**, 171 (1998).
53. Voskoboinikov, T. V., Chen, H. Y., and Sachtler, W. M. H., *Appl. Catal. B* **19**, 279 (1998).
54. Kögel, M., Sandoval, V. H., Schwieger, W., Tissler, A., and Turek, T., *J. Catal.* **182**, 470 (1999).
55. Feng, X., and Hall, W. K., *J. Catal.* **166**, 368 (1997).
56. Perez-Ramirez, J., Garcia-Cortes, J. M., Kapteijn, F., Mul, G., Moulijn, J. A., and Salinas-Martinez de Lecea, C., *Appl. Catal. B* **29**, 285 (2001).
57. Garcia-Cortes, J. M., J., P.-R., Illan-Gomez, M. J., Kapteijn, F., Moulijn, J. A., and Salinas-Martinez de Lecea, C., *Appl. Catal. B* **30**, 399 (2001).
58. Acke, F., and Skoglundh, M., *Appl. Catal. B* **20**, 235 (1999).
59. Long, R., and Yang, R. T., *Catal. Lett.* **52**, 91 (1998).
60. Xin, M., Hwang, I. C., and Woo, S. I., *Catal. Today* **38**, 187 (1997).
61. Shin, H. K., Hirabayashi, H., Yahiro, H., Watanabe, M., and Iwamoto, M., *Catal. Today* **26**, 13 (1995).
62. Lobree, L. J., Aylor, A. W., Reimer, J. A., and Bell, A. T., *J. Catal.* **181**, 189 (1999).
63. Ali, A., Alvarez, W., Loughran, C. J., and Resasco, D. E., *Appl. Catal. B* **14**, 13 (1997).
64. Misono, M., Hirao, Y., and Yokoyama, C., *Catal. Today* **38**, 157 (1997).
65. Descorme, C., Gelin, P., Lecuyer, C., and Primet, M., *Appl. Catal. B* **13**, 185 (1997).
66. Armor, J. N., *Catal. Today* **31**, 191 (1996).
67. Yogo, K., Ihara, M., Terasaki, I., and Kikuchi, E., *Catal. Lett.* **17**, 303 (1993).
68. Li, Z., and Flytzani-Stephanopoulos, M., *Appl. Catal. A* **165**, 15 (1997).

69. Traa, Y., Burger, B., and Weitkamp, J., *Micropor. Mesopor. Mat.* **30**, 3 (1999).
70. Amiridis, M. A., Zhang, T., and Farrauto, R. J., *Appl. Catal. B* **10**, 203 (1996).
71. Wang, X., Chen, H. Y., and Sachtler, W. M. H., *Appl. Catal. B* **26**, L227 (2000).
72. Li, Y., Battavio, P. J., and Armor, J. N., *J. Catal.* **142**, 561 (1993).
73. Feng, X., and Hall, W. K., *Catal. Lett.* **41**, 45 (1996).
74. Nishizaka, Y., and Misono, M., *Chem. Lett.* 2237 (1994).
75. Nishizaka, Y., and Misono, M., *Chem. Lett.* 1295 (1993).
76. Halasz, I., Brenner, A., and Ng, K. Y. S., *Catal. Lett.* **34**, 151 (1995).
77. Armor, J. N., *Catal. Today* **26**, 147 (1995).
78. Satsuma, A., Yamada, K., Mori, T., Niwa, M., Hattori, T., and Murakami, Y., *Catal. Lett.* **31**, 367 (1995).
79. Lezcano, M., Ribotta, A., Miro, E., Lombardo, E., Petunchi, J. O., Moreaux, C., and Dereppe, J. M., *J. Catal.* **168**, 511 (1997).
80. Maisuls, S. E., Seshan, K., Feast, S., and Lercher, J. A., *Appl. Catal. B* **29**, 69 (2001).
81. Gutierrez, L., Lombardo, E. A., and Petunchi, J. O., *Appl. Catal. A* **194-195**, 169 (2000).
82. Gutierrez, L., Boix, A., and Petunchi, J. A., *J. Catal.* **179**, 179 (1998).
83. Ogura, M., Sugiura, Y., Hayashi, M., and Kikuchi, E., *Catal. Lett.* **42**, 185 (1996).
84. Ogura, M., Hayashi, M., and Kikuchi, E., *Catal. Today* **42**, 159 (1998).
85. Denton, P., Giroir-Fendler, A., Praliaud, H., and Primet, M., *J. Catal.* **189**, 410 (2000).
86. Meunier, F. C., Breen, J. P., and Ross, J. R. H., *Chemical Communications* 259 (1999).

87. Yentekakis, I. V., Konsolakis, M., Lambert, R. M., Macleod, N., and Nalbantian, L., *Appl. Catal. B* **22**, 123 (1999).
88. Burch, R., and Ramli, A., *Appl. Catal. B* **15**, 63 (1998).
89. Efthimiadis, E. A., Lionta, G. D., Christoforou, S. C., and Vasalos, I. A., *Catal. Today* **40**, 15 (1998).
90. Burch, R., and Watling, T. C., *J. Catal.* **169**, 45 (1997).
91. Denton, P., Giroir-Fendler, A., Praliaud, H., and Primet, M., *Topics in Catal.* **16/17**, 377 (2001).
92. Jayat, F., Lembacher, C., Schubert, U., and Martens, J. A., *Appl. Catal. B* **21**, 221 (1999).
93. Chen, L. Y., Horiuchi, T., and Mori, T., *Catal. Lett.* **60**, 237 (1999).
94. Maunula, T., Ahola, J., and Hamada, H., *Appl. Catal. B* **26**, 173 (2000).
95. Mitome, J., Karakas, G., Bryan, K. A., and Ozkan, U. S., *Catal. Today* **42**, 3 (1998).
96. Burch, R., Breen, J. P., and Meunier, F. C., *Appl. Catal. B* **39**, 283 (2002).
97. Shimizu, K. I., Maeshima, H., Satsuma, A., and Hattori, T., *Appl. Catal. B* **18**, 163 (1998).
98. Konsolakis, M., Macleod, N., Isaac, J., Yentekakis, I. V., and Lambert, R. M., *J. Catal.* **193**, 330 (2000).

2. Reduction of nitric oxide by propene and propane on Ni-exchanged mordenite

The reduction of NO over Ni-exchanged mordenite in the presence of excess oxygen using propane and propene as reducing agents was studied. During ion exchange of the zeolite with Ni²⁺, Brønsted acid sites were formed resulting from the hydrolysis of divalent Ni²⁺ ions. The chemical state of the Ni ions and the density and strength of the acid sites strongly determine the activity and selectivity of the catalysts for the NO reduction. Non-reduced catalysts showed a high selectivity to N₂, while after partial reduction of the Ni ions significant concentrations of NO₂ and N₂O were formed. In addition, low concentrations of NO₂ were formed during reduction of NO with propane and related to the more demanding activation of the alkane. An optimum concentration of acid sites, which in turn depends on the nickel loading, is required to obtain high NO conversion with propane. Deactivation due to deposition of carbonaceous species was observed during the NO reduction with propene for samples with high concentration of acid sites.

2.1. Introduction

The reduction of NO_x with hydrocarbons using transition metal exchanged zeolites as catalysts is a promising route to replace ammonia-based reducing agents in the SCR process. CuZSM-5 has been studied extensively, since Cu has a unique activity for the decomposition of NO into its elements, but was rapidly deactivated in the presence of H_2O and/or SO_2 in the reactant gas stream [1, 2]. It was shown later that zeolites exchanged with other transition metals, such as FeZSM-5 [3-7] and CoZSM-5 [8-11], showed a similar selectivity for the reduction of NO to N_2 , but a higher stability in the presence of H_2O and SO_2 . Other metals such as Ni, Pt and Pd supported on ZSM-5 [12], FER [9, 12], MOR [13, 14], BEA [15, 16] and MCM-22 [15] as well as Ni supported on alumina [17, 18] are also known to be effective catalysts for the reduction of NO with hydrocarbons.

The catalytic activity of NiNaZSM-5 for the reduction of NO with various hydrocarbons was studied by Witzel *et al.* [12] At low space velocities (flow rate 75 ml/min and 0.25 g of catalyst), conversions around 90% were obtained at 400°C using isobutane as reducing agent. In addition they reported only a small influence of the type of charge balancing cation (i.e., H, Co, Ni, Cu, La, Mn, Ga) on the activity and selectivity of the catalysts. In contrast, Li and Armor [9, 10], found for transition metal-exchanged zeolites (prepared from the H form of the zeolite) that the type of zeolite and charge balancing cations strongly influences the activity of the catalysts for the NO reduction. In addition, the metal determines the preferred type of hydrocarbon used as reducing agent. CoZSM-5, MnZSM-5, NiZSM-5 and RhZSM-5 effectively reduce NO to N_2 with methane as well as other alkanes [10], whereas CuZSM-5 requires paraffins or olefins with at least three carbon atoms [19]. In general, the reaction mechanism for the reduction of NO appears to depend on the type of hydrocarbon used as reducing agent [19, 20], as the rupture of the

first C-H bond has been speculated to be the rate-limiting step in the reduction of NO with alkanes [12, 21].

The role of Brønsted acid sites in the selective reduction of NO by hydrocarbons is not unequivocally settled. For the catalytic reduction of NO with CH₄ over Pd/zeolites, protonic acidity is described to be essential [22-25]. Also for the reduction of NO by propene over CuZSM-5 a synergetic effect of the acidic and metal sites has been reported [26, 27]. In general, the generation of carbonaceous surface species, which are intermediates of the SCR reaction, has been attributed to the presence of acid sites [28]. In contrast, other authors have demonstrated the apparent irrelevance of Brønsted acidity for the SCR of NO by propene over Cu-exchanged mordenites [29] and ZSM-5 [30].

In order to understand the influence of metallic and Brønsted acidic sites on the catalytic performance of transition metal containing zeolites, a series of Ni ion exchanged zeolite samples with a carefully controlled concentration of metallic and Brønsted acidic sites was prepared. Possible synergistic effects of metallic and acidic sites on the activity for NO reduction were studied. Propane and propene were used to differentiate the effects of acid and cationic sites on the activation of the hydrocarbon.

2.2. Experimental

2.2.1. Catalyst preparation

NaMOR (Si/Al=8.6) was supplied by Tosoh. HMOR was prepared by ion exchange of the parent material (Na⁺-form) with an aqueous NH₄NO₃ solution, followed by calcination at 600°C for two hours (heating rate 2°C/min). Ni was incorporated into the Na⁺ and H⁺-forms of the zeolites by liquid phase ion exchange carried out in an aqueous solution of Ni(NO₃)₂ at 80°C under continuous

stirring for 24 h. The Ni loading of the zeolites was controlled by the concentration of Ni in the aqueous solution. Subsequently, the zeolite was separated from the solution by centrifugation, washed thoroughly with deionized water and dried overnight at 100°C. For a selected NiNaMOR sample, an additional calcination at 600°C and a further ion exchange with NaNO₃ solution were carried out in order to remove the protons formed by the hydrolysis of the Ni complex (sample indicated as NiNaMOR0.6be). One of the catalysts was reduced in H₂ at 350°C for 10 h (sample indicated as NiNaMORred).

2.2.2. Physicochemical characterization

The elemental composition of the samples was determined after solving the samples in HF by atomic absorption spectroscopy (AAS UNICAM 939).

The concentration of the acid sites was measured by temperature programmed desorption (TPD) of NH₃. After activation of the sample (~ 80 mg) in vacuum at 600°C for 1 h, NH₃ was adsorbed at 1 mbar pressure for 1 h at 150°C (unless otherwise stated). Weakly adsorbed ammonia was removed by evacuation of the sample at 150°C for 3 h. TPD was carried out from 150°C to 700°C with a heating rate of 10°C/min, the desorption of the probe molecules was detected in the gas phase with a mass spectrometer (Balzers QMG 420).

The nature of acid sites was determined by pyridine adsorption followed by IR-spectroscopy. Samples were prepared as self-supported wafers and activated at 600°C (heating rate 10°C/min) for 1 h. Spectra of activated samples were recorded at 120°C with a BRUKER IFS 88 FTIR spectrometer using a resolution of 4 cm⁻¹. Pyridine was adsorbed with a partial pressure of 1*10⁻² mbar at 120°C. A series of spectra was recorded until the sorption equilibrium of the probe molecules over the sample was achieved. The composition and concentration of acid sites for all catalysts are compiled in Table 2.1.

Table 2.1 Chemical composition and acid site concentration of the samples used

Sample	Si/Al ^a	Ni/Al ^a	Na/Al ^a	Ni loading (wt. %)	Acid site concentration [mmol/g]
NiNaMOR3.7	8.57	0.38	0.38	3.7	0.71
NiNaMOR3.0	8.63	0.30	0.53	3.0	0.65
NiNaMOR2.1	8.32	0.20	0.58	2.1	0.44
NiNaMOR1.3	9.17	0.14	0.80	1.3	0.23
NiNaMOR0.3	8.74	0.03	1.00	0.3	0.04
NiNaMORred	9.13	0.42	0.26	4.0	0.53
NiHMOR2.9	8.93	0.30	-	2.9	1.16
NaMOR	8.60	-	1.09	-	0.03
HMOR	8.97	-	-	-	1.33
NiNaMOR0.6be	10.06	0.07	0.99	0.6	0.09
NiNaMOR0.6	8.95	0.07	0.89	0.6	0.13
NiHNaMOR0.6	8.93	0.06	0.38	0.6	0.75
NiHMOR0.6	8.94	0.06	-	0.6	1.10

^a molar ratio

2.2.3. Catalytic measurements

The catalytic activity of the samples was studied in a continuous flow system with a fixed bed quartz reactor of 4 mm inner diameter containing 0.1 g of catalyst (particle size 300 μm). The reactant gas consisted of 1000 ppm NO, 1000 ppm C_3H_6 or C_3H_8 , 5% oxygen and He as the carrier gas. A total flow of 50 ml/min, resulting in a space velocity of 20000 h^{-1} , was used. The reaction products were analyzed with a chemiluminescence analyzer (NO- NO_2 analysis, TEI 42C) and a gas chromatograph (HP) with a TCD detector using a MS 5A column for the separation of N_2 , O_2 and CO and a Porapak Q column for N_2O , C_3H_6 , C_3H_8 and

CO₂ analysis. Before the reaction, the catalyst was activated under helium flow at 600°C for 1 h. Kinetic measurements were carried out at temperature intervals of 25°C between 150 and 600°C.

The absence of external diffusion limitations was verified by determining the activity of different flow rates by varying the catalyst mass to maintain constant space velocity.

2.3. Results

2.3.1. Influence of Nickel concentration

2.3.1.1 *Physicochemical characterization of samples with different Ni loading*

The IR-spectra of the activated NiNaMOR samples with different Ni content in the region of the stretching vibrations of the hydroxyl groups are shown in Fig. 2.1. IR-bands at 3740 and 3610 cm⁻¹, assigned to silanol and bridging hydroxyl groups, respectively, were observed on all NiNaMOR samples. With increasing Ni loading, the intensity of the bridging hydroxyl groups increased, indicating the formation of additional Brønsted acid sites after Ni²⁺ ion exchange of NaMOR. Additionally, the position of the band shifted from 3619 to 3602 cm⁻¹ for the samples with increasing nickel concentrations.

The acid site concentration was determined by NH₃ TPD after adsorption and outgassing at 150°C and 120°C. For both temperatures, linear correlations between the Ni loading and the concentration of acid sites were found (Fig. 2.2). The slope of the correlation after adsorption at 120°C was 1.9, which indicates that for each Ni²⁺ ion incorporated two acid sites were formed. However, the sites formed are not of equal acid strength, as indicated by the slope of 1.2 observed after adsorption at 150°C, because weaker sites were not detected at this temperature.

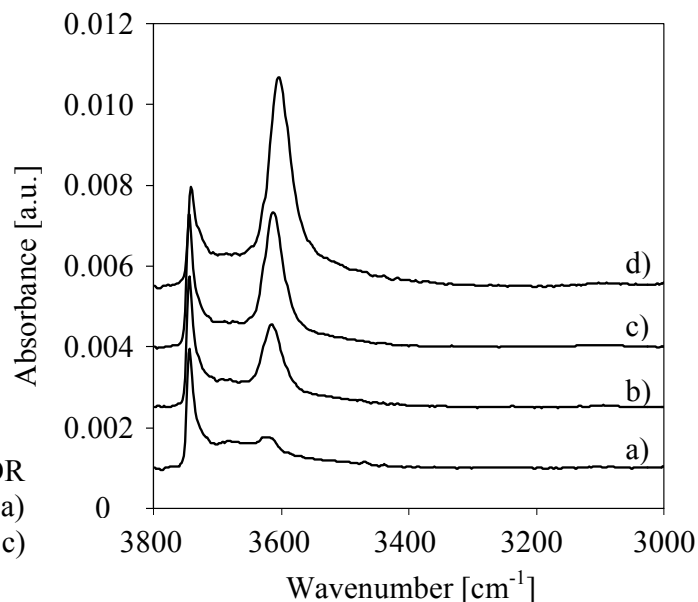


Figure 2.1 IR-spectra of NiNaMOR samples with different Ni loading. a) NiNaMOR1.3, b) NiNaMOR2.1, c) NiNaMOR3.0, d) NiNaMOR3.7.

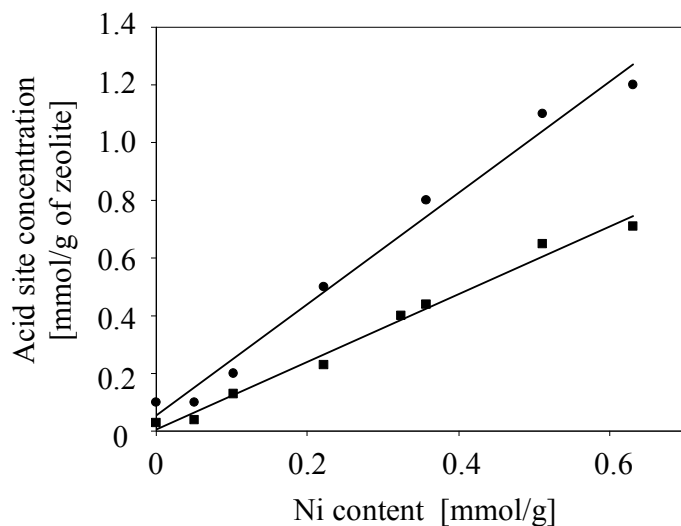


Figure 2.2 Acid site concentration of Ni-exchanged mordenite samples as a function of Ni loading, measured by NH_3 TPD after adsorption and outgassing at 120°C (●) and 150°C (■).

2.3.1.2 Catalytic measurements of samples with different Ni loading

The nitrogen-containing products observed during the reduction of NO with propane and propene were N_2 , N_2O and NO_2 . The carbon-containing products

formed during the reactions were oxidation products, i.e., CO₂ and CO, and cracking products, such as CH₄.

The activities of the Ni-containing mordenite samples prepared from the Na-form of the zeolite for the reduction of NO with propene and propane are compared in Table 2.2. For propene, the maximum NO conversion was observed at lower temperatures compared to propane, i.e., between 400 and 475°C, and between 450 and 500°C for propene and propane, respectively. Samples with a Ni loading below 1.4% showed much lower NO conversions with propane, while samples containing more Ni showed very similar NO conversions for both reducing agents. It has to be noted that for propane, the sample with the lowest Ni loading had a very low NO conversion (maximum 18%).

Table 2.2 Activity of NiNaMOR with different Ni loading during the reduction of NO with propene and propane

Sample	Propene			Propane		
	NO conv ^a [%]	Selectivity to N ₂ ^b [%]	T _{max} ^c [°C]	NO conv ^a [%]	Selectivity to N ₂ ^b [%]	T _{max} ^c [°C]
NiNaMOR3.7	80	96	425	80	91	450
NiNaMOR3.0	77 ^d	96 ^d	400 ^d	73	95	450
NiNaMOR2.1	76	95	400	73	95	450
NiNaMOR1.3	74	94	425	63	96	500
NiNaMOR0.3	50 ^d	90 ^d	475 ^d	18	75	500

^a Maximum NO conversion

^b Selectivity to N₂ at temperature of maximum NO conversion

^c Temperature at maximum NO conversion

^d Activity was determined from calibrated data obtained from the analysis of the gases with an infrared gas cell

The NO and hydrocarbon conversions for NiNaMOR2.1 during the reduction of NO with propene and propane are compared in Fig. 2.3. The maximum NO

conversions were 76% and 73% for reduction with propene and propane, respectively. A slightly lower temperature for the maximum NO conversion with propene compared to propane was observed, i.e., 400°C and 450°C for propene and

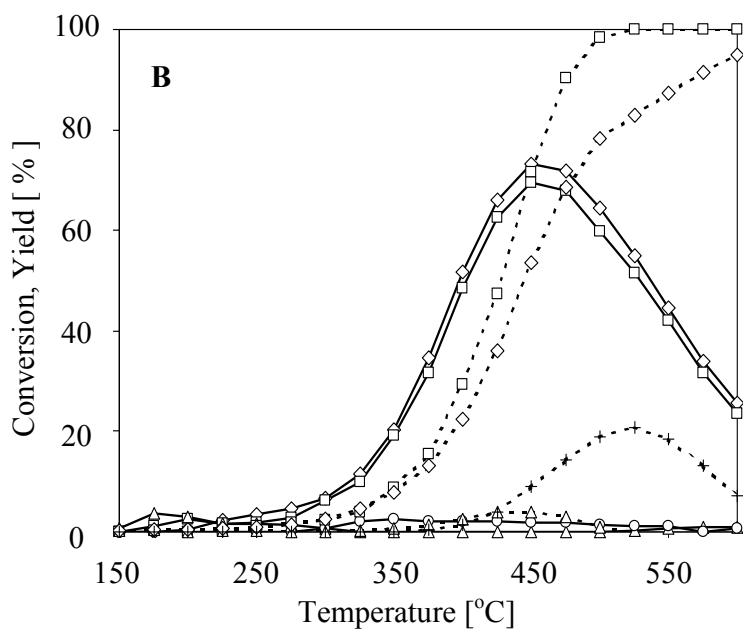
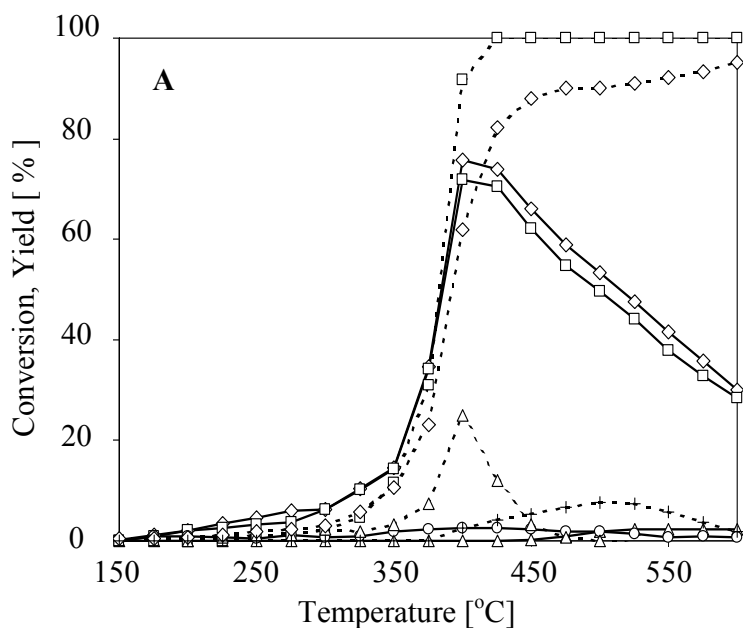


Figure 2.3 Reduction of NO with (A) propene and (B) propane on NiNaMOR2.1. Conversion of NO (—◇—) and propane or propene (—□—), and yields of N₂ (—□—), N₂O (—○—), NO₂ (—△—), CO₂ (—◇—), CO (—▲—) and CH₄ (—+—).

propane, respectively. However, the conversion of the reducing agent showed significant differences. The conversion of propene started in parallel to the NO conversion and reached a conversion level of 100% at 425°C, which is close to the temperature of the maximum NO conversion. In contrast, the conversion of propane was delayed with respect to the NO conversion and reached a conversion level of 100% at 525°C, which is 75°C above the temperature of the maximum NO conversion. A significant formation of CO was observed at the maximum NO conversion during NO reduction with propene, while only small amounts of CO were formed during the reaction with propane. A higher amount of CH₄ was formed using propane as reducing agent compared to propene. In general, only minor concentrations of N₂O were formed in both reactions, the highest N₂O concentration was observed at the temperatures corresponding to the maximum NO conversion. Fig. 2.4 compares the selectivities to N₂ during the reduction of NO with propene and propane on NiNaMOR2.1. For both reducing agents very high selectivities to N₂ were observed. At temperatures below the maximum NO conversion the selectivity to N₂ was higher for the reaction with propene due to the

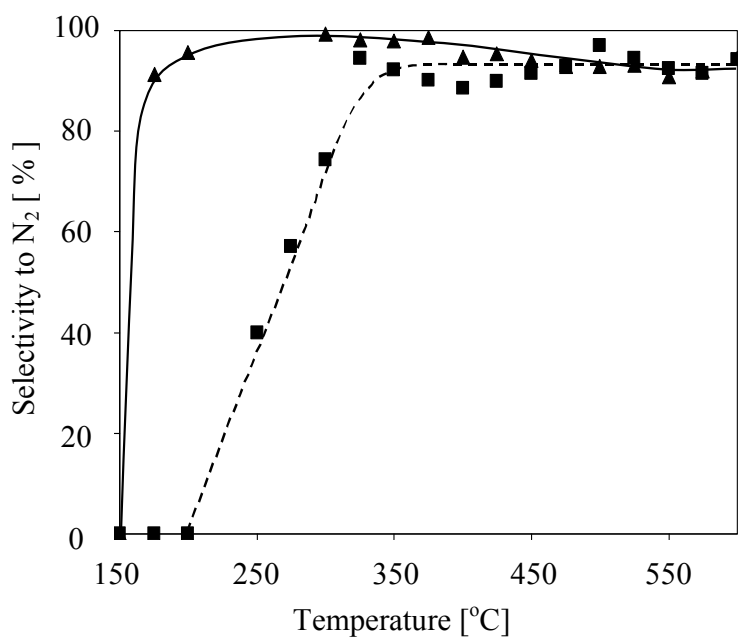


Figure 2.4 Selectivities to N₂ during the reduction of NO with propene (▲) and propane (■) over NiNaMOR2.1.

formation of moderate amounts of NO_2 in the reaction with propane. At temperatures above the maximum NO conversion, for propene the selectivities to N_2 decreased due to the formation of NO_2 .

2.3.1.3 *Influence of the type of charge balancing cation on the catalytic properties*

The influence of the type of charge-balancing cations, i.e., Na^+ or H^+ and the pre-treatment method on the maximum NO conversion and the yield of N_2 for the mordenite samples are summarized in Table 2.3. Independently of the type of reducing agent used, NaMOR was completely inactive for NO reduction. For HMOR, a maximum NO conversion of 5% was found for the reduction with propene, while with propane, a maximum NO conversion of 18% at 375°C was observed. The comparison of NiNaMOR3.0 and NiHMOR2.9 (see Fig. 2.5), clearly indicates that for both reducing agents, the main difference between Na^+ and H^+ containing catalysts is the temperature of the maximum NO conversion, which increases in the presence of acid sites. For the NO reduction with propane, the maximum NO conversion was reached at 450°C for NiNaMOR3.0, while for NiHMOR2.9 500°C were required. Higher temperatures for the maximum NO conversion were observed for propane in comparison to propene. In the case of propane, selectivities to N_2 and the formation of CH_4 were similar for both materials, while a larger concentration of CO was formed on NiHMOR2.9 compared to NiNaMOR3.0. For the reaction with propene, NiNaMOR3.0 was more active than at NiHMOR2.9 at temperatures below 350°C. At this temperature range small concentrations of N_2O were formed on both catalysts (not shown). At temperatures above 350°C, small amounts of NO_2 (yield < 7%) were formed on NiNaMOR3.0 and on NiHMOR2.9.

Table 2.3 Activity of NaMOR, HMOR and NiMOR with 3 wt% Ni for the reduction of NO

Sample	Propene			Propane		
	NO conv ^a [%]	Selectivity to N ₂ ^b [%]	T _{max} ^c [°C]	NO conv ^a [%]	Selectivity to N ₂ ^b [%]	T _{max} ^c [°C]
NaMOR	0	0	-	0	0	-
HMOR	5	74	600	18	84	375
NiNaMOR3.0	77 ^d	96 ^d	400 ^d	73	95	450
NiHMOR2.9	68	97	475	72	96	500
NiNaMORred	68 ^d	67 ^d	425 ^d	63	87	450

^a Maximum NO conversion

^b Selectivity to N₂ at temperature of maximum NO conversion

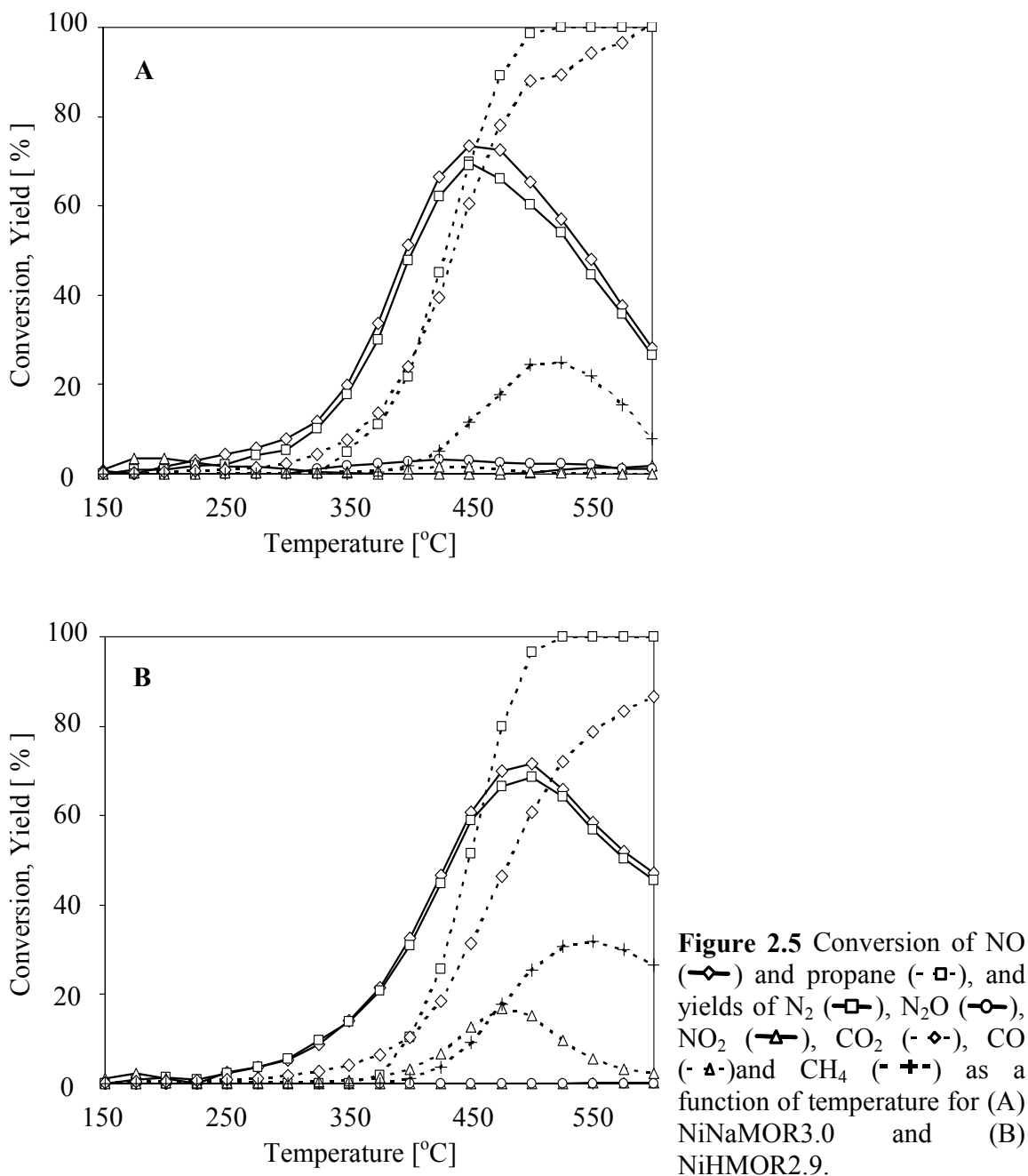
^c Temperature at maximum NO conversion

^d Activity was determined from calibrated data obtained from the analysis of the gases with an infrared gas cell

The NO conversion with propane NiNaMORred (pre-reduced) is shown in Fig. 2.6. For the pre-reduced catalyst (NiNaMORred) maximum NO conversions of around 65% were reached for both reducing agents. In comparison with the non-reduced samples, however, the N₂ yield was significantly lower due to the formation of N₂O at temperatures below 450°C (maximum N₂O yields approx. 19%) and of NO₂ at higher temperatures (NO₂ yields 13% for propene and 4% for propane). The formation of CO was not observed on the pre-reduced catalyst and CH₄ was only formed during the NO reduction with propane.

2.3.2. Influence of the acid site concentration

The influence of acid and metallic sites was studied using a series of samples with varying concentration of acid sites and constant Ni loading (0.6%).



Composition of the catalysts and the concentration of acid sites are compiled in Table 2.1. Two of these samples were prepared starting from the Na-form of mordenite, i.e., NiNaMOR0.6 and NiNaMOR0.6be. The latter sample was ion-exchanged with NaNO₃ after calcination in order to remove acid sites formed by the hydrolysis of the divalent Ni²⁺ cations. NiHMOR0.6 was prepared from the

protonic form of mordenite and NiHNaMOR0.6 was prepared from a partially protonic sample, which contained Na^+ cations and H^+ before the ion exchange. Integration of the curves during TPD of NH_3 indicated that the acid site concentration decreased in the order $\text{NiHMOR0.6} > \text{NiHNaMOR0.6} \gg \text{NiNaMOR0.6} > \text{NiNaMOR0.6be}$. The ratio between Brønsted and Lewis acid sites (B/L ratio), determined by pyridine adsorption followed by IR-spectroscopy [31], is summarized Table 2.4. The B/L ratio increased in the order $\text{NiNaMOR0.6be} < \text{NiNaMOR0.6} \ll \text{NiHNaMOR0.6} < \text{NiHMOR0.6}$.

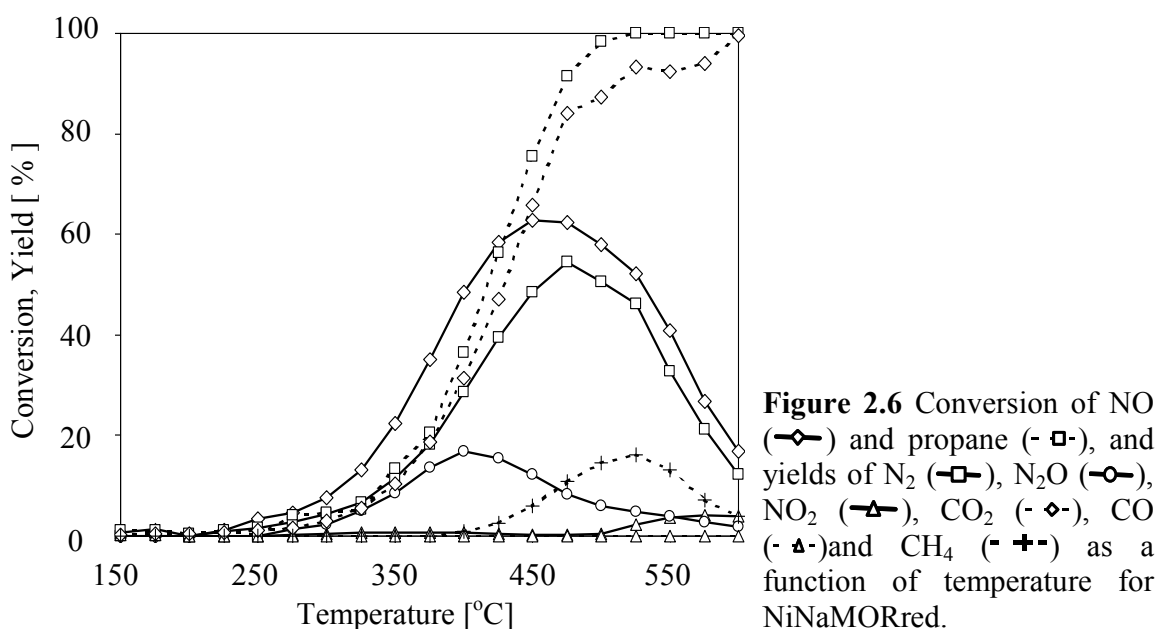
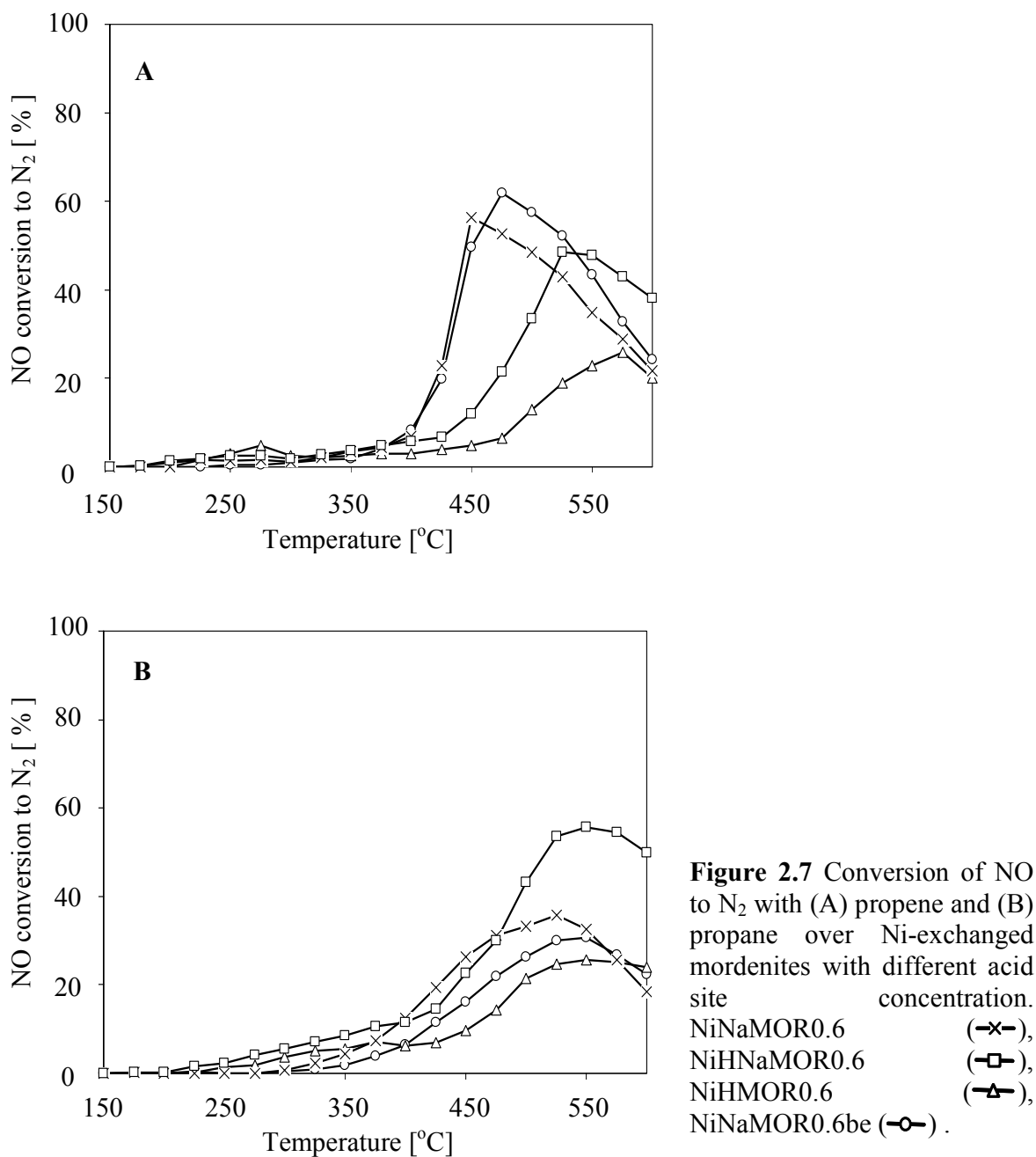


Table 2.4 Ratio between Brønsted and Lewis acid sites

Sample	Brønsted / Lewis ratio
NiNaMOR0.6be	0.04
NiNaMOR0.6	0.05
NiHNaMOR0.6	1.97
NiHMOR0.6	2.79

The NO conversions over the Ni-mordenite catalysts with 0.6 wt% Ni loading using propene and propane as reducing agents are compared in Fig. 2.7. When propene was used as reducing agent, the catalysts with the lowest concentration of acid sites (NiNaMOR0.6be and NiNaMOR0.6) showed the highest activities,



followed by the sample with intermediate concentration of acid sites (NiHNaMOR0.6), whereas the sample with the highest acid site concentration (NiHMOR0.6) was the least active. In contrast, for propane the catalyst with the intermediate concentration of acid sites (NiHNaMOR0.6) was the most active catalysts for the reduction of NO, followed by NiNaMOR0.6, NiNaMOR0.6be and NiHMOR0.6.

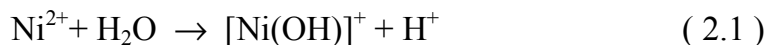
2.3.3. Effect of conversion on selectivity

The yields and selectivities of nitrogen containing reaction products as function of the NO conversion for NiNaMOR2.1 at 350°C are shown in Fig. 2.8. Independently of the reducing agent, the selectivity to N₂ increased and the selectivity to N₂O decreased with increasing conversion, while the formation of NO₂ was not observed.

2.4. Discussion

2.4.1. The acid-base properties of Ni²⁺ exchanged MOR

With increasing fraction of Ni²⁺ exchanged for Na⁺, a marked variation of the Brønsted and Lewis acid sites was found. The linear correlation with a slope of 1.9 between the concentration of Brønsted and Lewis acid sites (NH₃-TPD starting at 120°C) and the Ni content indicates that two acid sites are formed for each Ni atom incorporated during ion exchange (see Figs.2.1 and 2.2). One of these sites is concluded to result from the hydrolysis of the Ni²⁺Z⁻ complex and is located directly on the zeolite, the other is most probably associated with the NiOH⁺ groups of the Ni²⁺ (see Eq. 2.1).



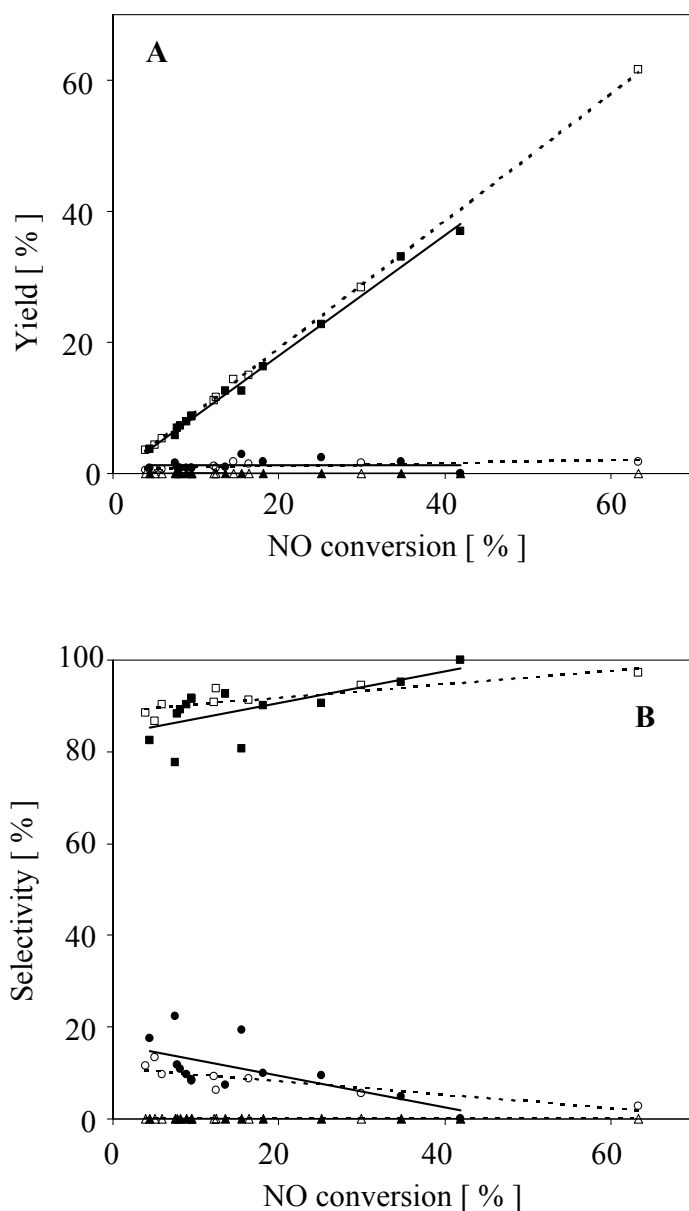


Figure 2.8 Reduction of NO with propane (solid symbols) and with propene (open symbols) over NiNaMOR2.1 at 350°C. (A) yield of N₂ (■,□), N₂O (●,○) and NO₂ (▲,△) vs. conversion, (B) selectivity to N₂ (■,□), N₂O (●,○), and NO₂ (▲,△) vs. conversion.

After equilibration with 1 mbar of NH₃ at 150°C, the slope of the correlation decreased to 1.2, which indicates that the two types of sites formed were not of equal acid strength and led to the speculation that most of the sites with the lower acidic strength, i.e., [Ni(OH)]⁺, were not detected by NH₃-TPD after adsorption at 150 °C. The difference between the slope of 1.9 observed and the theoretical value of 2 indicates that a minor fraction of Ni-oxide species is present in the samples.

The majority of the Ni atoms, however, were incorporated into the samples in the same chemical state and, therefore, allowed us to investigate the influence of the metal loading without effects of Ni species present in different chemical environments.

The formation of Brønsted acid sites during the ion exchange was confirmed by the increasing intensity of bridging hydroxyl groups in the IR spectra of the activated samples with increasing Ni loading. The shift of this IR band observed with increasing Ni concentration results from the different locations of the bridging hydroxyl groups formed inside the channels of mordenite. At low Ni concentrations, the band at 3619 cm^{-1} indicates that all Brønsted acid sites formed were located in the 12 member ring channels (main channels) of mordenite. With increasing Ni loading, bridging hydroxyl groups were also formed in the 8 member ring channels (side pockets), which results in a shift of the OH stretching vibrations to lower frequencies (see also refs. [32, 33]).

2.4.2. Catalytic conversion of NO with propene/propane

2.4.2.1 *Influence of the acid site concentration*

The complete inactivity of NaMOR in comparison to the moderate activity of HMOR for NO reduction clearly indicates that acid sites play a significant role in the NO reduction. The NO conversion level increased with the exchange degree of Na^+ by Ni^{2+} independently of the type of reducing agent. Thus, the activity of the Ni-containing catalysts is attributed to both, the presence of the metal cations and also to the formation of Brønsted acid sites during ion exchange.

The temperature required for the maximum NO conversion was lower for propene compared to propane, which indicates that the limiting step involves the activation of the hydrocarbon [34] as the presence of a carbon-carbon double bond facilitates the formation of carbenium ions [35]. The formation of NO_2 was

observed for all samples at temperatures below 350°C, when propane was used as reducing agent, which indicates that NO₂ is an intermediate during the reaction [13, 36, 37]. At low temperatures the catalysts are not sufficiently active to activate propane and, thus, NO₂ formed cannot react and is observed as a reaction product. This indicates that the activation of propane is slower than the oxidation of NO to NO₂ and, therefore, the former reaction appears to be the rate limiting step of the reaction [7, 12, 21, 38].

For catalysts with the same Ni loading of 0.6% the maximum in the NO conversion as function of the acid sites concentration observed (see Fig. 2.9) clearly points out that a balanced concentration of acid sites is required for the reduction of NO by propane, while for the NO reduction with propene the activity decreases with increasing concentration of acid sites. A high concentration of acid sites (e.g., in NiHMOR0.6) leads to rapid deactivation of the catalyst by propene oligomerization and coking [28], which causes blocking of active sites and pores [39]. For the NO reduction with propane a high concentration of acid sites also led to formation of carbonaceous species indicated by the low activity of NiHMOR0.6. In the temperature range between 325 and 550 °C, NO conversions are higher for the reduction with propane in comparison with propene, which we attribute to a potentially higher deposition of carbonaceous species in the latter case. Furthermore, it has been reported that the higher efficiency of propane compared to propene, is due to the lower degree of catalyst deactivation, since more carbonaceous material is deposited during the reaction using propene as reducing agent [40].

For samples with higher Ni loading, i.e., NiNaMOR3.0 and NiHMOR2.9, the effect of the acid site concentration was smaller (see Fig. 2.5). The main difference was observed in the temperature of maximum NO conversion, which was higher in the case of NiHMOR2.9 compared to NiNaMOR3.0. The difference in the maximum NO conversion was 9%, and 1% for propene and propane, respectively.

The inhibiting effect inherent to the presence of a high concentration of acid sites was not so pronounced compared to the samples with low Ni loading, i.e., NiNaMOR0.6 and NiHMOR0.6, therefore, we would like to speculate that the higher Ni loading suppresses the formation of carbonaceous species that potentially deactivate catalysts with a high concentration of acid sites.

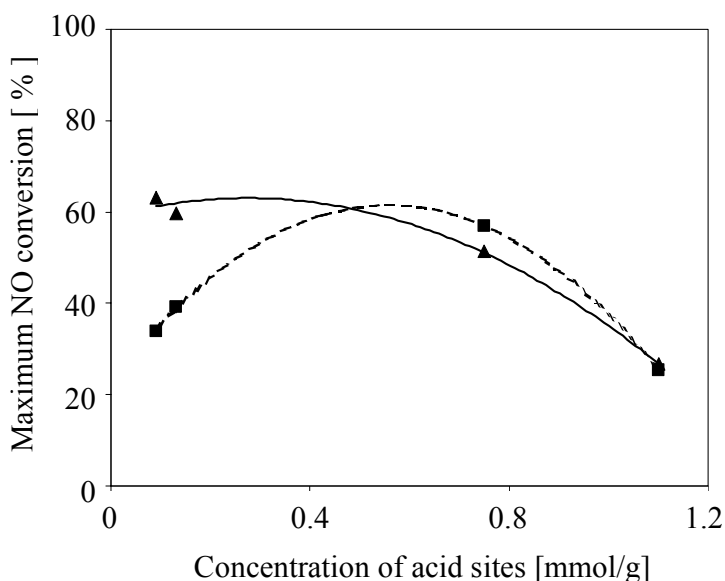


Figure 2.9 Variation of the maximum NO conversion with the total concentration of acid sites for the reduction of NO with propane (■) and propene (▲) over NiMOR samples with 0.6% Ni.

2.4.2.2 Influence of metal

Nickel was found to be present as Ni^{2+} located in the ion exchange positions inside the channels of mordenite and to remain highly dispersed even at Ni loadings of 3.7 wt%. The relation of the Ni concentration to the activity of the catalysts studied (based on the data shown in Table 2.2) is summarized in Fig. 2.10. For propene, at low Ni concentration (NiNaMOR0.3) the maximum NO conversion increases from almost zero (NaMOR) to 50%, but increased only to 80% for a catalyst with 3.7 wt% Ni. In contrast for the NO reduction with propane the catalyst with low Ni loading was less active (18 % NO conversion), but the activity increased up to 80% NO conversion for the catalysts with the highest Ni loading. The reduction of NO is typically limited by the availability of reducing agent. The

constant NO conversion at high Ni loading indicates that the unselective combustion of the hydrocarbon molecules prevails. Therefore, the concentration of the reducing agent at the active sites is insufficient for a further increase in the NO reduction.

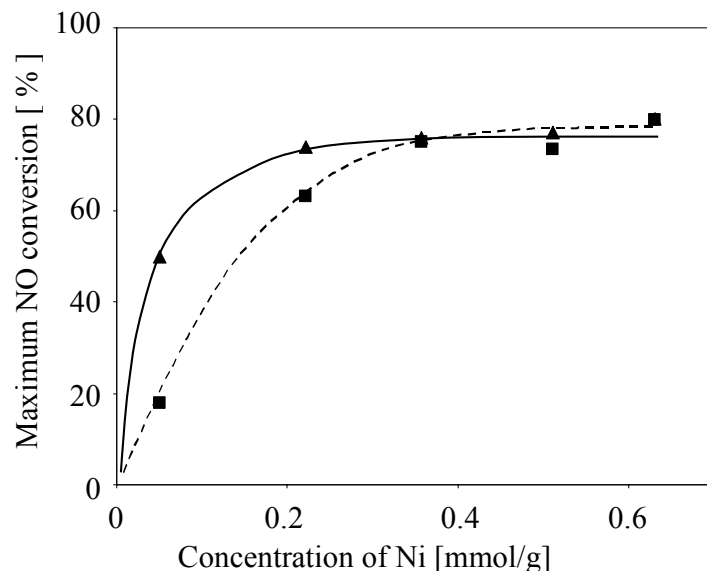


Figure 2.10 Variation of the maximum NO conversion with the concentration of Ni for the reduction of NO with propane (■) and propene (▲) over Ni-MOR

The significant formation of N_2O over the pre-reduced catalyst clearly indicates that the selectivity of the catalysts during the NO reduction is directly controlled by the nature of the metal-oxide species. Conceptually, Ni-oxide clusters formed from metallic Ni particles (pre-reduced NiNaMORred) during the reaction in oxidizing atmosphere should be larger compared to those formed from isolated Ni ions in the non-reduced samples. In addition, a minor fraction of the Ni particles might remain in a partially reduced state. The formation of N_2O is generally attributed to the presence of molecularly adsorbed NO, which reacts with N atoms adsorbed on the metal (oxide) surface [41-43]. Therefore, the simultaneous presence of large metal-oxide clusters formed and reduced Ni particles remaining in NiNaMORred favor a non-dissociative adsorption of NO, which leads to the enhanced N_2O formation. In addition, differences in the carbon product distribution were observed between non-reduced and reduced catalysts (see Figs. 2.5 and 2.6). The absence of CO

during the reduction of NO over NiNaMORred with both reducing agents, also indicates the presence of a small fraction metallic (reduced) Ni clusters, which are known to be effective catalyst for the total oxidation of alkanes [44].

2.5. Conclusions

Two Brønsted acid sites are formed for each Ni atom incorporated by hydrolysis after Ni²⁺ ion exchange of NaMOR. The hydroxyl groups associated with the Ni²⁺ ions are weaker acidic than the OH groups located on the zeolite. In the samples prepared from the sodium form of mordenite, the activity was enhanced by the increase in the nickel content, which is directly coupled to the increase in the acid site concentration. The activation of the hydrocarbon molecules occurs on the acid sites. Propene is easier to activate compared to propane due to the presence of the unsaturated carbon double-bond. However, an optimum concentration of acid sites, which depends on the nickel loading, is required to obtain high NO conversion with propane. For catalysts with an acid site concentration above the optimum, deactivation through carbonaceous species deposition is observed. For propene, a low acid site concentration enhances the activity of the catalyst.

For all non reduced catalysts studied a very high selectivity to N₂ was obtained. It is essential that Ni is present as highly dispersed Ni ions on the ion exchange positions of the zeolites. The formation of large Ni-oxide clusters and metallic Ni clusters, observed in the pre-reduced catalyst, decreases the selectivity to N₂ due to enhanced N₂O formation.

References

1. Traa, Y., Burger, B., and Weitkamp, J., *Micropor. Mesopor. Mat.* **30**, 3 (1999).
2. Yan, J. Y., Lei, G.-D., Sachtler, W. M. H., and Kung, H. H., *J. Catal.* **161**, 43 (1996).
3. Feng, X., and Hall, W. K., *Catal. Lett.* **41**, 45 (1996).
4. Feng, X., and Hall, W. K., *J. Catal.* **166**, 368 (1997).
5. Voskoboinikov, T. V., Chen, H. Y., and Sachtler, W. M. H., *Appl. Catal. B* **19**, 279 (1998).
6. Chen, H. Y., Voskoboinikov, T., and Sachtler, W. M. H., *J. Catal.* **180**, 171 (1998).
7. Chen, H. Y., Voskoboinikov, T., and Sachtler, W. M. H., *Catal. Today* **54**, 483 (1999).
8. Wang, X., Chen, H. Y., and Sachtler, W. M. H., *Appl. Catal. B* **26**, L227 (2000).
9. Li, Y., and Armor, J. N., *Appl. Catal. B* **3**, L1 (1993).
10. Li, Y., and Armor, J. N., *Appl. Catal. B* **2**, 239 (1993).
11. Maisuls, S. E., Seshan, K., Feast, S., and Lercher, J. A., *Appl. Catal. B* **29**, 69 (2001).
12. Witzel, F., Sill, G. A., and Hall, W. K., *J. Catal.* **149**, 229 (1994).
13. Kaucký, D., Vondrová, A., Dedecek, J., and Wichterlová, B., *J. Catal.* **194**, 318 (2000).
14. Li, Y., Battavio, P. J., and Armor, J. N., *J. Catal.* **142**, 561 (1993).
15. Corma, A., Palomares, A. E., and Fornes, V., *Res. Chem. Intermed.* **24**, 613 (1998).
16. Tabata, T., Kokitsu, M., Ohtsuka, H., Okada, O., Sabatino, L. M. F., and Bellussi, G., *Catal. Today* **27**, 91 (1996).

17. Shimizu, K. I., Maeshima, H., Satsuma, A., and Hattori, T., *Appl. Catal. B* **18**, 163 (1998).
18. Efthimiadis, E. A., Lionta, G. D., Christoforou, S. C., and Vasalos, I. A., *Catal. Today* **40**, 15 (1998).
19. Adelman, B. J., Beutel, T., Lei, G.-D., and Sachtler, W. M. H., *J. Catal.* **158**, 327 (1996).
20. Gaudin, C., Duprez, D., Mabilon, G., and Prigent, M., *J. Catal.* **160**, 10 (1996).
21. Cowan, A. D., Dumpelmann, R., and Cant, N. W., *J. Catal.* **151**, 356 (1995).
22. Ali, A., Alvarez, W., Loughran, C. J., and Resasco, D. E., *Appl. Catal. B* **14**, 13 (1997).
23. Lobree, L. J., Aylor, A. W., Reimer, J. A., and Bell, A. T., *J. Catal.* **181**, 189 (1999).
24. Misono, M., Hirao, Y., and Yokoyama, C., *Catal. Today* **38**, 157 (1997).
25. Nishizaka, Y., and Misono, M., *Chem. Lett.* 2237 (1994).
26. Xiao, F. S., Zheng, S., Sun, J., Yu, R., Qiu, S., and Xu, R., *J. Catal.* **176**, 474 (1998).
27. Xiao, F.-S., Zhang, W., Jia, M., Yu, Y., Fang Guoxingbatu, C., Zheng, S., Qiu, S., and Xu, R., *Catal. Today* **50**, 117 (1999).
28. Vergne, S., Berreghis, A., Tantet, J., Canaff, C., Magnoux, P., Guisnet, M., Davias, N., and Noiro, R., *Appl. Catal. B* **18**, 37 (1998).
29. Torre-Abreu, C., Ribeiro, M. F., Henriques, C., and Ribeiro, F. R., *Appl. Catal. B* **13**, 251 (1997).
30. Liese, T., and Grünert, W., *J. Catal.* **172**, 34 (1997).
31. Jentys, A., Kleestorfer, K., and Vinek, H., *Micropor. Mesopor. Mat.* **27**, 321 (1999).
32. Zholobenko, V. L., Makarova, M. A., and Dwyer, J., *J. Phys. Chem.* **97**, 5962 (1993).

33. Veefkind, V. A., Smidt, M. L., and Lercher, J. A., *Appl. Catal. A* **194-195**, 319 (2000).
34. Burch, R., and Hayes, M. J., *J. Mol. Catal. A* **100**, 13 (1995).
35. Nivarthi, G. S., Seshan, K., and Lercher, J. A., *Micropor. Mesopor. Mat.* **22**, 379 (1998).
36. Chen, H. Y., Wang, X., and Sachtler, W. M. H., *Appl. Catal. A* **194-195**, 159 (2000).
37. Stakheev, A. Y., Lee, C. W., Park, S. J., and Chong, P. J., *Catal. Lett.* **38**, 271 (1996).
38. Gutierrez, L., Boix, A., and Petunchi, J. A., *J. Catal.* **179**, 179 (1998).
39. Satsuma, A., Yamada, K., Mori, T., Niwa, M., Hattori, T., and Murakami, Y., *Catal. Lett.* **31**, 367 (1995).
40. d'Itri, J. L., and Sachtler, W. M. H., *Appl. Catal. B* **2**, L7 (1993).
41. Burch, R., and Ramli, A., *Appl. Catal. B* **15**, 63 (1998).
42. Garcia-Cortes, J. M., J., P.-R., Illan-Gomez, M. J., Kapteijn, F., Moulijn, J. A., and Salinas-Martinez de Lecea, C., *Appl. Catal. B* **30**, 399 (2001).
43. Xin, M., Hwang, I. C., and Woo, S. I., *Catal. Today* **38**, 187 (1997).
44. Aryafar, M., and Zaera, F., *Catal. Lett.* **48**, 173 (1997).

3. Structure-activity relations for Ni-containing zeolites during NO reduction Part 1 - Influence of acid sites

The influence of the zeolite structure on the catalytic properties for the reduction of NO with hydrocarbons was studied. A relation between the concentration and strength of acid sites and the activity of Ni-exchanged ZSM-5, MOR, and MCM-22 for the NO reduction with propane and propene was found. NiNaZSM-5, which contains a high concentration of strong acid sites, is the most active catalyst for the NO reduction with propane. NiNaZSM-5 and NiNaMCM-22 rapidly deactivate with propene as reductant due to the formation of carbonaceous deposits. The deposits block the pores. NiNaMOR is less affected by the deposits formed because of its large pore size and the relatively low concentration of strong Brønsted acid sites.

3.1. Introduction

Transition metal containing zeolites exhibit high activity and selectivity in the catalytic reduction of NO_x with hydrocarbons in oxidizing atmosphere. For copper-containing zeolites it is known that water inhibits the reaction and causes deactivation of the catalyst (1), while zeolites exchanged with other transition metals such as CoZSM-5 (2-5) and FeZSM-5 (6-10) remain active catalysts for the reduction of NO to N_2 also in the presence of H_2O or SO_2 . Ni, Pt and Pd supported on ZSM-5 (11), FER (3, 11), MOR (12, 13), BEA (14, 15) and MCM-22 (14) are also known to be effective catalysts for the reduction of NO with hydrocarbons.

In general, for transition metal containing zeolites the activity for the NO reduction depends on the type of metal and on the nature of the zeolite with respect to the strength and concentration of acid sites, pore dimensions and accessibility of acid sites. Corma *et al.* reported a similar activity of CuMFI and CuBEA with a CuO content higher than 6.5% for the reduction of NO with propane (16), while the activity of Cu-exchanged zeolites with a CuO content lower than 5.4% and of Co-exchanged zeolites decreases in the order MFI>BEA>MCM-22>Y and BEA>MFI>MCM-22, respectively (14). Li and Armor found that CoFER is more active than CoMFI for the reduction with methane (3). In the case of Fe containing zeolites, the activity for the reduction of NO with isobutane and propane decreases in the order FeBEA>FeMFI>>FeMOR \approx FeY (17).

Several authors suggest that the pore geometry is the main reason for the different activity of zeolite-based catalysts in NO reduction (17). Therefore, the difference in activity between the different zeolites should be more pronounced, when bulky hydrocarbons are used as reducing agents (11). The SCR activity of the zeolites with unidimensional channel systems is suggested to be limited by the low accessibility of the sites (17).

Brønsted acidity has been described to be essential for NO reduction with CH₄ over Pd/zeolites (18-21) and a synergetic effect of the acidic and metal sites has been proposed for the reduction of NO by propene over CuZSM-5 catalysts (22, 23). The formation of carbonaceous compounds, identified as reaction intermediates, has been attributed to the presence of acid sites (24). In modest contrast, some authors have reported that Brønsted acidity is not a prerequisite for catalytic activity in NO reduction with propene, although it may favor the reaction (25, 26). Others have suggested that Brønsted acid sites do not promote the selective reduction of NO by propene, because they contribute to coke formation, which suppresses the catalytic activity (27).

Influence of the pore geometry on the activity for the reduction of NO with propane and propene, has been studied over three zeolites (ZSM-5, MOR and MCM-22), with differing pore geometry and channel diameter, exchanged with the same concentration of Ni. The influence of the concentration and strength of acid sites and size of zeolite particles were related to the activity of the catalysts, while the effect of the metal will be discussed in detail in the second part of this study (28).

3.2. Experimental

3.2.1. Catalyst preparation

ZSM-5 (Si/Al = 15.6), mordenite (Si/Al=8.6) and MCM-22 (Si/Al = 16.4) were used. Mordenite in the sodium form was supplied by Tosoh, MCM-22 in the protonic form was supplied by Shell and ZSM-5 was synthesized in our laboratory according to ref. (29). MCM-22 and ZSM-5 were exchanged to the sodium form by liquid phase ion exchange with NaNO₃ solution at 50°C. The samples were

washed thoroughly with deionized water and dried over night in static air at 100°C. Ni was incorporated into the sodium form of the zeolites by liquid phase ion exchange carried out from an aqueous solution of Ni(NO₃)₂ at 80°C under continuous stirring for 24 h. Subsequently, the zeolite was separated from the ion exchange solution by centrifugation, washed thoroughly with deionized water and dried over night at 100°C.

3.2.2. Physicochemical characterization

The chemical composition of the samples was obtained by atomic absorption spectroscopy (AAS UNICAM 939). Crystal size of the zeolite samples was examined using a JEOL 500 Scanning Electron Microscope. The micro- and mesopore distributions were obtained on the basis of nitrogen adsorption measurements and the pore volume was calculated by using the t-plot method.

The concentration of acid sites was measured by temperature programmed desorption of NH₃ (NH₃-TPD). After activation of the sample (~ 80 mg) in vacuum at 600°C for 1 h, ammonia was adsorbed with a partial pressure of 1 mbar for 1 h at 150°C. Physisorbed ammonia was removed by evacuation ($p=10^{-3}$ mbar) of the sample at 150°C for 3 h. TPD was performed up to 750°C with a heating rate of 10°C/min. The molecules desorbing were monitored in the gas phase using a Balzer QMG 420 mass spectrometer. The type and strength of acid sites were determined by adsorption of pyridine and benzene followed by infrared spectroscopy, using a Bruker IFS-88 spectrometer equipped with a vacuum cell. Samples were pressed into self-supported wafers and activated at 600°C (increment 10°C/min) for 60 min. Infrared spectra of activated samples were recorded at 120 and 40°C. Pyridine was adsorbed at 120°C with a partial pressure of $1 \cdot 10^{-2}$ mbar, benzene was adsorbed at 40°C with a partial pressure of $1 \cdot 10^{-2}$ mbar.

3.2.3. Catalytic measurements

The catalytic activity of the samples was studied in a continuous flow system with a fixed bed quartz reactor of 4 mm inner diameter containing 0.1 g of catalyst (particle size of 300 μm). The reactant gas feed contained 1000 ppm of NO, 1000 ppm of C_3H_6 or C_3H_8 , 5% oxygen and He as the carrier gas. A total flow of 50 ml/min, resulting in a space velocity of 20000 h^{-1} , was used. The reaction products were analyzed by a chemiluminescence analyzer (TEI 42C) and a gas chromatograph (HP) equipped with a TCD detector using a molsieve column for separation of N_2 , O_2 and CO and a Porapak column for the analysis of N_2O , C_3H_6 , C_3H_8 and CO_2 . Before the reaction, the catalyst was pretreated *in situ* in helium flow at 600°C for 1 h. Kinetic measurements were carried out at temperature intervals of 25°C between 150 and 600°C.

3.3. Results

3.3.1. Physicochemical characterization

The composition of all samples studied is summarized in Table 3.1. The Na/Al ratio of approximately 1 for NaMOR and NaZSM-5 indicates that the samples were completely in the sodium form, while for NaMCM-22 with a Na/Al ratio of 0.7 a fraction of protons remained. All Ni containing samples had a Ni content of approximately 2 wt. %. The Si/Al ratio was not affected by the ion exchange with $\text{Ni}(\text{NO}_3)_2$ and increased in the order NiNaMOR < NiNaMCM-22 < NiNaZSM-5. Sodium was still present in NiNaMOR and NiNaZSM-5 after the ion exchange with Ni. The scanning electron micrographs of the three samples are shown in Fig. 3.1. NiNaMOR consisted of crystals with a size within the range 2-8 μm , while NiNaZSM-5 had homogeneous crystals of 3-4 μm size. NiNaMCM-22 consisted of

thin platelets of 1 μm size that formed agglomerates of approximately 15 μm . The surface area and pore volume of the Ni exchanged zeolites are summarized in Table 3.2. NiNaMOR had the largest micropore volume. The macro and mesopores surface volume is ascribed to the agglomeration of the primary zeolite particles.

Table 3.1 Chemical composition of Ni-exchanged samples

Sample	Si/Al ^a	Ni/Al ^a	Na/Al ^a	Ni loading [wt. %]
NaMOR	8.6	-	1.1	-
NaZSM-5	15.6	-	1.1	-
NaMCM-22	12.6	-	0.7	-
NiNaMOR	8.9	0.2	0.6	1.9
NiNaZSM-5	16.4	0.4	0.3	2.0
NiNaMCM-22	12.3	0.2	0.0	1.8

^a molar ratio

Table 3.3 summarizes the acidic properties of the samples. The acid site concentration determined by NH_3 -TPD was higher for NiNaMCM-22 and NiNaZSM-5 than for NiNaMOR. The composition of the unit cell of each sample was calculated from the elemental analysis. Table 3.4 summarizes the distribution of cations on the exchange positions for the three Ni-exchanged zeolites. The concentration of exchangeable sites and their occupation by Na^+ and the total Ni content were calculated from the elemental composition. The concentration of ion exchange sites occupied by $\text{H}^+/\text{[Ni(OH)]}^+$ was calculated from the concentration of acid sites determined by NH_3 -TPD. For NiNaZSM-5, the latter was corrected by

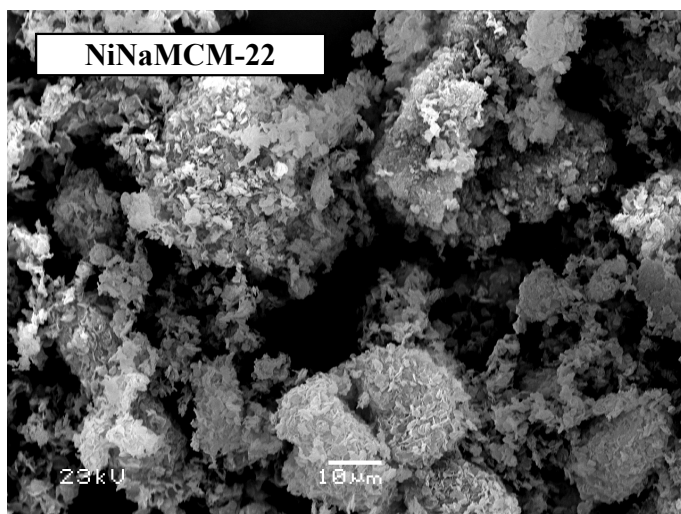
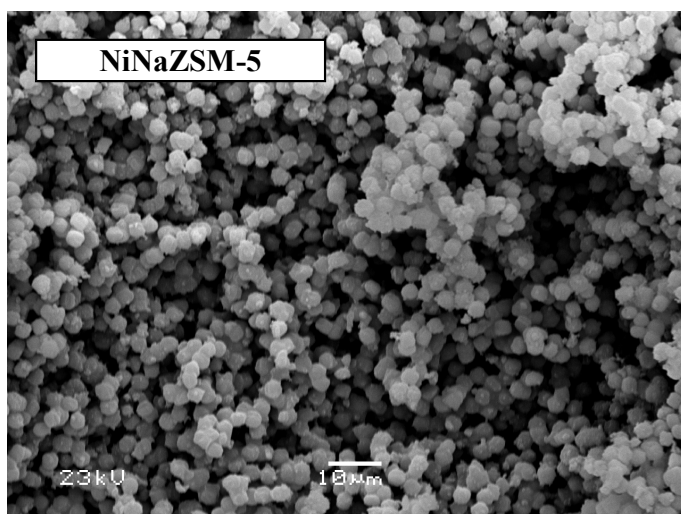
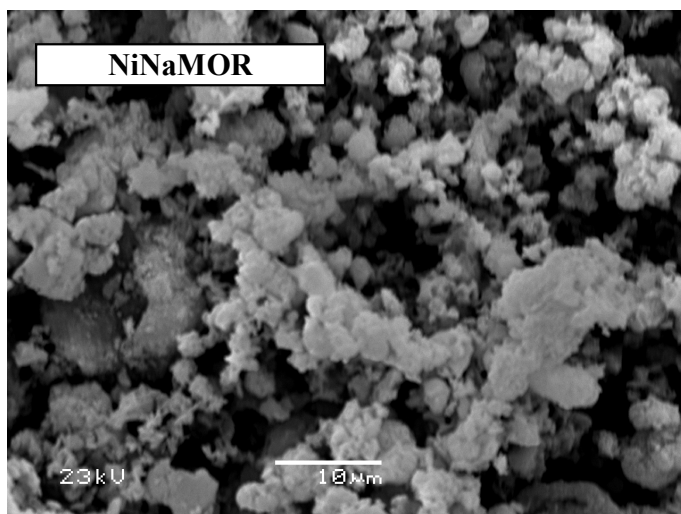


Figure 3.1 Scanning electron micrographs of Ni-exchanged zeolites.

Table 3.2 Textural properties of Ni-exchanged samples

Sample	Micropore surface area [m ² /g]	Macro and mesopore surface area [m ² /g]	Micropore volume [cm ³ /g]
NiNaMOR	267	106	0.104
NiNaZSM-5	227	101	0.087
NiNaMCM-22	214	233	0.066

Table 3.3 Acid site concentration determined by NH₃-TPD and ratio between Brønsted and Lewis acid sites determined by infrared spectroscopy of pyridine adsorption at 120°C and 1*10⁻² mbar

Sample	Acid site concentration [mmol/g]	Brønsted / Lewis ratio
NiNaMOR	0.4	0.4
NiNaZSM-5	0.7	0.2
NiNaMCM-22	0.8	0.3

the concentration of acid sites determined by NH₃-TPD for NaZSM-5. The sites occupied by Ni²⁺ were calculated from the difference of the total exchangeable sites and the sites occupied by Na⁺ and acid sites. Note that the calculated number of sites occupied by Ni²⁺ and the total concentration of Ni was identical for NiNaMOR and NiNaMCM-22, indicating that most of the [Ni(OH)]⁺ groups were not detected by NH₃-TPD at 150°C due to their weakly acidic character (30). We found previously that the amount of acid sites quantified by NH₃-TPD depends on

the temperature at which the adsorption and outgassing of NH_3 was done. The amount is larger when the adsorption temperature is lower and this is associated with the fact that H^+ and $[\text{Ni}(\text{OH})]^+$ have different strength, the former representing stronger acid sites. At 150°C , for NiNaMOR mainly H^+ could be quantified by NH_3 -TPD, while $[\text{Ni}(\text{OH})]^+$ was only partly detected (30). For NiNaZSM-5 the calculated number of exchangeable sites occupied by Ni^{2+} is lower than the total Ni experimentally determined. This points to the idea that the missing Ni in the calculated number of exchangeable sites occupied by Ni^{2+} was quantified as $[\text{Ni}(\text{OH})]^+$ and this implies that these acid sites are stronger than the corresponding ones in NiNaMOR and NiNaMCM-22. This difference might be related to the unequal location of Ni inside the structure of the three zeolites.

Table 3.4 Distribution of exchangeable sites of Ni-exchanged zeolites

Sample	Exchangeable sites [mmol/g]	Sites occupied by Na^+ [mmol/g]	Sites occupied by $\text{H}^+ / [\text{Ni}(\text{OH})]^+$ [mmol/g]	Sites occupied by Ni^{2+} [mmol/g]	Total Ni [mmol/g]
NiNaMOR	1.7	1.0	0.4	0.3	0.3
NiNaZSM-5	1.0	0.2	0.6	0.2	0.3
NiNaMCM-22	1.1	0.0	0.8	0.3	0.3

The infrared spectra after adsorption of pyridine at a partial pressure of $1 \cdot 10^{-2}$ mbar are shown in Fig. 3.2. The infrared band at 1545 cm^{-1} , assigned to pyridinium ions is characteristic for sorption on strong Brønsted acid sites, while Lewis acid sites are identified by the band at 1451 cm^{-1} , resulting from coordinately bound pyridine (31). The infrared spectra of NiNaMOR and NiNaZSM-5 showed a shoulder at 1443 cm^{-1} , which is assigned to pyridine sorbed on Na^+ cations (31-35). The complete disappearance of the bridged hydroxyls band ($\sim 3605 \text{ cm}^{-1}$) was

observed after the adsorption of pyridine on NiNaZSM-5 and NiNaMCM-22, while on NiNaMOR the area of the band decreased 88% (spectra not shown). This indicates that pyridine molecules enter all channels of ZSM-5 and MCM-22 and can reach all bridging hydroxyl groups present. For NiNaMOR only 88% of the bridged hydroxyl groups were found to interact with pyridine, while 12% of the bridging hydroxyl groups present in this material cannot be accessed by pyridine molecules. Following ref. (36) to evaluate the ratio of Brønsted acid sites located in the main channels and side pockets, the adsorption of n-hexane on the protonic form of mordenite (HMOR) was followed by infrared spectroscopy (not shown). 30% of the bridging hydroxyl groups were found not to be accessible to n-hexane and are, therefore, concluded to be located in the side pockets of H-MOR.

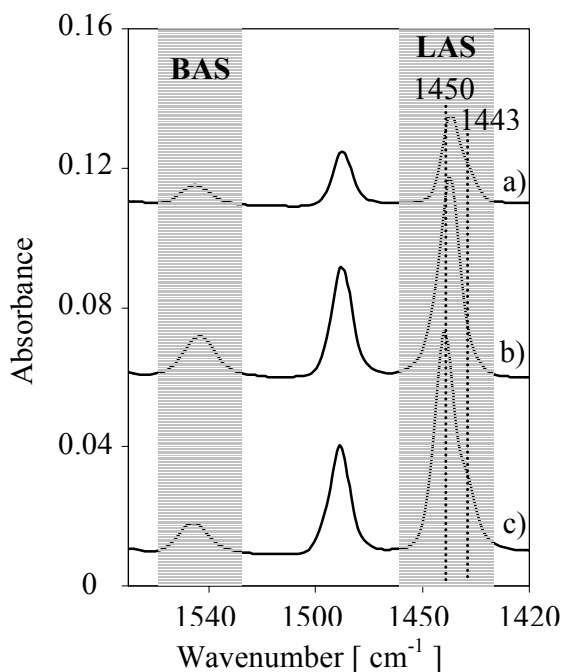


Figure 3.2 Infrared spectra of pyridine adsorption on a) NiNaMOR, b) NiNaMCM-22 and c) NiNaZSM-5. $T = 120^{\circ}\text{C}$, $p = 1 \cdot 10^{-2}$ mbar.

Table 3.3 summarizes the ratio between Brønsted and Lewis acid sites for the three samples determined by pyridine adsorption using the bands at 1544 cm^{-1} and 1450 cm^{-1} and the molar extinction coefficients reported by Emeis (37). In general,

the concentration of Lewis acid sites was higher than that of the Brønsted acid sites and the ratio followed the order: NiNaMOR>NiNaMCM22>NiNaZSM-5.

During adsorption of benzene the hydrogen bonding interaction causes a shift of the OH-stretching vibration of the Brønsted acid sites (framework bridging Si-OH-Al) to a lower frequency. The shifts in the frequency upon the adsorption of benzene on the three nickel samples are summarized in Fig. 3.3. The spectra shown were obtained from the subtraction of the spectra after benzene adsorption at $1 \cdot 10^{-2}$ mbar from the spectra of the activated samples. The shift can be directly correlated to the strength of the acid sites (38-41). The highest shift was observed for ZSM-5 ($\Delta\nu_{\text{OH}} = 342 \text{ cm}^{-1}$) followed closely by MOR ($\Delta\nu_{\text{OH}} = 335 \text{ cm}^{-1}$), while MCM-22 had the lowest shift ($\Delta\nu_{\text{OH}} = 295 \text{ cm}^{-1}$). In a recent paper Onida *et al.* have shown that the strength of H-bonding is under estimated when secondary interactions of the probe molecule with the surrounding walls take place (42). This occurs when relatively bulky molecules, like benzene, are used as probe molecules. They quantified the deviations as 17% and 27% for the shift of the OH stretching vibration when benzene was adsorbed on ZSM-5 and MCM-22, respectively. These deviations were employed to correct the $\Delta\nu_{\text{OH}}$ measured in the present work during benzene adsorption. New values of 400 cm^{-1} and 375 cm^{-1} were obtained for ZSM-5 and MCM-22, respectively. No deviation factor was reported for the adsorption of benzene on MOR. However, from the shift caused in the OH stretching vibration by propene adsorption, the similarity of the acid strength of the Brønsted acid sites in MOR and ZSM-5 has been reported (43). Therefore, we consider that the order of ZSM-5 \approx MOR>MCM-22, that we initially obtained for the strength of the acid sites is still valid and will be used for the interpretation of the difference in activities observed for the reduction of NO with hydrocarbons.

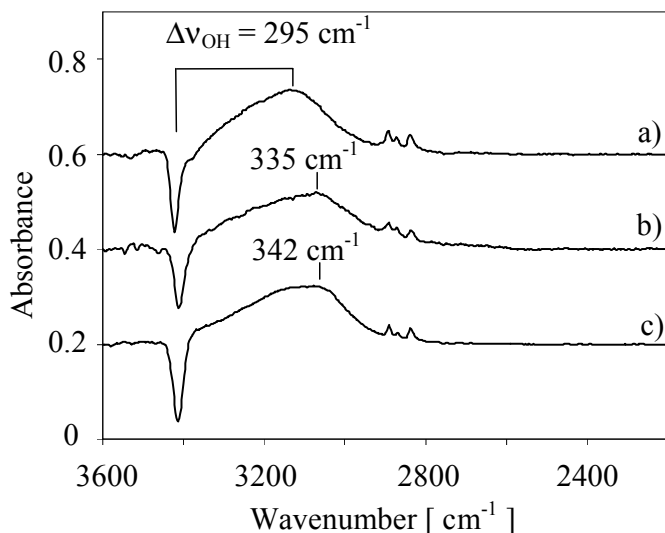


Figure 3.3 Infrared spectra of benzene adsorption on a). HMCM-22, b) HMOR and c) HZSM-5, $T = 40^{\circ}\text{C}$, $p = 1 \cdot 10^{-2}$ mbar.

The formation of oligomeric species was studied by temperature programmed desorption of propane and propene. Fig. 3.4A shows the comparison of the desorption peak of propane ($m/e = 29$) for the three zeolites. The intensity of the main desorption peak at $\sim 120^{\circ}\text{C}$ followed the order NiNaZSM-5 > NiNaMOR > NiNaMCM-22. In addition to propane, species with fragments in the range 49-52, 77, 78 and 79, among others, were observed. Desorption peaks corresponding to the mass 50 are shown in Fig. 3.4B. For NiNaMCM-22 this species desorbed at three different temperatures, one of them being as high as 720°C , for NiNaZSM-5 two desorption peaks at 150 and 430°C were observed, while for NiNaMOR only one desorption peak at 150°C was present. The intensities of these signals were 2 orders of magnitude lower than the signal of the main fragments of propane. Compounds associated to these masses are cyclic and partially aromatic intermediates, such as benzene and cyclohexadiene, which suggests that oligomerization and dehydrocyclization reactions of propane occurred at the catalyst surface.

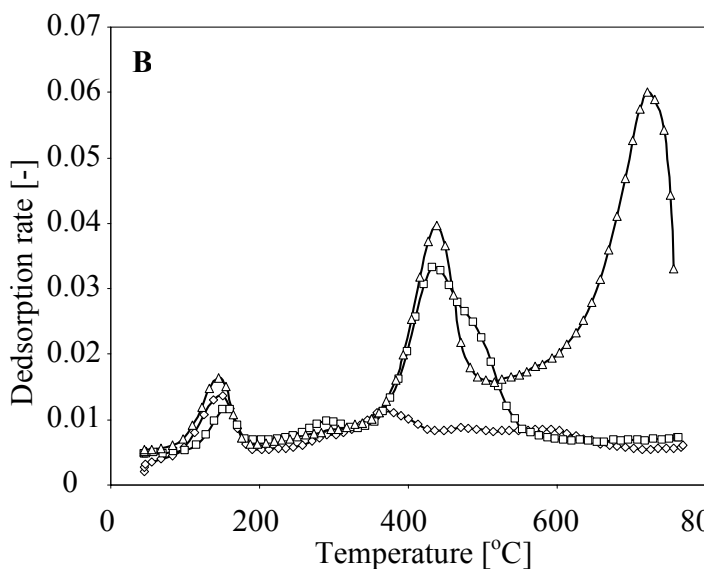
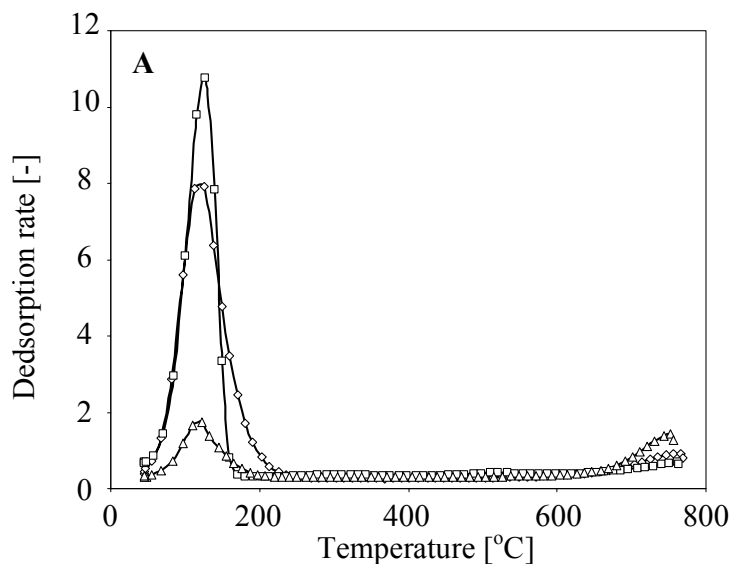


Figure 3.4 Temperature programmed desorption of propane adsorbed at 50°C of NiNaMOR (—◇—), NiNaZSM-5 (—□—), NiNaMCM-22 (—△—). A) $m/e = 29$, B) $m/e = 50$.

Similarly to propane, oligomeric species were observed during propene desorption from the three catalysts (experiment not shown). The signal of the oligomeric species is only one order of magnitude lower than the signal of the main fragments, indicating that the amount of oligomeric and cyclic species formed from the desorption of propene is higher than for propane. From the comparison of the temperatures of the peaks in the desorption curves, it was concluded that more

strongly adsorbed species are formed with NiNaZSM-5 and NiNaMCM-22 than with NiNaMOR.

3.3.2. Kinetic measurements

3.3.2.1 *Reduction of NO with propane*

The conversions of NO to N₂ with propane obtained for the nickel-exchanged zeolites are shown in Fig. 3.5. The maximum NO conversion and the temperature of maximum NO conversion followed the order NiNaZSM-5 > NiNaMOR > NiNaMCM-22. In general the NO conversion started at lower temperatures compared to the propane conversion. The ratio of N₂ molecules formed to propane molecules converted, used to assess the efficiency of the reducing agent, is shown in Fig. 3.6. A ratio of approximately 1 was observed at temperatures below 375°C. It decreased to 0.2 at higher temperatures indicating that at low temperatures one molecule of propane reduced selectively two NO molecules, while at higher temperatures the direct oxidation of the hydrocarbon dominated. According to Fig. 3.5, the sharp decrease in the N₂/C₃H₈ ratio corresponds to C₃H₈ conversion of above 10%. The slope of the curves is the same for the three samples at higher temperatures indicating a similar efficiency of C₃H₈ for the three catalysts.

The selectivities of the nitrogen-containing products of the three catalysts are compared in Fig. 3.7. The distribution of products was similar for the three catalysts. N₂ was the main product of the NO reduction, at temperatures above 400°C, selectivities to N₂ were higher than 95%. At temperatures below 350°C, small amounts of NO₂ were formed over the three catalysts. Selectivity to N₂ increased with increasing temperature, while selectivity to NO₂ decreased. Only at low temperatures the formation of small amounts of N₂O was observed.

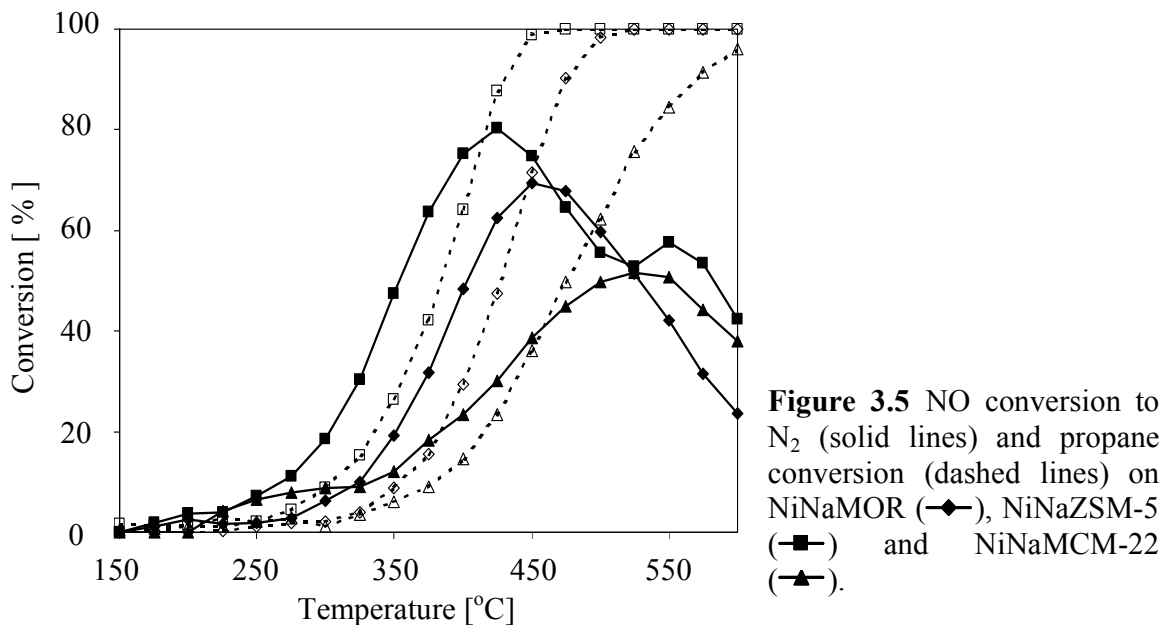
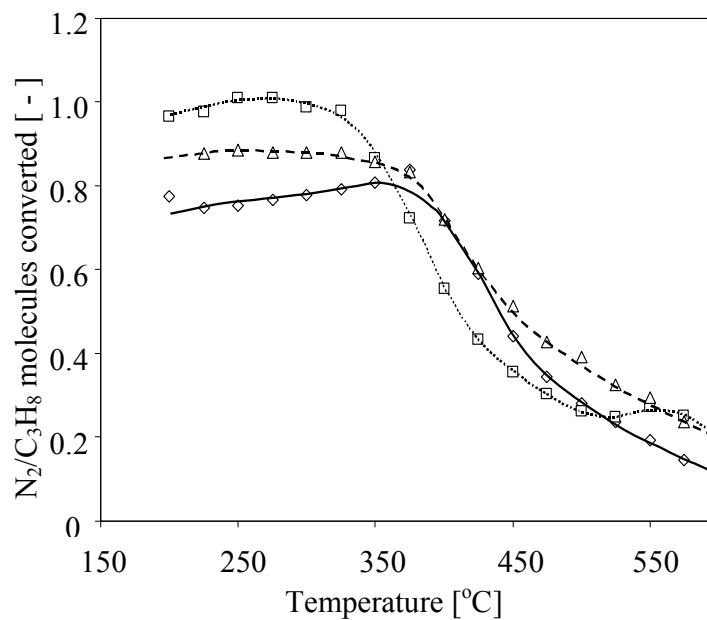


Figure 3.6 Ratio between N_2 formed and C_3H_8 on NiNaMOR (\blacklozenge), NiNaZSM-5 (\square), NiNaMCM-22 (\blacktriangle) during the reduction of NO with propane.



3.3.2.2 Reduction of NO with propene

Fig. 3.8 compares the NO and propene conversions during the reduction of NO with propene. The activities of NiNaZSM-5 and NiNaMCM-22 were significantly

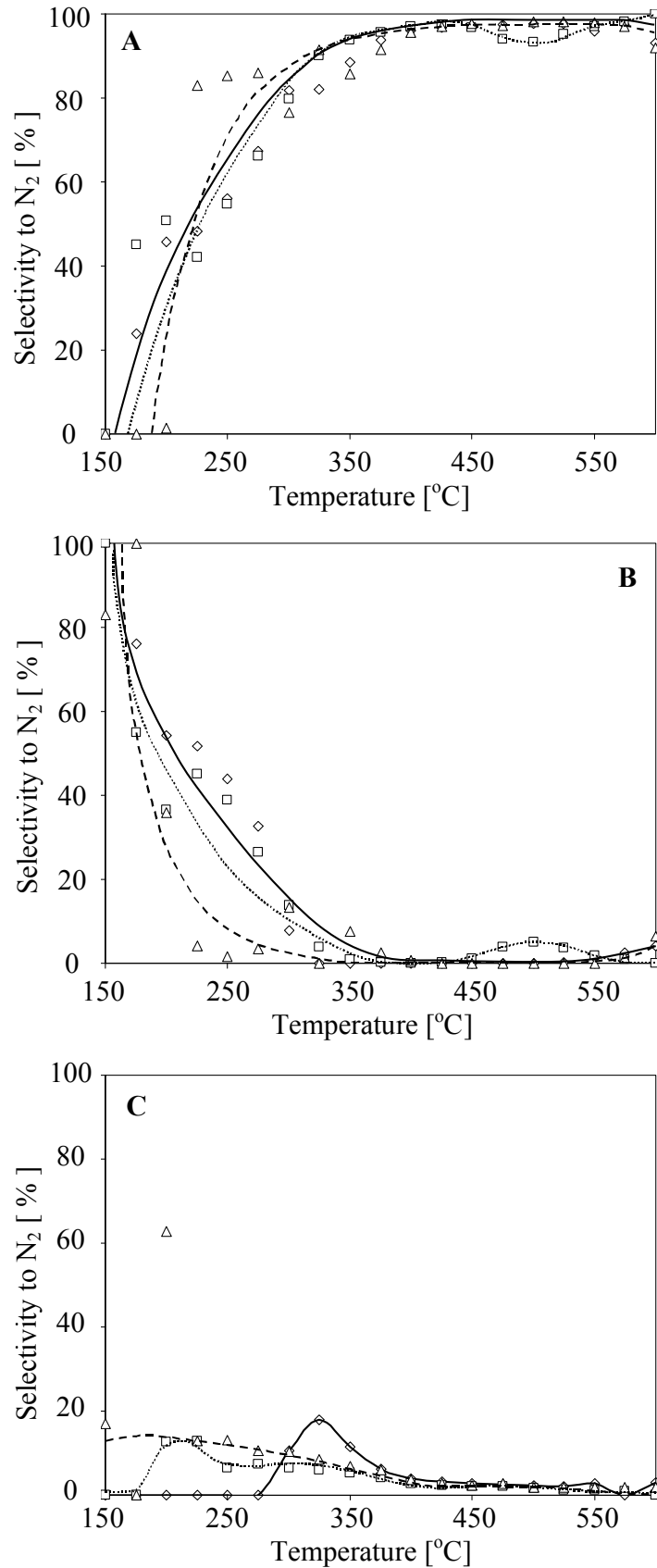


Figure 3.7 Selectivities to A) N₂, B) NO₂, C) N₂O during the reduction of NO with propane on NiNaMOR (—◇—), NiNaZSM-5 (---□---), NiNaMCM-22 (-△-).

lower for the reduction of NO with propene compared to propane. NiNaMOR was found to be the most active catalyst, with a NO conversion to N_2 of 72% at 400°C. The conversion of propene started increasing almost in parallel to the conversion of NO for NiNaMOR, while for NiNaZSM-5 and NiNaMCM-22, 100% conversion of propene was reached at temperatures below the maximum NO conversion. In general, propene was less efficient for the reduction of NO than propane. The ratio between N_2 molecules formed and propene molecules converted indicated that for NiNaMOR two molecules of propene are required to reduce one molecule of NO at temperatures below the maximum NO conversion (400°C) and even lower ratios were obtained for NiNaZSM-5 and NiNaMCM-22.

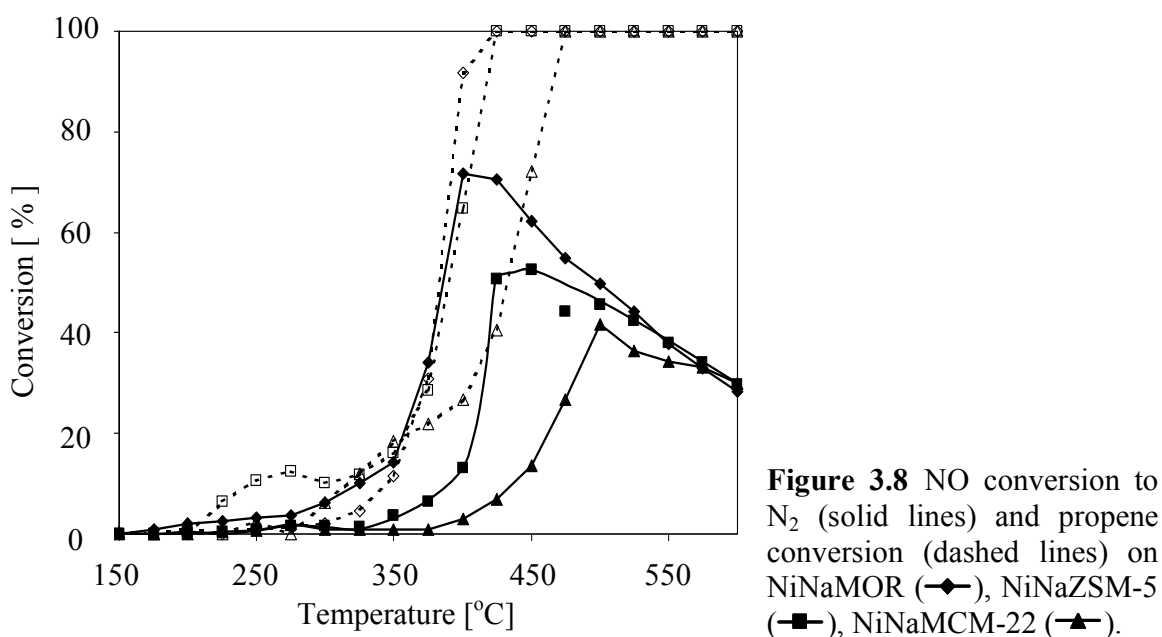


Fig. 3.9 shows the selectivities of the nitrogen products during the reduction of NO with propene. At temperatures above 250°C, N_2 was the main product. At lower temperatures, more N_2O was formed over NiNaZSM-5 and NiNaMOR than in the case of propane. For propene, NO_2 was formed only at high temperatures when propene was directly oxidized, in contrast to the reduction of NO with

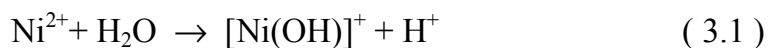
propane, where NO₂ is formed at low temperatures. Higher amounts of N₂O were observed in the case of NiNaMCM-22, in comparison with NiNaZSM-5 and NiNaMOR.

3.4. Discussion

3.4.1. Acid sites

The catalytic activity for the reduction of NO with propane and propene of Ni-exchanged zeolites was found to depend on the structure and acidity of the zeolites. From the three materials studied NiNaZSM-5 is the most active for the reduction of NO with propane, followed by NiNaMOR and NiNaMCM-22. For the reduction of NO with propene, NiNaMOR was the most active catalysts followed by NiNaZSM-5 and NiNaMCM-22. The NO conversion with propene was significantly lower compared to propane for NiNaZSM-5 and NiNaMCM-22. Note that the activity for the reduction of NO with propane and propene of NiNaMOR catalysts has been found to depend on the acid site concentration (30). For the same type of material a balanced concentration of acid sites is necessary to obtain high NO conversion with propane, while a low acid site concentration enhances the activity for the reduction of NO with propene (30).

During ion exchange of Na⁺ with Ni²⁺ Brønsted acid sites were formed by hydrolysis according to Eq. 3.1.



Therefore, the concentration of acid sites is primarily determined by the Ni content. Since the Ni-exchanged zeolites studied here had the same Ni content a similar acid site concentration was expected. However, acid site concentration of NiNaMCM-22 and NiNaZSM-5 determined by NH₃-TPD was higher than that of

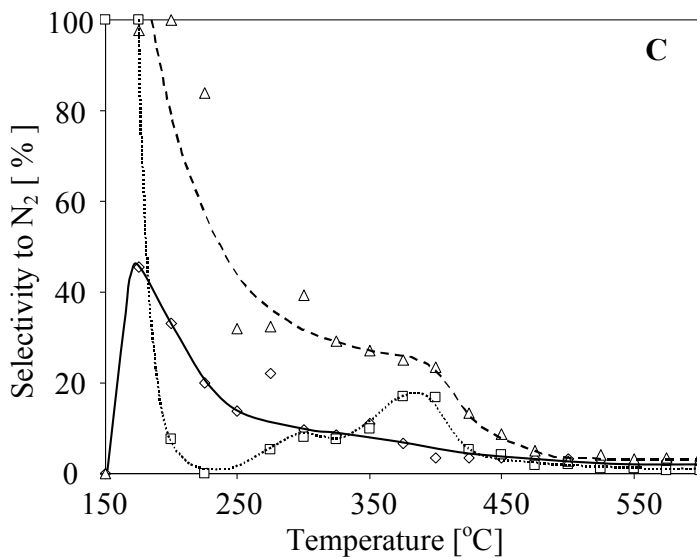
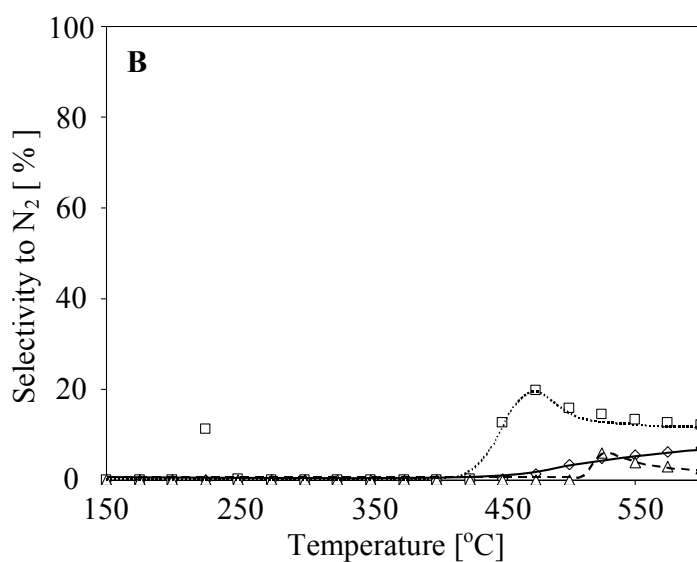
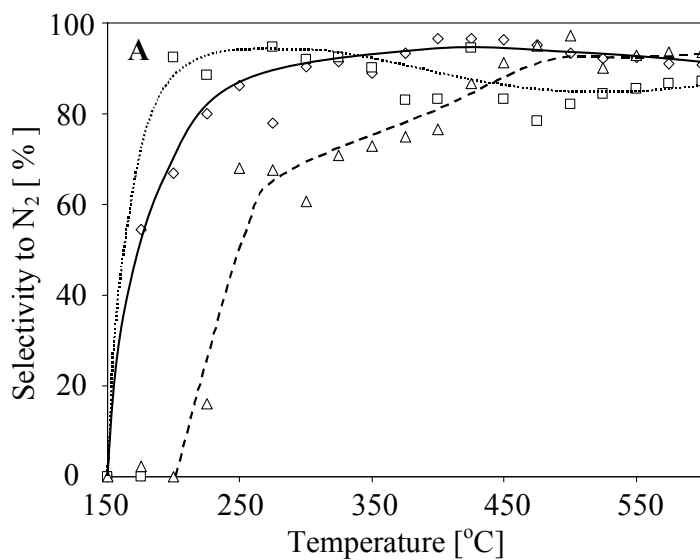


Figure 3.9 Selectivities to A) N₂, B) NO₂, C) N₂O during the reduction of NO with propene on NiNaMOR (—◇—), NiNaZSM-5 (··□··), NiNaMCM-22 (—△—).

NiNaMOR. Note that NiNaMCM-22 contained an additional fraction of acid sites already present in the parent material. The slightly higher concentration of acid sites in NiNaZSM-5 is tentatively attributed to the stronger acidic character of the $[\text{Ni}(\text{OH})]^+$ groups present in this material in comparison to NiNaMOR and NiNaMCM-22. This was observed from the comparison of the calculated exchangeable sites occupied by Ni^{2+} and the total concentration of Ni determined by elemental analysis (see Table 3.4), for NiNaZSM-5 the former being lower than the latter. The exchangeable sites occupied by Ni^{2+} were calculated from the difference of the total exchangeable sites and the sites occupied by Na^+ and acid sites. The latter was determined by NH_3 -TPD and quantified according to the strength of the acid sites not only H^+ but $[\text{Ni}(\text{OH})]^+$ also. For NiNaZSM-5, the missing sites occupied by Ni^{2+} might have been quantified as $[\text{Ni}(\text{OH})]^+$ implying a stronger acid character of these species in comparison with the corresponding ones of NiNaMOR and NiNaMCM-22. The difference in the strength of the acid sites can be attributed to the location of Ni on the ion exchange sites in the structure of the three zeolites.

All Brønsted acid sites on NiNaZSM-5 and NiNaMCM-22 were accessible for pyridine, while on NiNaMOR 12% of the Brønsted acid sites could not be accessed by pyridine. The dimensions of the 10-member-ring channel systems are $5.3 \times 5.6 \text{ \AA}$ and $5.1 \times 5.5 \text{ \AA}$ for ZSM-5 and $4.0 \times 5.9 \text{ \AA}$ and $4.0 \times 5.4 \text{ \AA}$ for MCM-22. MOR possesses, in addition to the 12-member-ring channels ($6.5 \times 7.0 \text{ \AA}$), 8-member-ring side pockets of smaller dimensions ($2.6 \times 5.0 \text{ \AA}$). The acid sites not accessible by pyridine in NiNaMOR are located in the side pockets. Since Brønsted acid sites were the result of the hydrolysis after ion exchange, we assume that Ni^{2+} ions are in close proximity to the acid sites. Therefore, a small fraction of Ni, similar to that of the acid sites, should be located in the side pockets of the zeolite.

Conceptually, the strength of acid sites is determined by the Si/Al ratio and influenced by the confinement related to the location of the OH groups inside the

pores, channels and cages of the zeolites (38, 44). The shift of the stretching vibration of the OH groups to lower frequencies during the adsorption of benzene indicates that the Brønsted acid sites on ZSM-5 and MOR were stronger acidic than those of MCM-22.

3.4.2. Catalytic activity

The activity of the samples for the reduction of NO with propane followed the same order than the strength of the acid sites. This indicates that the rate-limiting step during the reduction of NO with propane is primarily related to the strength of the acid sites, and apparently determines the activity of the catalyst.

The concentration of acid sites in NiNaMOR is, however, lower than in NiNaZSM-5, while the strength of the acid sites is similar for both samples. Therefore, the activity for the reduction of NO with propane for NiNaMOR is slightly lower than that of NiNaZSM-5.

Small amounts of NO₂ were observed at low temperatures, during the reduction of NO with propane, while at the temperature of the maximum NO conversion NO₂ was completely absent on all three catalysts. It has been proposed that the reaction occurs *via* NO oxidation (17). Nitrites and nitrates formed from the oxidation of NO (45, 46) react with hydrocarbons forming a nitrogen-containing carbonaceous deposit on the catalyst, which further reacts to N₂ (9, 17, 47). Thus, the presence of NO₂ in the gas phase at the outlet of the reactor indicates that the activation of propane is the rate-limiting step at low temperatures (10). In contrast, for propene NO₂ was present only at high temperatures, when the reducing agent was directly oxidized. This model is supported by the general concept that olefins are more easily activated on acid sites than alkanes, due to the presence of the C=C double bonds, which facilitates the formation of carbenium ions (48).

The activation of propane might lead to the formation of propene by dehydrogenation of propane molecules on the Ni²⁺ ions shown to act as Lewis acid

sites (49, 50). The same extent of propane dehydrogenation is expected to occur on the three catalysts since the loading of Ni is similar. The activation of the olefin formed takes also place on the acid sites. In contrast with the reduction of NO with propene, the amount of olefin is limited during NO reduction with propane and reacts more efficiently with the adsorbed nitrites and nitrates to form N₂. We concluded from the catalytic results obtained during the NO reduction with propene that the reaction was not limited by the concentration of acid sites. Therefore, the strength of the acid sites itself plays an important role for the activation of propene formed by propane dehydrogenation during the reduction of NO with propane.

Oligomerization reactions took place during the desorption of propane and propene from the Ni exchanged samples, occurring to a higher extent for propene than for propane due to its olefinic nature. The extent of oligomerization follows the order NiNaMCM-22 > NiNaZSM-5 >> NiNaMOR, which is identical to the order observed for the concentration of acid sites indicating that a higher concentration of acid sites favors the oligomerization of the hydrocarbons. Carbonaceous deposits blocking the active sites (10, 24, 27, 51) might also be formed. In addition, more strongly adsorbed oligomeric species were obtained for the materials with higher acid site concentration, e.g., NiNaZSM-5 and NiNaMCM-22.

For the NO reduction with propene the activity followed the order NiNaMOR > NiNaZSM-5 > NiNaMCM-22. In contrast to the reduction of NO with propane a strong inverse correlation of the activity for the NO reduction with propene with the concentration of acid sites is deduced from the characterization and the catalytic results. NiNaMOR, which contains the lowest concentration of acid sites was the most active for the reduction of NO with propene, while NiNaMCM-22 having the highest concentration of acid sites of the three materials, was the least active. The difference in activity of the three catalysts for the reduction of NO with

propene is attributed to the formation of carbonaceous species that deposit on the materials. NiNaZSM-5 and NiNaMCM22 with higher concentration of acid sites and smaller pore size are more affected than NiNaMOR.

The Brønsted acid sites are only located in the micropores of the zeolite. The macro and mesopore surface corresponds to the intra-particle void space formed by the agglomeration of particles in the material. The maximum N_2 yield for the reduction of NO with propane and propene are plotted against the micropore volume in Fig. 3.10. No relation was found between the N_2 yield for the reduction of NO with propane and the micropore volume, while a linear correlation was found between the maximum N_2 yield obtained from the reduction of NO with propene and the micropore volume. This indicates that for propene the limitation in the activity of the catalysts is related to the blocking of pores.

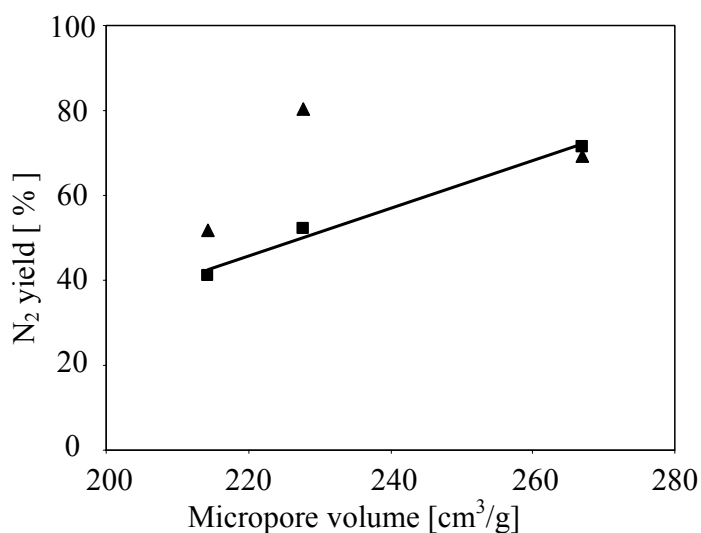


Figure 3.10 Relation between N_2 yield during the NO reduction with propene (■) and propane (▲) and micropore volume.

3.5. Conclusions

NiNaZSM-5 was found to be the most active catalyst for the reduction of NO with propane compared to NiNaMOR and NiNaMCM-22. The higher activity of NiNaZSM-5 is related to the high concentration and strength of the acid sites present in the material. At low temperatures, the rate-limiting step appears to be

related to the activation of the alkane associated to the formation of olefins by dehydrogenation on the Ni²⁺ ions. The activation of propene formed in this way is promoted by the presence of strong acid sites.

Oligomerization of hydrocarbons related to the formation of carbonaceous deposits occurs on the three materials, being more severe in the case of propene. A high concentration of acid sites promotes the formation of carbonaceous deposits, which led to a partial blocking of the pores. NiNaMOR, the material with the largest pore diameter and the largest micropore volume experiences the least severe deactivation resulting from the largest pore volume and the lowest concentration of acid sites, and it is, therefore, the most active among the three catalysts for the reduction of NO with propene.

References

1. Traa, Y., Burger, B., and Weitkamp, J., *Micropor. Mesopor. Mat.* **30**, 3 (1999).
2. Wang, X., Chen, H. Y., and Sachtler, W. M. H., *Appl. Catal. B* **26**, L227 (2000).
3. Li, Y., and Armor, J. N., *Appl. Catal. B* **3**, L1 (1993).
4. Li, Y., and Armor, J. N., *Appl. Catal. B* **2**, 239 (1993).
5. Maisuls, S. E., Seshan, K., Feast, S., and Lercher, J. A., *Appl. Catal. B* **29**, 69 (2001).
6. Feng, X., and Hall, W. K., *Catal. Lett.* **41**, 45 (1996).
7. Feng, X., and Hall, W. K., *J. Catal.* **166**, 368 (1997).
8. Voskoboinikov, T. V., Chen, H. Y., and Sachtler, W. M. H., *Appl. Catal. B* **19**, 279 (1998).
9. Chen, H. Y., Voskoboinikov, T., and Sachtler, W. M. H., *J. Catal.* **180**, 171 (1998).

10. Chen, H. Y., Voskoboinikov, T., and Sachtler, W. M. H., *Catal. Today* **54**, 483 (1999).
11. Witzel, F., Sill, G. A., and Hall, W. K., *J. Catal.* **149**, 229 (1994).
12. Kaucký, D., Vondrová, A., Dedecek, J., and Wichterlová, B., *J. Catal.* **194**, 318 (2000).
13. Li, Y., Battavio, P. J., and Armor, J. N., *J. Catal.* **142**, 561 (1993).
14. Corma, A., Palomares, A. E., and Fornes, V., *Res. Chem. Intermed.* **24**, 613 (1998).
15. Tabata, T., Kokitsu, M., Ohtsuka, H., Okada, O., Sabatino, L. M. F., and Bellussi, G., *Catal. Today* **27**, 91 (1996).
16. Corma, A., Fornes, V., and Palomares, E., *Appl. Catal. B* **11**, 233 (1997).
17. Chen, H. Y., Wang, X., and Sachtler, W. M. H., *Appl. Catal. A* **194-195**, 159 (2000).
18. Ali, A., Alvarez, W., Loughran, C. J., and Resasco, D. E., *Appl. Catal. B* **14**, 13 (1997).
19. Lobree, L. J., Aylor, A. W., Reimer, J. A., and Bell, A. T., *J. Catal.* **181**, 189 (1999).
20. Misono, M., Hirao, Y., and Yokoyama, C., *Catal. Today* **38**, 157 (1997).
21. Nishizaka, Y., and Misono, M., *Chem. Lett.* 2237 (1994).
22. Xiao, F. S., Zheng, S., Sun, J., Yu, R., Qiu, S., and Xu, R., *J. Catal.* **176**, 474 (1998).
23. Xiao, F.-S., Zhang, W., Jia, M., Yu, Y., Fang Guoxingbatu, C., Zheng, S., Qiu, S., and Xu, R., *Catal. Today* **50**, 117 (1999).
24. Vergne, S., Berreghis, A., Tantet, J., Canaff, C., Magnoux, P., Guisnet, M., Davias, N., and Noirot, R., *Appl. Catal. B* **18**, 37 (1998).
25. Ma, A. Z., Muhler, M., and Grünert, W., *Appl. Catal. B* **27**, 37 (2000).
26. Liese, T., and Grünert, W., *J. Catal.* **172**, 34 (1997).

27. Torre-Abreu, C., Ribeiro, M. F., Henriques, C., and Ribeiro, F. R., *Appl. Catal. B* **13**, 251 (1997).
28. Chapter 4 of this thesis.
29. Robson, H., "Verified syntheses of zeolitic materials", (Second Revised Edition ed.), p. 266. Elsevier Science B.V., Amsterdam, 2001.
30. Chapter 2 of this thesis.
31. Ward, J. W., *J. Catal.* **22**, 237 (1971).
32. Jentys, A., Kleestorfer, K., and Vinek, H., *Micropor. Mesopor. Mat.* **27**, 321 (1999).
33. Auroux, A., and Datka, J., *Appl. Catal. A* **165**, 473 (1997).
34. Li, Y. G., Xie, W. H., and Yong, S., *Appl. Catal. A* **150**, 231 (1997).
35. Yamada, K., Kondo, S., and Segawa, K., *Micropor. Mesopor. Mat.* **35-36**, 227 (2000).
36. Eder, F., Stockenhuber, M., and Lercher, J. A., *J. Phys. Chem. B* **101**, 5414 (1997).
37. Emeis, C. A., *J. Catal.* **141**, 347 (1993).
38. Juamain, D., and Su, B. L., *Catal. Today* **73**, 187 (2002).
39. Su, B. L., and Norberg, V., *Zeolites* **19**, 65 (1997).
40. Su, B. L., and Norberg, V., *Langmuir* **14**, 7410 (1998).
41. Jentys, A., and Lercher, J. A., *Stud. Surf. Sci. Catal.* **46**, 585 (1989).
42. Onida, B., Bonelli, B., Borello, S., Fiorilli, S., Geobaldo, F., and Garrone, E., *Stud. Surf. Sci. Catal.* **142**, 143 (2002).
43. Geobaldo, F., Spoto, G., Bordiga, S., Lamberti, C., and Zecchina, A., *J. Chem. Soc., Faraday Trans.* **93**, 1243 (1997).
44. Hunger, B., Heuchel, M., Clark, L. A., and Snurr, R. Q., *J. Phys. Chem. B* **106**, 3882 (2002).
45. Adelman, B. J., Beutel, T., Lei, G.-D., and Sachtler, W. M. H., *J. Catal.* **158**, 327 (1996).

46. Campa, M. C., Pietrogiacomini, D., Tuti, S., Ferraris, G., and Indovina, V., *Appl. Catal. B* **18**, 151 (1998).
47. Gaudin, C., Duprez, D., Mabilon, G., and Prigent, M., *J. Catal.* **160**, 10 (1996).
48. Nivarthi, G. S., Seshan, K., and Lercher, J. A., *Micropor. Mesopor. Mat.* **22**, 379 (1998).
49. Hoang, D. L., Berndt, H., Miessner, H., Schreier, E., Volter, J., and Lieske, H., *Appl. Catal. A* **114**, 295 (1994).
50. Kanazirev, V. I., and Price, G. L., *J. Mol. Catal. A* **96**, 145 (1995).
51. Satsuma, A., Yamada, K., Mori, T., Niwa, M., Hattori, T., and Murakami, Y., *Catal. Lett.* **31**, 367 (1995).

4. Structure-activity relations for Ni-containing zeolites during NO reduction Part 2 - Influence of metal

The influence of the metal in Ni-containing zeolites used as catalysts for the reduction of NO with propane and propene was studied. For the fresh catalysts Ni is located in ion exchange positions for NiNaMOR, NiNaZSM-5 and NiNaMCM-22. The formation of carbonaceous deposits, the removal of Al from framework positions and the migration of Ni ions were identified as main reasons for the changes observed in the activity of the catalysts during the NO reduction with hydrocarbons. Under reaction conditions Ni either forms NiO clusters or migrates to sites where it is not accessible for the reactants.

4.1. Introduction

The reduction of nitric oxide with hydrocarbons using transition metal exchanged zeolites represents an alternative for the use of NH_3 as reducing agent in the selective catalytic reduction of NO_x . Typically transition metals such as Co (1-4), Fe (5-9) and Ni (2, 3, 10) supported on zeolites are investigated as potential catalysts for the reduction of NO using hydrocarbons as reductant (11).

Several authors have pointed out that the coordination of the metal ions at different cationic sites of the zeolites (12, 13) may affect the relative diffusivities of the reactants and/or the activation of the hydrocarbon molecules (13-15). Li and Armor suggested that on ferrierite Co ions located in 8-membered rings are less active for NO reduction with methane than sites in 10-membered rings. Kaucký et al. reported the influence of the location of Co cations in zeolites on the catalytic activity for the reduction of NO with methane (13). In general, α -type Co ions, bound to framework oxygens of the wall of the main channel were found to be the most active Co ions in mordenite and ferrierite, while in ZSM-5 β -type Co ions, coordinated to the deformed six-membered ring at the intersection of straight and sinusoidal channels possess the highest activity. It is described that the stabilization of isolated metal cations at short distances within the zeolite structure might be the reason for the high SCR activity of metal-exchanged zeolites (13). In the case of FeZSM-5 a binuclear iron complex has been proposed as the active site for the reduction of NO with hydrocarbons (7, 8, 16).

The deactivation of catalysts during the reduction of NO with hydrocarbons might either result from the formation of carbonaceous deposits, which block the active sites (9, 17, 18) or from changes in the catalyst structure. The formation of carbonaceous species was found to be more severe when unsaturated reducing agents (e.g. olefins) are used (17) and for highly acidic catalysts (18). For alumina-

supported Pt catalysts metal sintering during NO reduction in the presence of excess of oxygen at temperatures below 500 °C (18, 19) was observed. Cu- (20-22) and Ag-exchanged zeolite catalysts (23) are known to sinter under the flow of the reaction mixture due to the presence of steam. In addition, deactivation of the zeolite based catalysts due to removal of Al^{3+} from framework positions (dealumination) during the NO reduction with methane was observed for H-mordenite (24) and for Cu-ZSM-5 in the presence of H_2O due to the formation of inactive species like copper aluminate (25). Petunchi et al. reported for CuZSM-5 at temperatures above 350 °C a severe deactivation of the catalysts resulting from dealumination (22).

The effect of the type and concentration of acid sites on the activity of Ni-exchanged MOR, ZSM-5 and MCM-22 zeolites was discussed in the first part of this study (26). In this part, the role of Ni and of structural changes of the metal and the zeolite support on the catalytic properties of Ni exchanged zeolites for NO reduction are discussed.

4.2. Experimental

4.2.1. Preparation of samples

Ni-exchanged MOR (Si/Al=8.6), ZSM-5 (Si/Al = 15.6) and MCM-22 (Si/Al = 16.4) were prepared by liquid phase ion exchange of the sodium form of the zeolites carried out from an aqueous solution of $Ni(NO_3)_2$ at 80 °C under continuous stirring for 24 h. Subsequently, the zeolite was separated from the ion exchange solution by centrifugation, washed thoroughly with deionized water and dried over night at 100 °C.

4.2.2. Characterization

The adsorption of CO was followed by IR-spectroscopy, using a Bruker IFS-88 spectrometer equipped with a vacuum cell. Samples were pressed into self-supported wafers and activated at 500 °C for 60 min. The increase in temperature during the activation was done in steps at 150, 250 and 300 °C for 30 min using a ramp of 10 °C/min. Spectra of activated samples were recorded at 50 °C and CO was adsorbed at the same temperature using partial pressures between $1 \cdot 10^{-3}$ to 1 mbar.

^{27}Al -MAS-NMR spectra were measured on a Bruker MSL-300 NMR spectrometer at a field strength of 7.5 T and a spinning frequency of 15 kHz speed at a frequency of 78.205 MHz with 1.0 μs excitation pulses and recycle times of 0.1 s. The samples were pressed into 4 mm ZrO_2 -rotors. The ^{27}Al chemical shifts were referenced to 1 M aqueous solution of $\text{Al}(\text{NO}_3)_3$ ($\delta=0.0$ ppm).

X-ray absorption spectra were measured at HASYLAB, DESY (Hamburg, Germany) on beamline X1 using the Si (111) monochromator. The intensity of higher order reflections was minimized by detuning the second crystal of the monochromator to 60 % of the maximum intensity. The samples were prepared as self-supporting wafers having a total absorption of 2.5 to optimize the signal to noise ratio. Fresh samples were activated *in situ* at 600°C for 1 h in a stainless steel cell. X-ray absorption spectra were recorded at the Ni edge (8333 eV) and analyzed with the WINXAS97 software (27). The local environment of the Ni atoms was determined from the EXAFS using phase-shift and amplitude functions for Ni-O and Ni-Ni calculated assuming multiple scattering processes (FEFF Version 8.10) (28).

4.2.3. Catalytic measurements

The catalytic activity of the samples was studied in a continuous flow system with a fixed bed quartz reactor of 4 mm inner diameter containing 0.1 g of catalyst (particle size 300 μm). The reactant gas feed contained 1000 ppm of NO, 1000 ppm of C_3H_6 or C_3H_8 , 5 % O_2 and He as the carrier gas. A total flow of 50 ml/min, resulting in a space velocity of 20000 h^{-1} , was used. The reaction products were analyzed by a chemiluminescence analyzer (TEI 42C) and a gas chromatograph (HP) equipped with a TCD detector using a Molsieve column for separation of N_2 , O_2 and CO and a Porapak column for N_2O , C_3H_6 , C_3H_8 and CO_2 analysis. Before the reaction, the catalysts were pretreated *in situ* under helium flow at 600 °C for 1 h.

The activity and the deactivation of the catalysts during the reaction were investigated by an extended procedure consisting of three cycles. In the first cycle the activity was followed at temperatures between 150 and 600 °C in intervals of 25 °C (cycle 1). This cycle was followed immediately by cycle 2, where the activity was measured during the decrease of the temperature between 600 and 150 °C at intervals of 25 °C. Subsequently, the samples were treated in oxygen at 600 °C for 1 h followed a third cycle between 150 and 600 °C with intervals of 25 °C (cycle 3). During all cycles the activity was followed at each temperature for 2 h.

4.3. Results

4.3.1. Changes in activity after NO reduction

As reported previously in part I (26) the catalytic activities of the three Ni containing catalysts followed the order NiNaZSM-5 > NiNaMOR > NiNaMCM-22

for NO reduction with propane and NiNaMOR > NiNaZSM-5 > NiNaMCM-22 for NO reduction with propene. The activity of the catalysts for the reduction of NO with propane during the three temperature cycles are compared in Fig. 4.1. For all catalysts the temperature where the maximum NO conversion was reached increased after the first cycle, while the activity during the second and third cycle was nearly identical. For NiNaMOR and NiNaZSM-5 the same level of NO conversion was reached in all cycles, e.g., 69 % and 80 %, while for NiNaMCM-22 a significant decrease from 51 % to 39 % in the maximum activity after the first cycle was observed. In the case of NiNaMOR changes in the activity were observed at temperatures above 325 °C, while for NiNaZSM-5 and NiNaMCM-22 the differences in NO conversion were already observed above 175 °C. The smallest differences between the first and the second temperature cycle were observed for NiNaMOR. The selectivity to nitrogen containing products was not affected by the temperature cycles.

When propene was used as reducing agent deactivation caused by marked coke formation for NiNaZSM-5 and NiNaMCM-22 was observed (26). Therefore, for these catalysts a different activity during the second and third temperature cycle was observed during the reduction of NO with propene as shown in Fig. 4.2. In contrast, for NiNaMOR the changes in the activity were independent of the type of reducing agent and similarly than for the reduction with propane, for the reduction with propene the activity of the second and third cycles was equal.

The differences in the activity observed between the first and the subsequent cycles indicate that irreversible changes took place in the materials during the first temperature increase in the presence of reactive substrates. In order to determine the temperature where structural changes occur, the NO reduction with propane was studied for NiNaMOR and NiNaZSM-5 during extended time at constant temperature as shown in Fig. 4.3. For NiNaZSM-5 (Fig. 4.3A) the conversion of

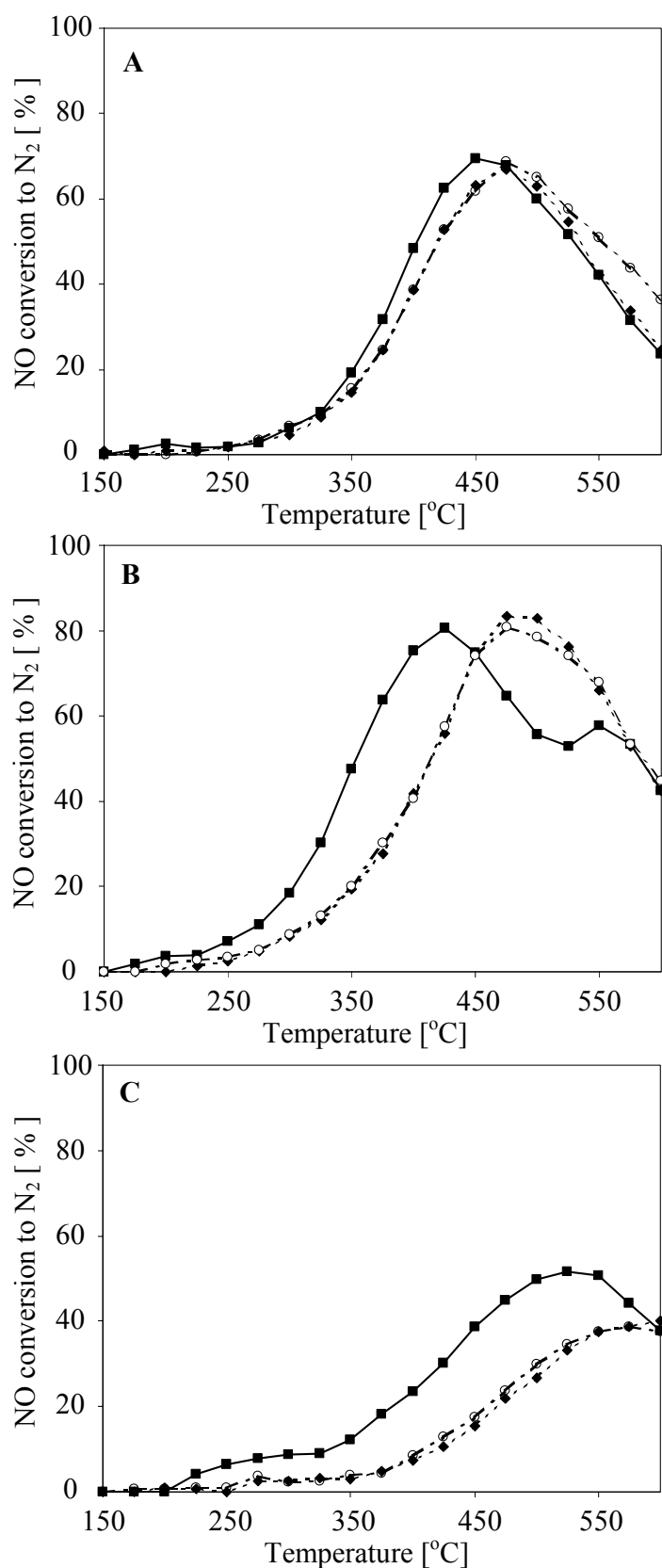


Figure 4.1 NO conversion to N₂ during NO reduction with propane ramp upwards 1 (—■), ramp downwards 1 (—◆), ramp upwards 2 (—◻) on (A) NiNaMOR, (B) NiNaZSM-5 and (C) NiNaMCM-22.

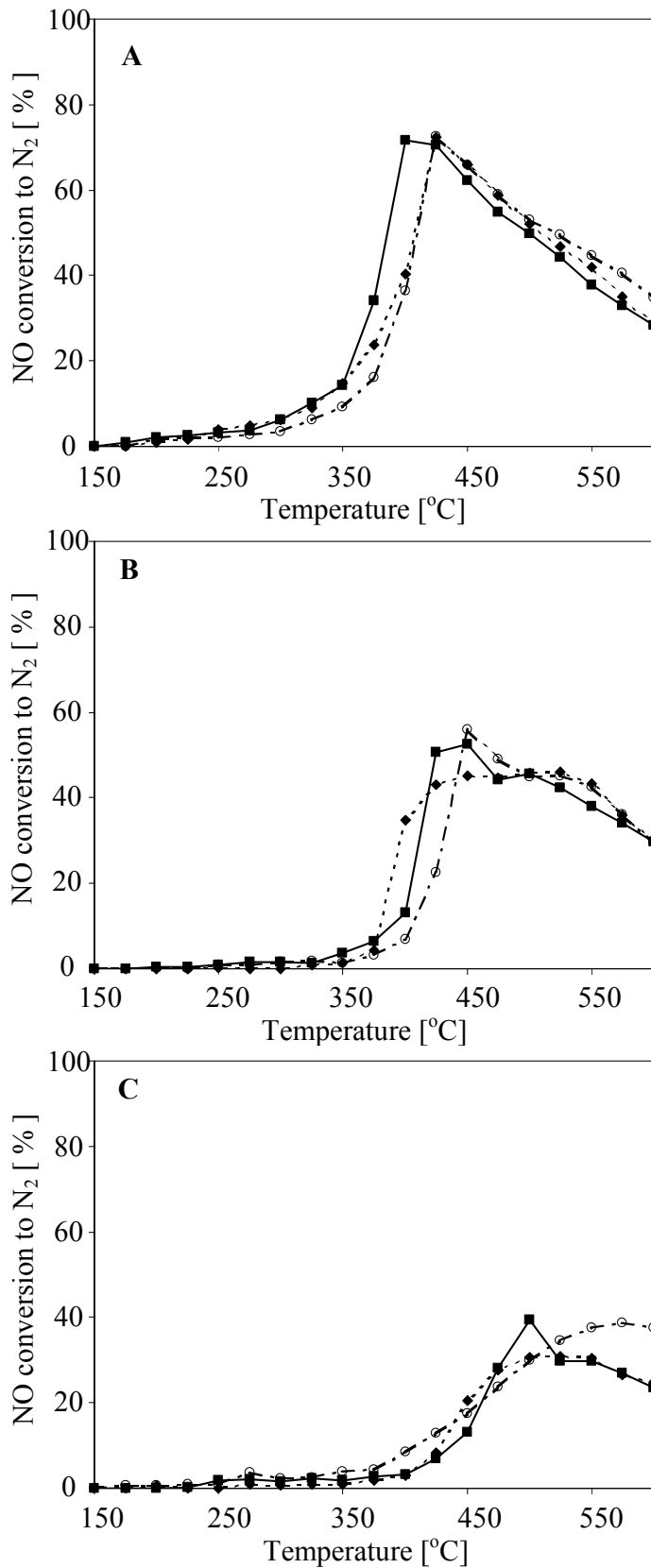
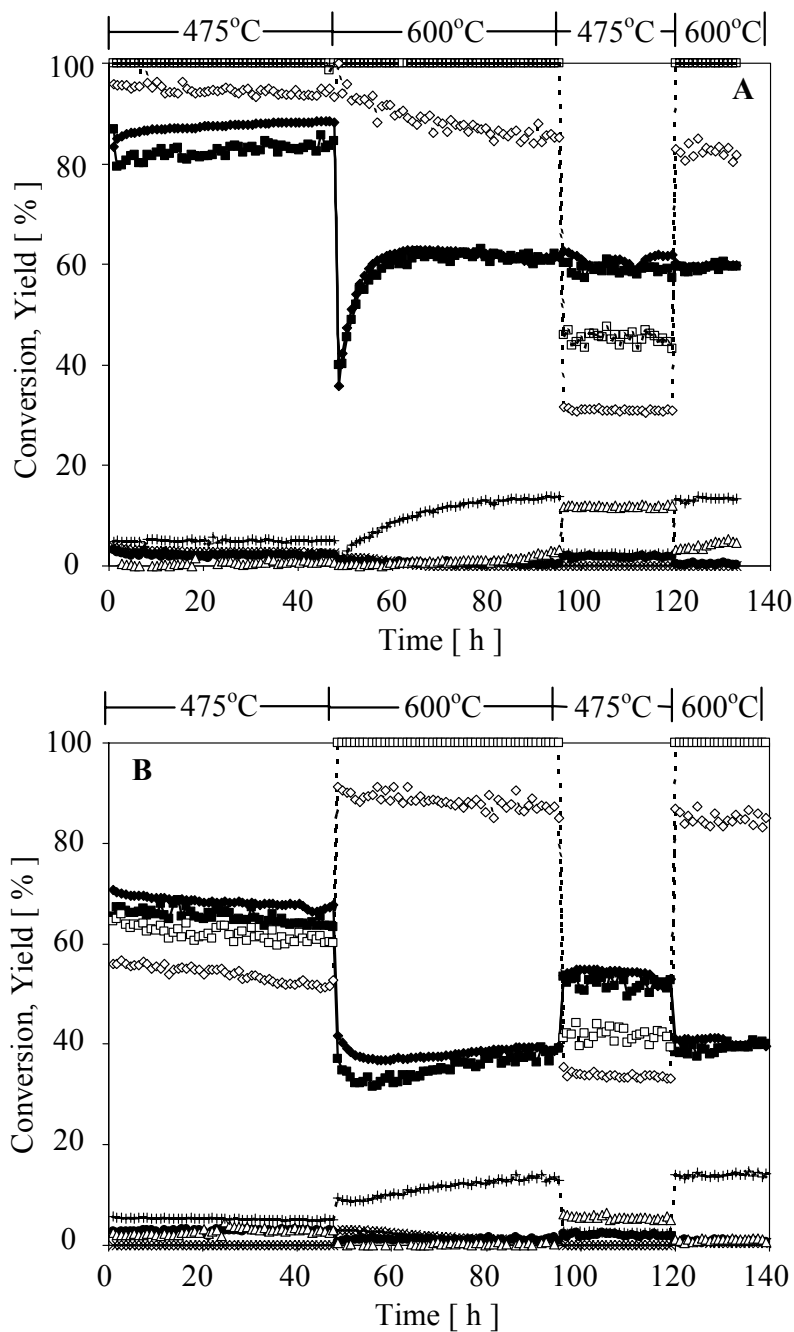


Figure 4.2 NO conversion to N₂ during NO reduction with propene ramp upwards 1 (—■—), ramp downwards 1 (—◆—), ramp upwards 2 (—○—) on (A) NiNaMOR, (B) NiNaZSM-5 and (C) NiNaMCM-22.



NO at 475 °C increased from 83 % at 1 h to 88 % after 48 h, while the selectivities of nitrogen products did not change during this time. After increasing the temperature to 600 °C, the NO conversion decreased to 42 % and finally reached

59 % during a period of 10 h. Initially, small concentrations of NO₂ were observed, however, after 10 h the selectivity improved and N₂ was the only nitrogen containing product. The formation of CO₂ decreased with time and that of CH₄ increased. After 48 h of reaction at 600 °C, the temperature was changed back to 475 °C. Then, the conversions of NO and propane were much lower than those obtained with the fresh sample, i.e., 60 % and 45 %, respectively, while the selectivity to CO was much higher. The conversion and selectivity were stable during the following 24 h at 475 °C. After a subsequent temperature increase to 600 °C the same conversion and selectivity was observed as during the first experiments at 600 °C.

For NiNaMOR (Fig. 4.3B) only small variations in the conversions and selectivities were observed for the fresh catalyst for the reaction of NO with propane at 475 °C during 48 h, i.e., NO and propane conversion decreased from 70 % to 68 % and from 64 % to 60 %, respectively. After temperature was increased to 600 °C the NO conversion initially decreased to 41 % and reached during the subsequent 30 h 39 % passing through a minimum of 37 %. After the stepwise change in temperature small concentrations of NO₂ were formed during the first hours, while after longer time on stream N₂ became the only nitrogen product being detected. In addition, the selectivity of the carbon containing products changed significantly during this period of time. Similarly to NiNaZSM-5, the amount of CO₂ decreased with time, while the amount of CH₄ increased. However, the changes observed for NiNaMOR were less pronounced than those reported for NiNaZSM-5 above. After 48 hours of reaction at 600 °C, the temperature was lowered to 475 °C and the NO conversion reached 54 %, which was slightly lower than the conversion of the fresh catalyst (68 %), and remained constant for the following 24 h. After an increase to 600 °C the conversions and selectivities reached the same levels than during the first cycle at 600 °C.

4.3.2. Characterization

The ^{27}Al -NMR spectra of the fresh samples and after NO reduction with propane and propene are shown in Fig. 4.4. For all samples a signal at 52 ppm, assigned to Al located in tetrahedral positions, was observed (6, 24). For NiNaMCM-22 an unresolved asymmetric doublet, which corresponds to different framework sites, was observed (29-31). For NiNaMCM-22 and for all samples after the NO reduction with propane and propene, a signal near 0 ppm was observed, which is assigned to Al in octahedral positions and indicates the presence of extraframework Al-oxide species (6, 24), formed during the calcination of the sample (NiNaMCM-22) (29-32) and during the NO reduction. In addition, the change in the shape of the doublet at ~ 50 ppm for MCM-22 is associated with the dealumination of the zeolite structure (32). Table 4.1 summarizes the fraction of Al present in octahedral positions in fresh samples and samples after the reduction of NO with propane and propene.

The IR spectra (region of the hydroxyl groups) of the activated catalysts and after NO reduction with propane and propene are shown in Fig. 4.5. The bands observed at 3745, 3680 and 3610 cm^{-1} correspond to terminal Si-OH groups, Al-OH groups on extraframework Al-oxide species and to bridging SiOHAl groups (Brønsted acid sites), respectively (33-36). In general, for all samples the intensity of the band at 3610 cm^{-1} decreased after the reaction. Decreases in the range from 32 % to 93 % were observed for the area of the band of the bridged hydroxyl groups in the spectra of the samples after reaction in comparison with the spectra of the fresh samples. The intensity of the band at 3680 cm^{-1} was higher compared to the fresh samples. Changes in the intensity of the band at 3745 cm^{-1} were not observed.

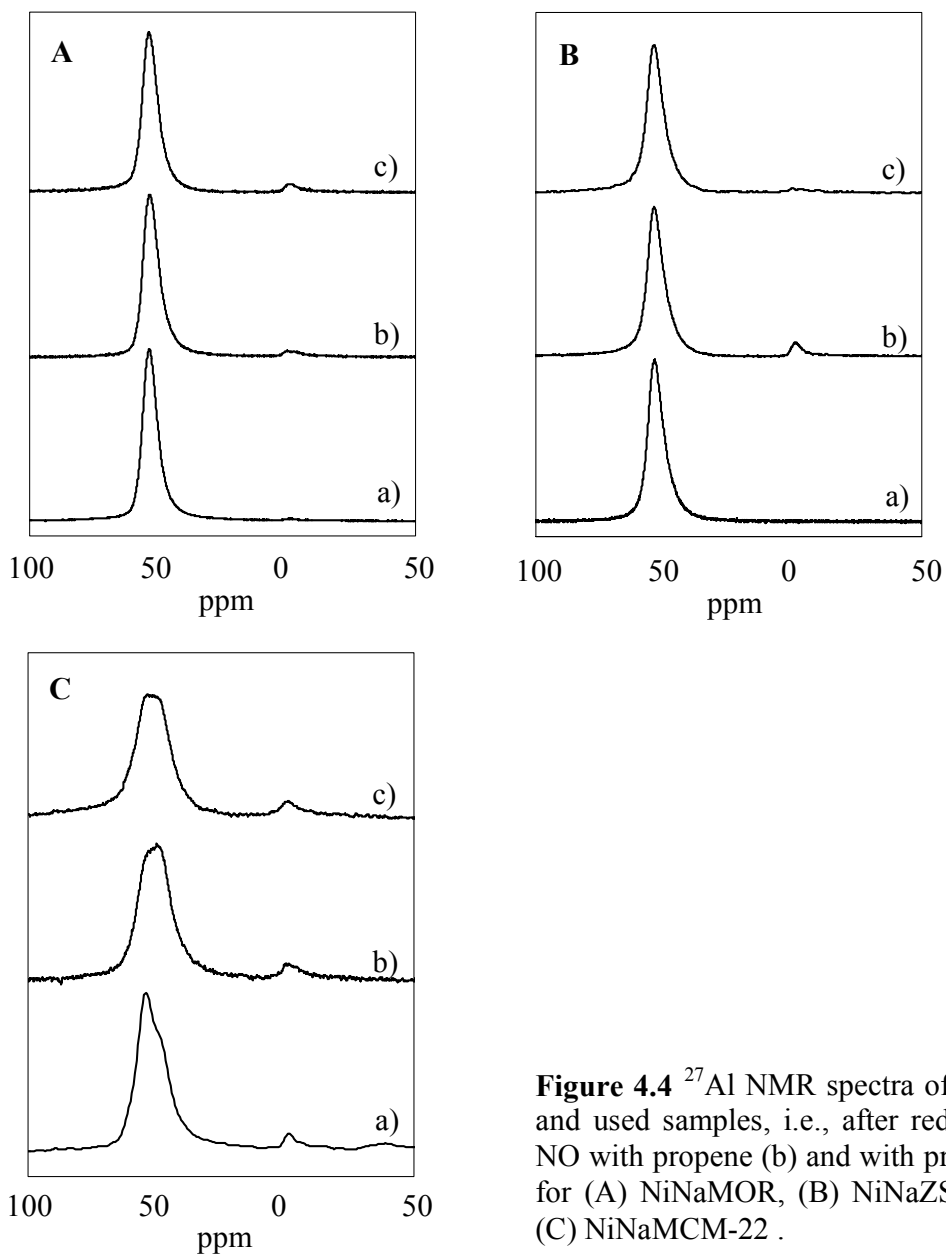


Figure 4.4 ^{27}Al NMR spectra of fresh (a) and used samples, i.e., after reduction of NO with propene (b) and with propane (c) for (A) NiNaMOR, (B) NiNaZSM-5 and (C) NiNaMCM-22 .

The IR spectra during adsorption of CO at partial pressures between 1 and 10^{-3} mbar on NiNaZSM-5 are shown in Fig. 4.6. At a CO partial pressure of 1 mbar bands at 2213, 2136, 2092 cm^{-1} and a shoulder at 2220 cm^{-1} were observed. The IR bands at 2220 and 2213 cm^{-1} were assigned to $\text{Ni}^{2+}\text{-CO}$ species (37). The bands at 2136 and 2092 cm^{-1} were assigned to the symmetric and asymmetric stretching vibration of dicarbonyl species on Ni^+ ions, i.e., $\text{Ni}^+\text{-(CO)}_2$ (37-40). At a CO

Table 4.1 Fraction of Al present in octahedral positions.

Sample	Fraction of Al in octahedral positions [%]
NiNaMOR fresh	0.0
NiNaMOR (propene) ^a	4.6
NiNaMOR (propane) ^b	2.4
NiNaZSM-5 fresh	0.7
NiNaZSM-5 (propene) ^a	2.4
NiNaZSM-5 (propane) ^b	3.3
NiNaMCM-22 fresh	4.7
NiNaMCM-22 (propene) ^a	5.6
NiNaMCM-22 (propane) ^b	6.1

^a After the reduction with propene^b After the reduction with propane

partial pressure of 0.1 mbar the intensities of the bands at 2220, 2213, 2136 and 2092 cm⁻¹ decreased. In addition, a new band at 2109 cm⁻¹, which was assigned to monocarbonyl species, i.e., Ni⁺-CO (37-40), was observed. This band reached a maximum in intensity at a CO partial pressure of 10⁻² mbar and decreased at 10⁻³ mbar. At this partial pressure the bands at 2092 and 2136 cm⁻¹ were not observed. This indicates, that with decreasing CO partial pressure Ni dicarbonyl species are replaced by monocarbonyl species followed by the desorption of CO. The presence of Ni⁺-CO and Ni⁺-(CO)₂ species was not unexpected, as the reduction of Ni²⁺ to Ni⁺ by dehydration in vacuum at temperatures above 300 °C has previously been reported (40, 41). When the temperature is increased very slowly (42), water removed from the sample reduces Ni, according to Eq. 4.1 (40).



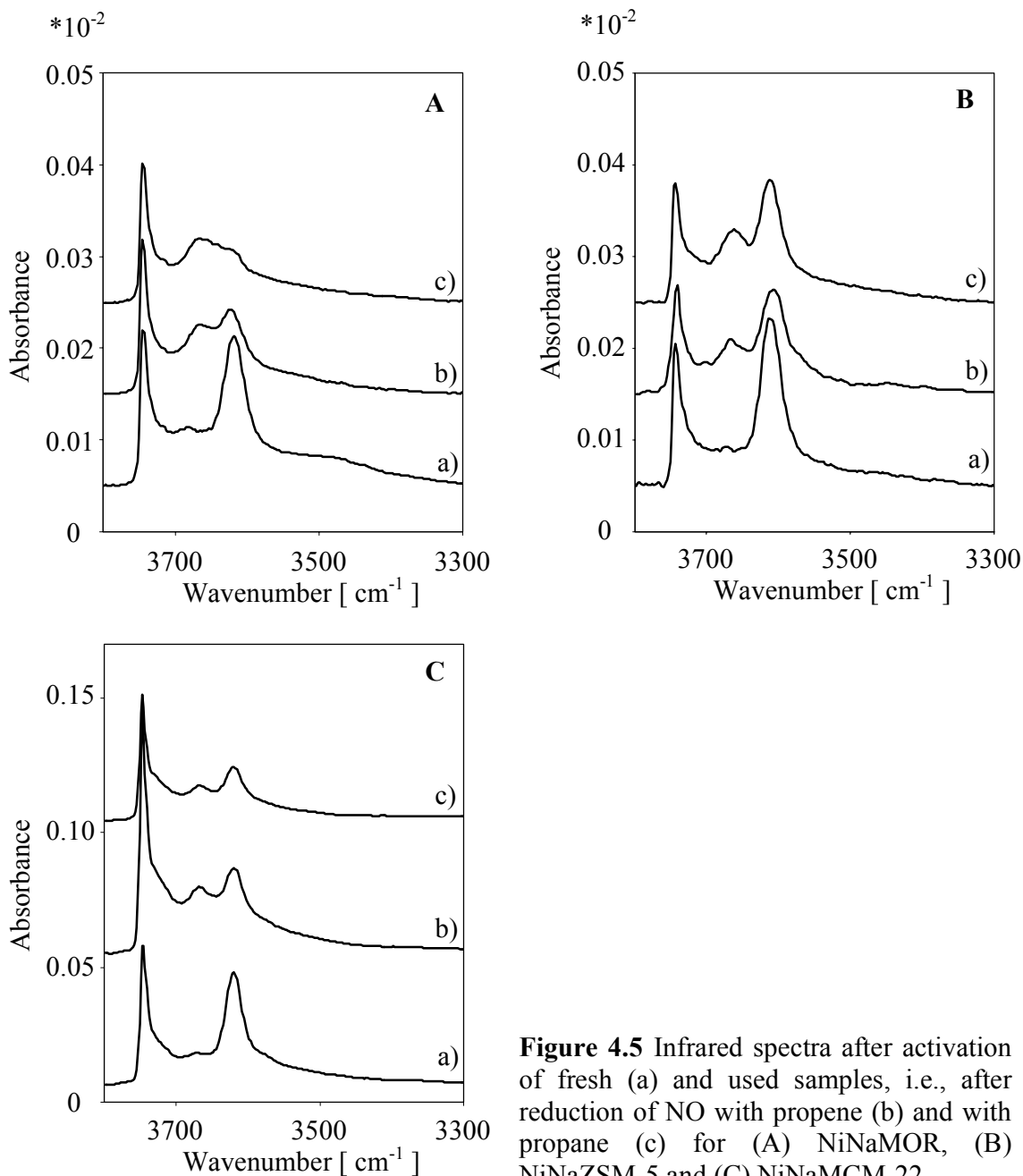


Figure 4.5 Infrared spectra after activation of fresh (a) and used samples, i.e., after reduction of NO with propene (b) and with propane (c) for (A) NiNaMOR, (B) NiNaZSM-5 and (C) NiNaMCM-22.

Spectra during the adsorption of CO with a partial pressure of 10^{-2} mbar on the fresh catalysts and after NO reduction with propene and propane are shown in Fig. 4.7. For the fresh NiNaMOR (Fig. 4.7A) the intensity of the band at 2108 cm^{-1} ($\text{Ni}^+ \text{-CO}$) was lower compared to NiNaZSM-5 and NiNaMCM-22 and was not

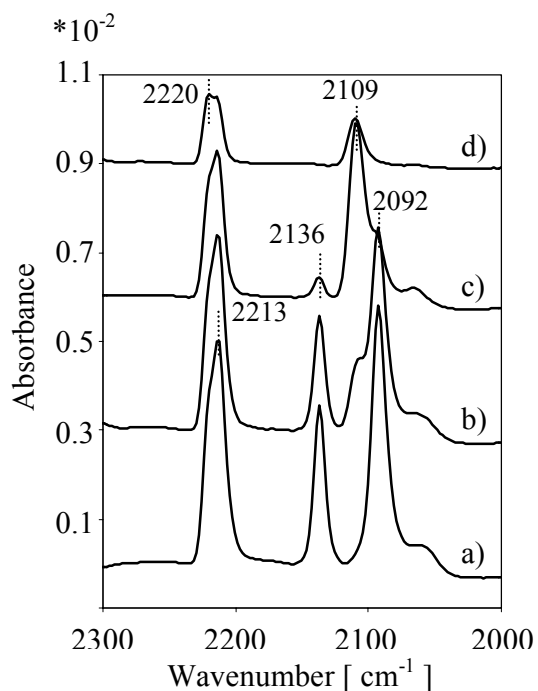


Figure 4.6 Infrared spectra of CO adsorption on fresh NiNaZSM-5 at 50°C, at 1 mbar (a), $1 \cdot 10^{-1}$ mbar (b), $1 \cdot 10^{-2}$ mbar (c) and $1 \cdot 10^{-3}$ mbar (d).

present in the spectra after the reaction, while the intensity of the band at 2213 cm^{-1} was not affected. For the fresh NiNaZSM-5 (Fig. 4.7B), two different Ni^{2+} -CO species at 2220 and 2213 cm^{-1} were observed, while for the samples after reaction only the band at 2213 cm^{-1} was present. In addition, Ni^+ -CO species were clearly observed for the fresh NiNaZSM-5, while after the NO reduction with propene the intensity of the corresponding bands was very weak and for the sample after NO reduction with propane Ni^+ -CO species were absent. In the spectra for NiNaMCM-22 after NO reduction with propane and propene (Fig. 4.7C) the intensity of the bands at 2113 and 2095 cm^{-1} , corresponding to CO interacting with Ni^+ , was much lower in comparison with the fresh sample, while the band at 2213 cm^{-1} was not affected by the state of the sample. In general, for all samples studied the intensity of the bands assigned to CO interacting with Ni^{2+} ions was almost the same, when comparing fresh and used samples, while IR bands resulting from the adsorption of CO on Ni^+ were much lower for the catalyst studied after the NO reduction.

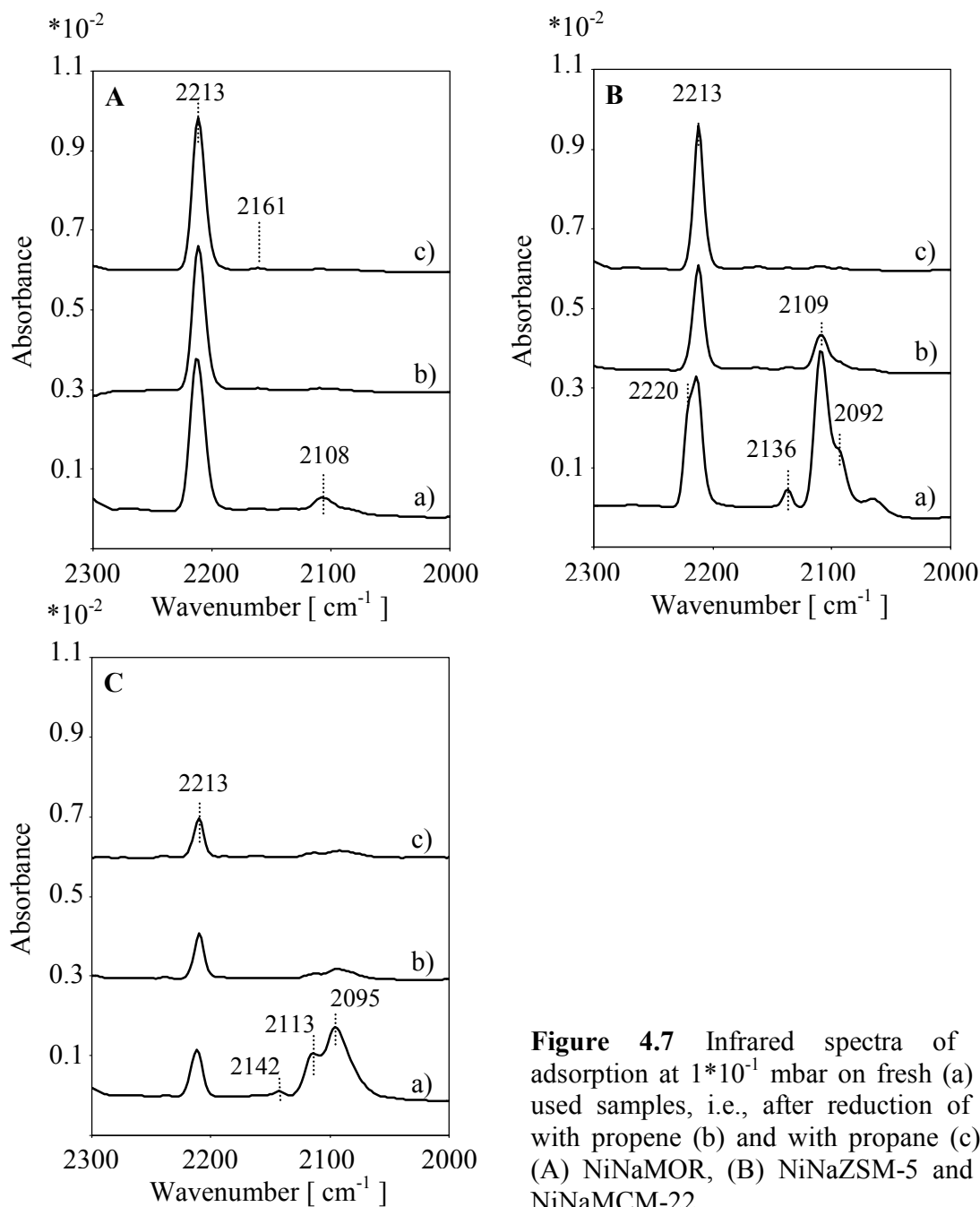


Figure 4.7 Infrared spectra of CO adsorption at $1 \cdot 10^{-1}$ mbar on fresh (a) and used samples, i.e., after reduction of NO with propene (b) and with propane (c) for (A) NiNaMOR, (B) NiNaZSM-5 and (C) NiNaMCM-22.

The energies of the Ni-K X-ray absorption edge, which can be related to the average charge of the Ni atoms in the samples, are summarized in Table 4.2. For the fresh samples and for NiO the shift in the edge position of +2.7 eV, with respect to metallic Ni was observed, while the samples after the reaction exhibited an increase in the edge energy of +3.8 eV.

Table 4.2 Energy position of the Ni-K edge of Ni samples

Sample	Edge position half-height ^c	
	eV	Δ eV
Ni foil	8339.5	
NiO	8342.2	2.7
NiNaMOR fresh	8342.1	2.6
NiNaMOR (propene) ^a	8343.2	3.7
NiNaMOR (propane) ^b	8343.2	3.7
NiNaZSM-5 fresh	8342.2	2.7
NiNaZSM-5 (propene) ^a	8343.2	3.7
NiNaZSM-5 (propane) ^b	8343.3	3.8
NiNaMCM-22 fresh	8342.3	2.8
NiNaMCM-22 (propene) ^a	8343.5	4.0
NiNaMCM-22 (propane) ^b	8343.2	3.7

^a After the reduction with propene

^b After the reduction with propane

^c The energy corresponds to the absorption at half-height of the edge, i.e. absorbance = 0.5 in the normalized spectra

The magnitude of the Fourier transformed EXAFS (weighted with k^2) of the samples before and after the reduction of NO with propane and propene are compared in Fig. 4.8 and the results of the analysis of the EXAFS are summarized in Table 4.3. In principle, two contributions of Ni-oxide species at 1.6 and 2.5 Å, assigned to Ni-O and to Ni-Ni, were observed in all samples. In the fresh samples mainly Ni-O contributions were present and the low number of O neighbors ($N_{\text{Ni-O}} \sim 3$), the absence of Ni-Ni contributions ($N_{\text{Ni-Ni}} < 0.8$) and the slightly shorted distance between Ni and O compared to Ni-oxide indicates that the Ni ions are mainly located on ion exchange positions. After the NO reduction a significant

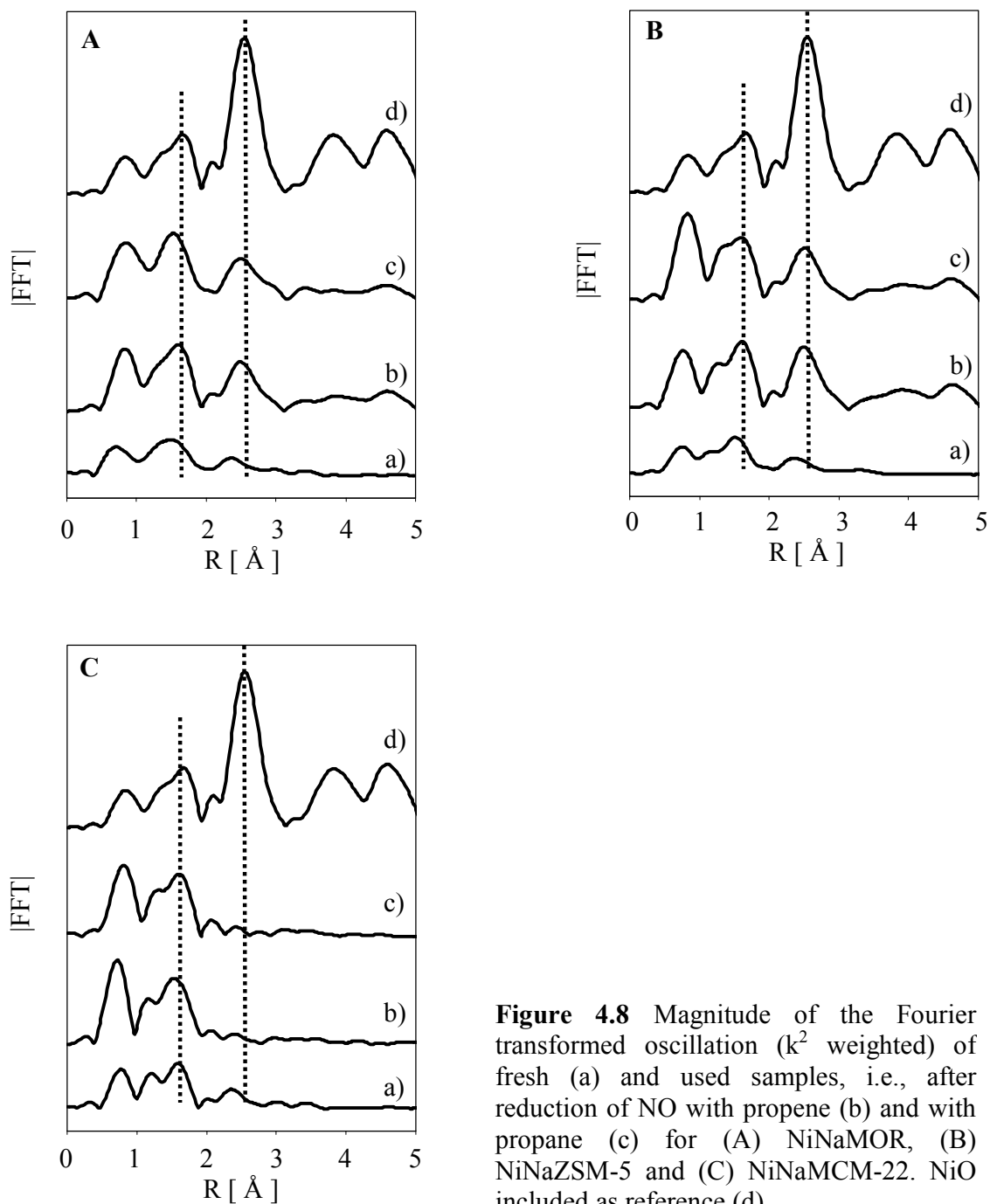


Figure 4.8 Magnitude of the Fourier transformed oscillation (k^2 weighted) of fresh (a) and used samples, i.e., after reduction of NO with propene (b) and with propane (c) for (A) NiNaMOR, (B) NiNaZSM-5 and (C) NiNaMCM-22. NiO included as reference (d).

increase in the Ni-Ni and to a lesser extent in the Ni-O contributions was observed, which points to the formation of larger Ni-oxide species on NiNaMOR and NiNaZSM-5 during the reaction. In contrast, for NiNaMCM-22 only Ni-O

Table 4.3 Coordination parameters for Ni-exchanged zeolites determined by X-ray absorption spectroscopy

Sample	Ni-O			Ni-Ni		
	N	R [Å]	$\Delta\sigma^2$ [Å ²]	N	R [Å]	$\Delta\sigma^2$ [Å ²]
Ni foil				12	2.488	
NiO	6	2.084		12	2.947	
NiNaMOR fresh	2.95	2.020	0.0072	0.79	2.958	0.0034
NiNaMOR (propene) ^a	4.63	2.052	0.0043	4.81	2.951	0.0062
NiNaMOR (propane) ^b	4.51	2.052	0.0026	4.18	2.935	0.0053
NiNaZSM-5 fresh	2.81	2.005	0.0072	0.73	2.958	0.0074
NiNaZSM-5 (propene) ^a	4.22	2.054	0.0025	4.45	2.945	0.0039
NiNaZSM-5 (propane) ^b	4.67	2.056	0.0044	3.91	2.954	0.0038
NiNaMCM-22 fresh	3.16	2.024	0.0072	0.68	2.843	0.0034
NiNaMCM-22 (propene) ^a	3.91	2.036	0.0022	0	0	0
NiNaMCM-22 (propane) ^b	3.34	2.043	0.0013	0	0	0

^a After the reduction with propene^b After the reduction with propane

similar to the fresh samples, were observed after the reaction. Table 4.4 summarizes the size of the NiO clusters formed after the reduction of NO with propane and propene. The size of the clusters of NiO formed in NiNaMOR and NiNaZSM-5 after the reduction of NO with propane and propene ranges from 6.5 Å to 8 Å. It was determined from a relation obtained between the cluster size and the number of neighbors in spherical clusters built with the crystallographic parameters for NiO.

Table 4.4 Size of NiO clusters in samples after the reduction of NO with propane and propene

Sample	Size of cluster [Å]
NiNaMOR fresh	0
NiNaMOR (propene) ^a	8.0
NiNaMOR (propane) ^b	7.0
NiNaZSM-5 fresh	0
NiNaZSM-5 (propene) ^a	7.4
NiNaZSM-5 (propane) ^b	6.5
NiNaMCM-22 fresh	0
NiNaMCM-22 (propene) ^a	0
NiNaMCM-22 (propane) ^b	0

^a After the reduction with propene^b After the reduction with propane

4.4. Discussion

In principle two reasons, i.e., the deposition of carbonaceous species on the catalyst and structural changes of the material, might account for the deactivation of the catalysts during the reduction of NO with propane and propene. As already described in ref. (43) the formation of carbonaceous deposits depends markedly on the type of reducing agent and the reaction temperature. With propene a higher concentration of carbonaceous deposits is generally formed, which leads to a lower activity of the Ni containing catalysts for the reduction of NO with propene than for the reduction with propane.

During the reduction of NO with propane a decrease in the activity of the catalysts after the first cycle (from 150 to 600 °C) was observed for all three materials studied, while the activity between the second (600 °C to 150 °C) and the

third cycle (150 °C to 600 °C) did not change. The intermediate oxidation of the catalysts at 600 °C in O₂, carried out between cycle 2 and 3, should sufficiently remove coke species formed (17, 22) and, therefore, restore the initial activity of the catalysts if coke formation is the main reason for the deactivation. The activity of the catalysts during cycle 3, however, remained at the level of the second cycle, which indicates that irreversible changes of the catalyst (and not carbon deposition) are the main reason for the catalyst deactivation after high temperature reactions.

The effect of the formation of carbonaceous species is demonstrated in the NO reduction experiments carried out for an extended time at 475 °C and 600 °C. After exposing NiNaZSM-5 and NiNaMOR to the reaction mixture at 475 °C immediately after the activation, NO conversion levels of 88 % and 68 % were obtained. For NiNaZSM-5 the NO conversion was higher compared to that obtained at 475 °C during the experiment performed by varying the temperature between 150 and 600 °C, i.e., 65 %, (see Fig. 4.1B) which indicates that a partial deactivation (most likely through deposition of carbonaceous species) during such temperature variations is taking place. In contrast, for NiNaMOR the same NO conversion was observed in both experiments (see Fig. 4.1A and Fig. 4.3B), which confirms that the formation of carbonaceous species in NiNaMOR is lower compared to NiNaZSM-5, due to the lower concentration of acid sites (26). After 50 h of reaction at 475 °C the temperature was increased to 600 °C for 50 h and the NO conversion decreased for both catalysts. It is interesting to note that for NiNaZSM-5 an induction period of 10 h was observed at 600 °C, where the NO conversion increased from 42 to 59 %. After changing the reaction temperature back to 475 °C both catalysts showed a lower activity compared to the first part of the experiment. For NiNaZSM-5 the NO conversion decreased from 88 % to 60 %, due to a severe and irreversible deactivation of the catalysts. For NiNaMOR the NO conversion decreased from 68 % to 54 %, indicating that changes of the

catalyst structure resulting from the reaction at 600 °C were smaller in comparison with NiNaZSM-5.

During the NO reduction with propene the difference in activity during all three cycles was very small. Having already shown that the presence of carbonaceous species is the main reason for the lower activity of the catalysts compared to the NO reduction with propane (26), a reversible formation of coke during the reaction is proposed. The oxidation treatment between cycle 2 and 3 most probably removes the coke species formed. During the third reaction cycle, however, the formation of carbonaceous species occurs in a similar extent as during the first cycle and, therefore, the activity of the catalysts during the first and third cycle is the same. In addition, structural changes of the catalysts, similar to the reaction with propane, most probably occur, but have only a minor effect on the activity of the MOR based catalysts.

As shown in ref (26) the type and strength of the acid sites have a significant influence on the activity of the catalyst for the NO reduction with propane. Therefore, the decrease in the activity observed during the reaction at high temperatures is attributed to the removal of Brønsted acid sites resulting from the partial dealumination of the zeolites. In addition, Al³⁺ located in the zeolite framework act as anchor positions for the Ni-ions and thus dealumination additionally leads to an enhanced formation of Ni-oxide clusters within the zeolite pores. For all samples, the formation of extraframework Al-oxide species was detected by IR spectroscopy and by ²⁷Al-NMR. After the reaction an intense IR band assigned to extraframework Al-oxide species was observed, which had only a weak intensity in the fresh samples. A small fraction of Al present in octahedral positions in the fresh NiNaMCM-22 and NiNaZSM-5 was detected by ²⁷Al-NMR, while for NiNaMOR the signal at 0 ppm was not observed. After the reaction, octahedral Al species could be detected in all catalysts (see Table 4.1), the highest concentration was observed in NiNaMOR after the reaction with propene and in

NiNaMCM-22 after the reaction with propene and propane. Ion exchange positions in the investigated zeolites are occupied by protons, Ni and Na ions. From the spectra of the activated samples a decrease of 32 % - 93 % in the area of the infrared band at 3610 cm^{-1} attributed to the bridged hydroxyl groups, was observed when comparing fresh and used samples. Comparing this decrease with the appearance of a small peak associated to octahedral Al in the ^{27}Al -NMR corresponding to a fraction of 2.4 % - 6.1 % of the total Al (see Table 4.1), might indicate the preferential dealumination of aluminum atoms associated to bridged hydroxyl groups.

The area of the bands of CO adsorbed at 0.1 mbar on Ni^+ and Ni^{2+} in the samples after reaction was integrated. We assumed that the molar extinction coefficients of these species are similar and calculated the percentage of decreased area in comparison with fresh samples. The results are summarized in Table 4.5. The smallest difference in the IR spectra during CO adsorption between fresh and used samples was observed for NiNaMOR, which perfectly agrees with the minor decrease in activity observed during the NO reduction at $600\text{ }^\circ\text{C}$. For NiNaZSM-5 and NiNaMCM-22 the intensity of the bands assigned to CO adsorption on monovalent Ni^+ decreased significantly after reaction compared to the fresh catalysts (>60 %). In general, the presence of CO interacting with monovalent Ni proves the existence of isolated Ni ions in the catalysts, because only single Ni^{2+} ions can be partially reduced to Ni^+ by H_2O present in the zeolite structure (40, 41). Therefore, the spectra of CO adsorption showing the disappearance of the band corresponding to CO interacting with Ni^+ indicates that the deactivation NiNaZSM-5 and NiNaMCM-22 during the reaction at $600\text{ }^\circ\text{C}$ results from a decrease in the availability of isolated Ni ions.

The migration of Ni from isolated ion exchange positions into larger Ni-oxide species was also observed by EXAFS. In the fresh catalysts Ni was present as Ni^{2+} at ion exchange positions as indicated by the number of O neighbors of around 3

and the minor Ni-Ni contributions ($N_{\text{Ni-Ni}} \sim 0.7$). The minor extent of Ni-Ni contributions might indicate the presence of Ni^{2+} ions on cation sites next to each other surrounded by oxygen atoms of the zeolite framework. Similar structures have been observed previously for Ni-exchanged Y zeolite prepared by solid-state ion exchange (44). Note that the contributions of the closest oxygen neighbors are only weakly affected by the formation of Ni-oxide species. It is not possible to differentiate between the contributions to the EXAFS from oxygen atoms from the zeolite lattice and from Ni-oxide clusters, while the presence of next nearest Ni neighbors unequivocally demonstrates the existence of Ni-oxide species. For the NiNaMOR and NiNaZSM-5 catalysts the increase in the Ni-O and Ni-Ni coordination numbers suggests the formation of Ni-oxide particles. However, for NiNaMCM-22, which did not show such an increase it is concluded that the Ni ions remain on ion exchange positions after the NO reduction at 600 °C. The decrease in the accessibility of the Ni ions observed during the CO adsorption on the NiNaMCM-22 after reaction indicates that changes associated with the metal ions occurred, which are tentatively attributed to the migration of Ni to less accessible ion exchange positions.

The position of the X-ray absorption edge depends on the effective charge density of the adsorbing atom and reflects the tendency of an atom to bind the electrons (45). The position of the Ni-K edge of the fresh and used samples was 2.7 and 3.8 eV higher than that of reduced Ni. For the fresh samples the same position as for NiO was observed indicating that Ni was in an oxidation state of +2 in the Ni-exchanged zeolites. O'Grady *et al.* assigned an increase of the Ni-K edge energy of 1.5 eV to a change of +1 in the oxidation state of Ni (46, 47). Therefore, for the used samples the increase in the edge energy of +1 eV with respect to the NiO might indicate the simultaneous presence of species formally charged as Ni^{2+} and Ni^{3+} . However, a change in the local environment of Ni, in this case represents a more likely explanation of the +1 eV energy shift observed for the samples after

the reaction of NO with propane and propene in comparison with the fresh samples and the reference NiO. The decrease of the main edge energy has been reported to be due to the loss of nearest neighbors for Raney Ni catalysts (48). Therefore we suggest that the shift of the Ni K absorption edge to higher energies is related to the gain of new nearest neighbors as a consequence of the formation of NiO clusters.

Table 4.5 Decrease of the area of the bands of adsorbed CO at 0.1 mbar for samples after the reduction of NO with propane and propene in comparison with fresh samples.

Sample	Decrease of accessibility of isolated Ni ions [%]
NiNaMOR (propene) ^a	34
NiNaMOR (propane) ^b	31
NiNaZSM-5 (propene) ^a	57
NiNaZSM-5 (propane) ^b	72
NiNaMCM-22 (propene) ^a	66
NiNaMCM-22 (propane) ^b	67

^a After the reduction with propene

^b After the reduction with propane

In summary, all experiments indicate that the reduction of NO with propane and with propene in the presence of excess of oxygen cause structural changes of the Ni exchanged zeolites. These changes can be differentiated into (i) reversible changes resulting from the deposition of carbonaceous species and (ii) irreversible changes such as the dealumination of the zeolite and the migration of Ni. For NiNaMOR Ni oxide clusters of 8.0 Å and 7.0 Å size are formed during the reduction of NO with propene and propane but the accessibility of Ni for the reactants decreased only ~ 30 %. Therefore, this catalyst was only slightly deactivated under reaction

conditions. For NiNaZSM-5 a part of Ni migrates and forms Ni oxide clusters of 7.4 Å and 6.5 Å size, resulting in a decreased accessibility of active sites of 57 % and 72 % during the reduction of NO with propene and propane. For NiNaMCM-22, a decrease in the accessibility 67 % indicates that Ni migrates to positions where it is more difficult to be accessed under reaction conditions. Formation of NiO clusters was not observed for this material. Dealumination observed from the increase or appearance of a fraction of Al located in octahedral positions by ^{27}Al NMR, might cause the migration of Ni in the three cases.

4.5. Conclusions

Changes in the activity of Ni-exchanged zeolites were observed after the reduction of NO with propane and propene. The main reasons for such changes are related to (i) the deposition of carbonaceous species on the catalysts and (ii) structural changes associated to Ni and Al.

The effects of the deposition of carbonaceous species on the catalytic surface were more pronounced for those materials that contained a higher concentration of acid sites. A significant increase in the NO conversion was observed for NiNaZSM-5 exposed to the reaction mixture at 475 °C directly after activation, in comparison with the conversion obtained at 475 °C for a sample that has been exposed to the reaction mixture while varying temperatures between 150 °C and 600 °C, since the formation of the carbonaceous species is the highest at temperatures below 475 °C.

In the fresh materials, nickel is present as Ni^{2+} ions located in ion exchange positions in NiNaMOR, NiNaZSM-5 and NiNaMCM-22. Dealumination of the samples due to their exposure to the reaction mixtures at high temperatures caused the decrease of accessible Ni ions. For NiNaZSM-5 and to a lower extent for NiNaMOR the decrease in the accessibility of Ni resulted from the formation of

Ni-oxide clusters, while for NiNaMCM-22 Ni ions migrated to less accessible positions. In all cases, the reduced accessibility accounts for the decrease in the catalytic activity.

Acknowledgements

The authors acknowledge the staff of the beamline X1 (Dr. N. Haack, Dr. E. Welter and M. Herrmann) at Hasylab DESY, Hamburg, Germany for their kind help.

References

1. Wang, X., Chen, H. Y., and Sachtler, W. M. H., *Appl. Catal. B* **26**, L227 (2000).
2. Li, Y., and Armor, J. N., *Appl. Catal. B* **3**, L1 (1993).
3. Li, Y., and Armor, J. N., *Appl. Catal. B* **2**, 239 (1993).
4. Maisuls, S. E., Seshan, K., Feast, S., and Lercher, J. A., *Appl. Catal. B* **29**, 69 (2001).
5. Feng, X., and Hall, W. K., *Catal. Lett.* **41**, 45 (1996).
6. Feng, X., and Hall, W. K., *J. Catal.* **166**, 368 (1997).
7. Voskoboinikov, T. V., Chen, H. Y., and Sachtler, W. M. H., *Appl. Catal. B* **19**, 279 (1998).
8. Chen, H. Y., Voskoboinikov, T., and Sachtler, W. M. H., *J. Catal.* **180**, 171 (1998).
9. Chen, H. Y., Voskoboinikov, T., and Sachtler, W. M. H., *Catal. Today* **54**, 483 (1999).
10. Witzel, F., Sill, G. A., and Hall, W. K., *J. Catal.* **149**, 229 (1994).
11. Traa, Y., Burger, B., and Weitkamp, J., *Micropor. Mesopor. Mat.* **30**, 3 (1999).

12. Li, Y., and Armor, J. N., *J. Catal.* **150**, 376 (1994).
13. Kaucký, D., Vondrová, A., Dedecek, J., and Wichterlová, B., *J. Catal.* **194**, 318 (2000).
14. Sobalik, Z., Dedecek, J., Kaucký, D., Wichterlová, B., Drozdova, L., and Prins, R., *J. Catal.* **194**, 330 (2000).
15. Chajar, Z., Le Chanu, V., Primet, M., and Praliaud, H., *Catal. Lett.* **52**, 97 (1998).
16. Marturano, P., Drozdova, L., Kogelbauer, A., and Prins, R., *J. Catal.* **192**, 236 (2000).
17. d'Itri, J. L., and Sachtler, W. M. H., *Appl. Catal. B* **2**, L7 (1993).
18. Giroir-Fendler, A., Denton, P., Boreave, A., Praliaud, H., and Primet, M., *Topics in Catal.* **16/17**, 237 (2001).
19. Denton, P., Giroir-Fendler, A., Praliaud, H., and Primet, M., *J. Catal.* **189**, 410 (2000).
20. Quincoces, C. E., Kikot, A., Basaldella, E. I., and Gonzalez, M. G., *Ind. Eng. Chem. Res.* **38**, 4236 (1999).
21. Li, Y., Battavio, P. J., and Armor, J. N., *J. Catal.* **142**, 561 (1993).
22. Petunchi, J. O., and Hall, W. K., *Appl. Catal. B* **3**, 239 (1994).
23. Li, Z., and Flytzany-Stephanopoulos, M., *Appl. Catal. B* **22**, 35 (1999).
24. Lezcano, M., Ribotta, A., Miro, E., Lombardo, E., Petunchi, J. O., Moreaux, C., and Dereppe, J. M., *J. Catal.* **168**, 511 (1997).
25. Yan, J. Y., Lei, G.-D., Sachtler, W. M. H., and Kung, H. H., *J. Catal.* **161**, 43 (1996).
26. Chapter 3 of this thesis.
27. Ressler, T. J., *Physique IV* **7**, C2 (1997).
28. Ankudinov, A. L., and Rehr, J. J., *Phys. Rev. B.* **62**, 2437 (2000).
29. Santos Marques, A. L., Fontes Monteiro, J. L., and Pastore, H. O., *Micropor. Mesopor. Mat.* **32**, 131 (1999).

30. Lawton, S. L., Fung, A. S., Kennedy, G. J., Alemany, L. B., Chang, C. D., Hatzikos, G. H., Lissy, D. N., Rubin, M. K., Timken, H. K. C., Steuernagel, S., and Woessner, D. E., *J. Phys. Chem.* **100**, 3788 (1996).
31. Kolodziejski, W., Zicovich-Wilson, C., Corell, C., Perez-Pariente, J., and Corma, A., *J. Phys. Chem.* **99**, 7002 (1995).
32. Meriaudeau, P., Tuan, V. A., Nghiem, V. T., Lefevbre, F., and Ha, V. T., *J. Catal.* **185**, 378 (1999).
33. Stockenhuber, M., and Lercher, J. A., *Microporous Mater.* **3**, 457 (1995).
34. Jentys, A., Lugstein, A., and Vinek, H., *J. Chem. Soc., Faraday Trans.* **93**, 4091 (1997).
35. Moreau, F., Ayrault, P., Gnep, N. S., Lacombe, S., Merlen, E., and Guisnet, M., *Micropor. Mesopor. Mat.* **51**, 211 (2002).
36. Zholobenko, V. L., Makarova, M. A., and Dwyer, J., *J. Phys. Chem.* **97**, 5962 (1993).
37. Hadjiivanov, K., Knözinger, H., and Hihaylov, M., *J. Phys. Chem. B* **106**, 2618 (2002).
38. Bonneviot, L., Cai, F. X., Che, M., Kermarec, M., Legendre, O., Lepetit, C., and Olivier, D., *J. Phys. Chem. B* **91**, 5912 (1987).
39. Kermarec, M., Olivier, D., Richard, M., Che, M., and Bozon-Verduraz, F., *J. Phys. Chem. B* **86**, 2818 (1982).
40. Kasai, P. H., Bishop, R. J. J., and McLeod, D. J., *J. Phys. Chem.* **82**, 279 (1978).
41. Prakash, A. M., and Kevan, L., *J. Phys. Chem.* **100**, 19587 (1996).
42. Choo, H., Hong, S. B., and Kevan, L., *J. Phys. Chem. B* **105**, 1995 (2001).
43. Chapter 2 of this thesis.
44. Förster, H., and Hatje, U., *Solid State Ionics* **101**, 425 (1997).
45. Tadjeddine, A., Lahrichi, A., and Tourillon, G., *J. Electroanal. Chem.* **360**, 261 (1993).

46. O'Grady, W. E., Pandya, K. I., Swider, K. E., and Corrigan, D. A., *J. Electrochem. Soc.* **143**, 1613 (1996).
47. Marco, J. F., Gancedo, J. R., Gracia, M., Gautier, J. L., Rios, E., and Berry, F. J., *J. Solid State Chem.* **153**, 74 (2000).
48. Rothe, J., Hormes, J., Schild, C., and Pennemann, B., *J. Catal.* **191**, 294 (2000).

5. On the surface reactions during NO reduction with propene and propane on Ni-exchanged mordenite

The reduction of NO with propene and propane on Ni-exchanged mordenite was investigated by *in situ* infrared spectroscopy. Nitrates and nitro compounds were formed on the surface of the catalyst upon exposure to NO and O₂. In the presence of propene carbonaceous deposits consisting of oxygenated carbon species, condensed aromatic compounds and polyenes were formed on the surface. The concentration of deposits on the surface of the catalyst was considerably lower for propane. Isocyanates associated with Ni were identified as reactive intermediates during the reduction of NO to N₂. Oxygenated carbon species contribute to the formation of CO₂ and might be involved in the formation of isocyanates.

5.1. Introduction

Reduction of NO_x by hydrocarbons over metal-exchanged zeolites is a potential alternative to the NH_3 -SCR for the control of emissions in the presence of excess of oxygen. A wide range of transition metals such as Cu (1-3), Co (4-7), Fe (8-12), Ni (5, 6, 13) in combination with different zeolite structures were found to be active catalysts for the reduction of NO using hydrocarbons as reducing agents (2).

In the search of a catalyst with potential for the commercial application, understanding of the reaction mechanism is crucial. Different reaction mechanisms have been proposed in the literature. However, the complexity of the process has made it difficult to establish a commonly accepted mechanism. However, a general consensus about the role of oxygen for the formation of oxidized nitric oxide species (adsorbed NO_x) (10, 11, 14-16) and for the removal of carbonaceous species from the active metal sites (11, 17) exists. Nitrites (ONO^-) (18), nitro compounds (NO_2^-) (17, 19) and nitrates (NO_3^-) (14, 20-23) formed on the catalyst surface interact with the hydrocarbon molecules. Organic nitro (24, 25), organic nitrite (11, 26, 27) and nitroso (28, 29) compounds have also been suggested to take part in the NO_x reduction process. Isocyanates ($-\text{NCO}$) (15, 19, 24, 26, 27, 30, 31), nitriles ($-\text{CN}$) (18, 32), ammonia (24, 27) are intermediates reported leading to the formation of nitrogen. Fig. 5.1 shows a concise summary of the reaction mechanisms reported in literature.

The present contribution uses the assignment of bands obtained from a systematic IR study of the adsorption of NO, $\text{NO} + \text{O}_2$, C_3H_6 , C_3H_8 , $\text{C}_3\text{H}_6 + \text{O}_2$, $\text{C}_3\text{H}_8 + \text{O}_2$, over Ni loaded NaMOR to identify reaction intermediates for the reduction of NO with propane and propene. A reaction mechanism that agrees with observations made from kinetic experiments is proposed.

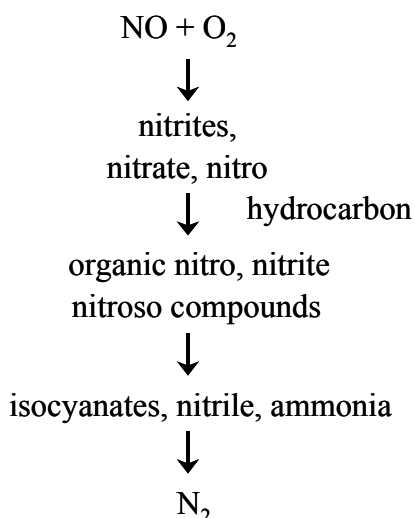


Figure 5.1 Concise summary of reaction mechanisms reported in the literature.

5.2. Experimental

5.2.1. Catalyst preparation

Mordenite (Si/Al=8.6) in the sodium form supplied by Tosoh, was used as parent material. Ni was incorporated by liquid phase ion exchange using an aqueous solution of $\text{Ni}(\text{NO}_3)_2$ at 80°C under continuous stirring for 24 h. Subsequently, the zeolite was separated from the solution by centrifugation, washed thoroughly with deionized water and dried overnight at 100°C . The chemical compositions of the sample is summarized in Table 5.1, details about the characterization of metallic and acid sites are reported in ref. (33, 34).

Table 5.1 Chemical composition and acid site concentration of the sample used

Sample	Si/Al*	Ni/Al*	Na/Al*	Ni loading (wt. %)	Acid site concentration [mmol/g]
NiNaMOR	8.9	0.2	0.6	1.9	0.40

*molar ratio

5.2.2. In situ infrared spectroscopy

IR measurements were performed with a Perkin Elmer 2000 FT-IR spectrometer in a cell allowing collecting spectra during the NO reduction (35). Samples were pressed into self-supported wafers and activated in He at 450°C (temperature increment 10°C/min) for 60 min. The adsorption of the reactants spectra of activated samples were recorded and subtracted from the spectra during the adsorption to enhance the changes in the spectra. During the NO reduction the flow of reactants (50 ml/min) was maintained over the sample for 1 h and subsequently the sample was flushed with He for 1 h. Desorption of the strongly adsorbed surface species was carried out by increasing the temperature with an increment of 5°C/min until 450°C. Spectra were collected during the adsorption, the purge with He and the temperature programmed desorption.

5.2.3. Catalytic measurements

The catalytic activity of the samples was studied in a plug flow system with a quartz reactor of 4 mm inner diameter containing 0.1 g of catalyst (particle size 300 µm). Concentrations of the reactants were 1000 ppm of NO, 1000 ppm of C₃H₆ or C₃H₈, 5% oxygen, the carrier gas was He. A total flow of 50 ml/min, resulting in a space velocity of 20000 h⁻¹, was used. The reaction products were analyzed by a chemiluminescence analyzer (TEI 42C) and a gas chromatograph (HP) with a TCD detector using a Molsieve column for separation of N₂, O₂ and CO and a Porapak column for N₂O, C₃H₆, C₃H₈ and CO₂ analysis. Before the reaction, the catalyst was pretreated *in situ* under helium flow at 600°C for 1 h. Kinetic measurements were carried out at temperature intervals of 25°C between 150 and 600°C.

5.3. Results

5.3.1. Kinetics of the reduction of NO in the absence of oxygen

Fig. 5.2 shows the reduction of NO with propane in the absence and in the presence of 5% oxygen on NiNaMOR. In the absence of O₂ the conversion of NO started increasing above 450°C and reached 100% at 550°C, while the N₂ yield was only 84%. The only nitrogen product observed in gas phase was N₂ and the carbon-containing products were CO₂, CO, CH₄, C₃H₆. The formation of CO and CO₂ resulted from the direct oxidation of C₃H₈ with O₂ being formed during the reduction of NO. C₃H₆ is a product of the dehydrogenation of C₃H₈ (36), while CH₄ results from cracking of C₃H₈ (37) or hydrogenolysis of C₃H₈ (38-40). From the mass-balance of carbon and nitrogen containing species a lack in the amount of product molecules formed was obtained. For example, at 600°C, 40% of C₃H₈ was converted, while the yields of CO₂, CO, CH₄ and C₃H₆ were only 8%, 5%, 10% and 6%, respectively, giving a sum of 29 %. This indicates that at high temperatures in the absence of oxygen a significant amount of coke containing carbon and nitrogen is deposited on the catalyst. In the presence of oxygen the maximum NO conversion of 73% was reached at 450°C. A high selectivity to N₂ was observed. The main carbon-containing product was CO₂, while small amounts of CO are attributed to the incomplete combustion of C₃H₈. CH₄ was also present in the outlet of the reactor. The reaction rate of the NO reduction with propane was enhanced by the presence of O₂ indicating the important role of this gaseous species in the mechanism.

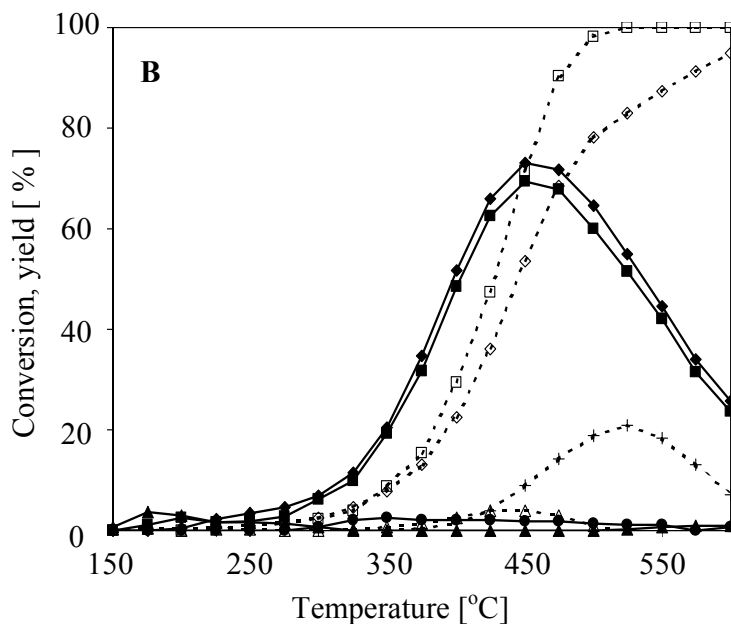
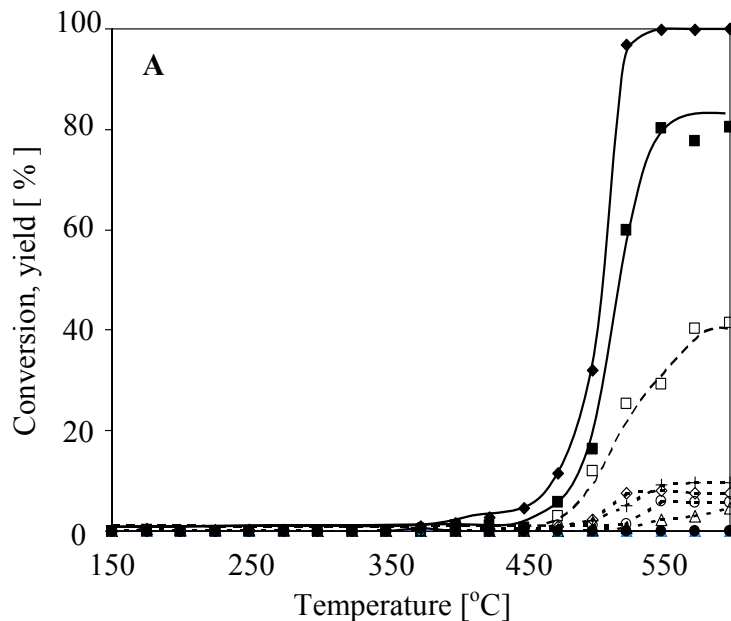


Figure 5.2 Conversion of (—◆—) NO and (---□---) propane, and yields of (—■—) N₂, (—●—) N₂O, (—▲—) NO₂, (---◇---) CO₂, (---△---) CO, (---⊕---) C₃H₆ and (---+---) CH₄ as a function of temperature for NiNaMOR during the reduction of NO with propane (A) in the absence of oxygen and (B) in the presence of excess of oxygen.

5.3.2. In situ infrared studies

5.3.2.1 NO and NO₂ adsorption, NO oxidation

The infrared spectra of NiNaMOR during the exposure to NO, NO + O₂, and NO₂ at 300°C are shown in Fig. 5.3. After exposing the sample to NO (Fig. 5.3,

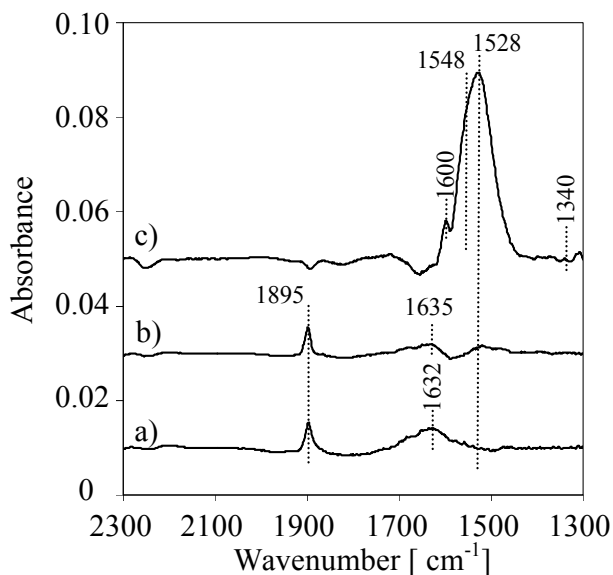


Figure 5.3 Infrared spectra of the adsorption of (a) NO, (b) NO + O₂ and (c) NO₂ on NiNaMOR at 300°C.

spectrum a) two weak bands at 1895 and 1632 cm⁻¹, assigned to mononitrosyl species (11, 16, 23, 26, 41-43) and bridging bidentate nitrate species (16, 44) were observed. Similar bands were observed after 60 minutes of exposure of the sample to NO + O₂ (Fig. 5.3, spectrum b). In addition a very weak band at 1528 cm⁻¹, indicating the presence of monodentate nitrate species (21, 44, 45) was observed. The introduction of NO₂ (Fig. 5.3, spectrum c) leads to the appearance of a broad band at 1528 cm⁻¹ assigned to surface monodentate nitrates. Bands at 1600, 1548 and 1340 cm⁻¹ were also visible. The bands at 1600 and 1340 are characteristic of nitro compounds (44). The band at 1548 cm⁻¹ was assigned to chelating bidentate nitrate species (44, 46). The bands observed after the exposure of the sample to NO₂ were much more intense than those obtained after exposure to NO and NO + O₂.

5.3.3. Reactivity of adsorbed nitrogen oxygen species with hydrocarbons

At 150°C, a sample previously exposed to a flow of NO + O₂ was further purged with He for 1 h (Fig. 5.4A, spectrum a). A very intense band at 1521 cm⁻¹,

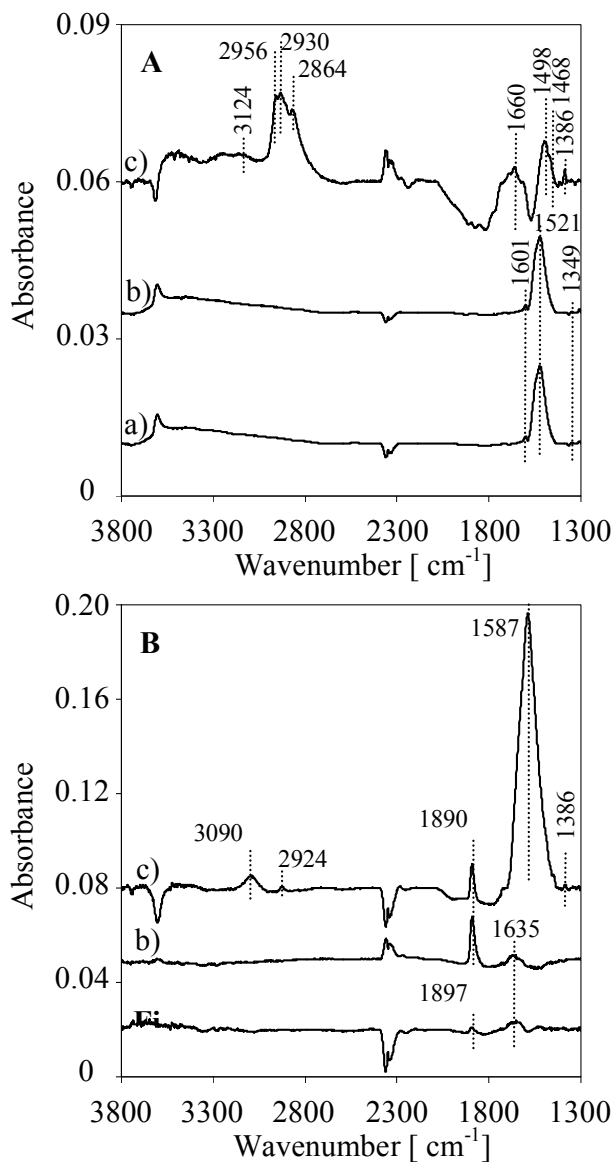


Figure 5.4 Infrared spectra of NiNaMOR after adsorption of NO + O₂ followed by (a) purge with He. Further exposure to (b) C₃H₈ and (c) C₃H₆ at (A) 150°C and (B) 300°C.

assigned to monodentate nitrate species was visible. Two weak bands at 1601 and 1349 cm⁻¹ were also present. These bands are tentatively assigned to nitro compounds. This sample was then exposed to a flow of C₃H₈ and purged with He (Fig. 5.4A, spectrum b). The introduction of C₃H₈ caused the appearance of a weak band at 2967 cm⁻¹ attributed to C-H stretching vibrations (47). The band disappeared upon purging the reactor with He (Fig. 5.4A, spectrum b).

In a similar procedure, surface NO_x species were produced by the adsorption of $\text{NO} + \text{O}_2$ followed by He purge at 150°C . The introduction of C_3H_6 to this sample led to drastic changes in the spectrum. All the adsorbed species remained after purging (Fig. 5.4A, spectrum c). Bands in the region $3000\text{-}2800\text{ cm}^{-1}$ assigned to CH_2 and CH_3 stretching vibrations appeared (23, 46, 47). A broad and weak band at 3124 cm^{-1} ascribed to OH of an allyl oxime was also present. The intense band at 1521 cm^{-1} corresponding to monodentate nitrate was replaced by a band at 1498 cm^{-1} , with a shoulder at 1468 cm^{-1} possibly related to light aromatics (25, 47). A band at 1660 cm^{-1} , which can be assigned to organic nitrito compounds, appeared (47). Bands at 1460 and 1386 cm^{-1} are attributed to CH_2 and CH_3 deformation vibrations (47, 48).

The sample was also exposed to $\text{NO} + \text{O}_2$ at 300°C and subsequently purged with He (Fig. 5.4B, spectrum a). The introduction of C_3H_8 to this sample (Fig. 5.4B, spectrum b) caused the replacement of the band at 1897 cm^{-1} assigned to mononitrosyl species by a band at 1890 possibly due to the presence of an allene species, $\text{C}=\text{C}=\text{CH}_2$ (47). No further changes were observed for C_3H_8 . In the case of the introduction of C_3H_6 , the weak bands in the range $1800\text{-}1300\text{ cm}^{-1}$ present in the sample after adsorption of $\text{NO} + \text{O}_2$ at 300°C were rapidly masked by the intense band that extended in the region $1700\text{-}1400\text{ cm}^{-1}$ with a maximum at 1587 cm^{-1} , assigned to carbonaceous deposits. Bands at 3090 , 2924 and 1386 cm^{-1} attributed to asymmetric stretching vibration of unsaturated CH_2 , stretching vibration of CH_2 and CH_3 deformation (47), respectively, also appeared when C_3H_6 was adsorbed. A band at 1890 cm^{-1} corresponding to surface allene species was also observed.

5.3.3.1 Reaction mixture

Fig. 5.5A shows the adsorption of NO + O₂ + C₃H₆ at 150°C and 300°C. The assignments of the bands present in the spectrum at 150°C are summarized in Table 5.2. Bands assigned to amine (3305 cm⁻¹) (47), allyl oxime (3125, 1670, 1465, 1436 and 1386 cm⁻¹) (26, 47), C-H stretching vibrations (2954, 2930 and 2860 cm⁻¹), acrolein (1670 cm⁻¹) (25), bridging bidentate nitrates (1638 cm⁻¹), C=C (1638 cm⁻¹) (14, 22, 48), nitro compounds (1602 and 1345 cm⁻¹), carboxylates (1602 and 1436 cm⁻¹) (25), acetates (1465 cm⁻¹) (46, 49) and formates (1386 cm⁻¹) (49) were observed, when the mixture was introduced into the cell at 150°C (Fig. 5.5A, spectrum a). The broad band at 1530 cm⁻¹ may actually consist of two overlapping bands at 1550 and 1520 cm⁻¹, which can be assigned to organic nitro compounds (46, 50, 51) and surface monodentate nitrates, respectively. The band at 1670 cm⁻¹ is assigned to organic nitrito compounds, because its wavenumber is very close to 1662 cm⁻¹ previously related to these species (46). The band at 1602 cm⁻¹, however, might contain contributions from aromatic species (24). Very weak bands were observed at 2275 and 2188 cm⁻¹, which are assigned to -NCO bonded to Al³⁺ (52-54) and to Ni²⁺ (50, 51). In addition a weak band at 2146 cm⁻¹ assigned to -CN species (50) was observed.

When the reaction mixture (NO + C₃H₆ + O₂) was introduced into the cell at 300°C (Fig. 5.5A, spectrum b), a broad band at 3108 cm⁻¹ and a weak band at 2934 cm⁻¹ appeared. The former is assigned to an OH stretching vibration of an allyl oxime (CH₂=CH-CH=N-OH) and the latter to a stretching vibration of CH₂. A very weak band at 3392 cm⁻¹, attributed to the asymmetric stretching vibration of amines, was also observed. Since the first minutes of exposure a very broad band with a maximum at 1599 cm⁻¹ and a shoulder at 1648 cm⁻¹ was observed. A band at 2268 cm⁻¹ due to Al³⁺-bound NCO was also present. A band of weak intensity at 2190 cm⁻¹, assigned to Ni²⁺-bound NCO appeared. The asymmetry of the band at

Table 5.2 Assignment of infrared bands during adsorption of NO + C₃H₆ + O₂ at 150°C.

Wavenumber [cm ⁻¹]	Assignment	Species	Ref.
3305	ν_s (NH ₂)	R-NH ₂	(47)
3125	ν_{as} (=CH ₂) ν (OH) of an allyl oxime	C=N-OH	(47) (26, 47)
2954	ν_{as} (CH ₃)		(47)
2930	ν_{as} (CH ₂)		(47)
2860	ν_s (CH ₂)		(47)
2275	out-of-phase ν (N=C=O)	Al ³⁺ -NCO	(52-54)
2188	out-of-phase ν (N=C=O)	Ni ²⁺ -NCO	(52-54)
2146	ν (C \equiv N)	C \equiv N	(14, 41)
	ν (C=O) of acrolein		(25)
1670	ν (N=O) of organic nitrito compound ν (C=N) of an allyl oxime	R-O-N=O C=N-OH	(44, 46) (47)
1638	ν (C=C) (ν_3) bridging bidentate nitrate	$\begin{array}{c} \text{O} \\ \\ \text{N} \\ / \quad \backslash \\ \text{O} \quad \text{O} \\ \quad \\ \text{M} \quad \text{M} \end{array}$	(14, 22, 48) (44)
	ν_{as} (CO ₂) of a carboxylate	$\begin{array}{c} \text{O} \quad \text{O} \\ \backslash \quad / \\ \text{N} \\ \\ \text{M} \end{array}$	(25)
1602	Aromatic species or polyenes ν_{as} (NO ₂) of nitro compound		(24) (44)
1550	ν_{as} (NO ₂) of organic nitro compound	R-NO ₂	(25, 44, 50, 51)
1520	(ν_3) monodentate nitrate	$\begin{array}{c} \text{O} \quad \text{O} \\ \backslash \quad / \\ \text{N} \\ \\ \text{O} \\ \\ \text{M} \end{array}$	(21, 44, 45)
1465	ν (C-O) of an acetate group CH ₂ , CH ₃ deformation		(46, 49) (47)
1436	ν_s (CO ₂) of a carboxylate OH deformation of an allyl oxime	C=N-OH	(25) (47)
1386	CHO deformation of a formate group CH ₃ deformation		(49) (47)
1344	ν_s (NO ₂) of nitro compound ν_s (NO ₂) of organic nitro compound	$\begin{array}{c} \text{O} \quad \text{O} \\ \backslash \quad / \\ \text{N} \\ \\ \text{M} \end{array}$	(44) (44)

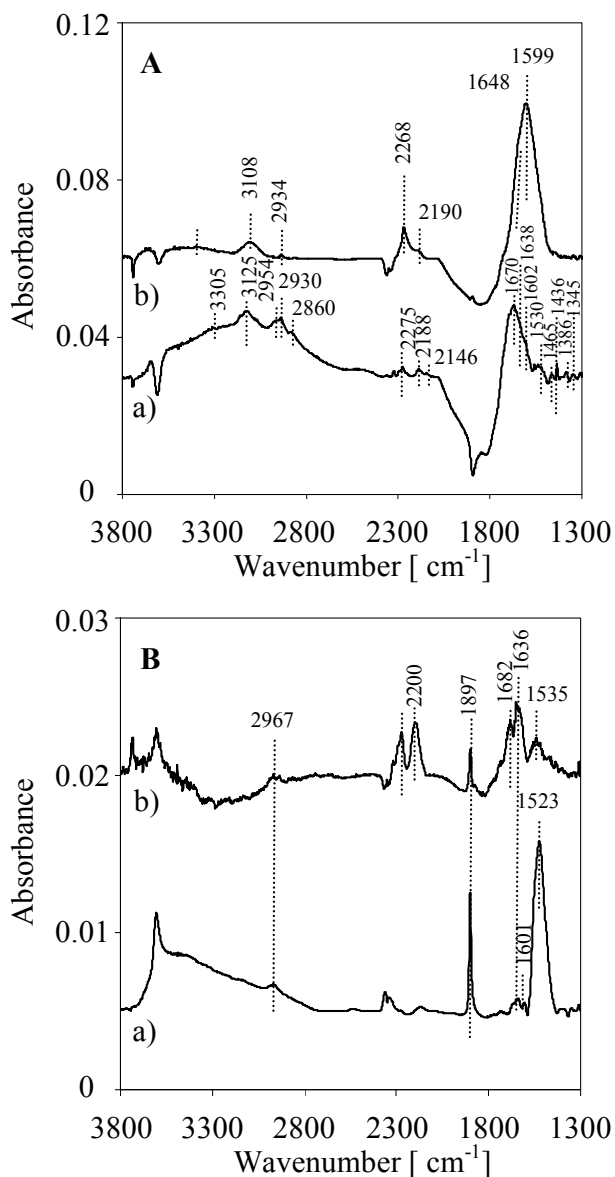


Figure 5.5 Infrared spectra of the adsorption of (A) NO + O₂ + C₃H₆ and (B) NO + O₂ + C₃H₈ on NiNaMOR at (a) 150°C and (b) 300°C.

2268 cm⁻¹ indicates the presence of an overlapping band at approximately 2245 cm⁻¹. The broad band observed in the region 1730-1450 cm⁻¹ with a maximum at 1599 cm⁻¹ is attributed to the presence of carbonaceous deposits on the sample. According to the position of the band, it can be assigned to aromatic compounds, e.g., alkyl-substituted naphthalenes, and polyenes whose characteristic bands appear at 1510-1540 cm⁻¹ and 1570-1620 cm⁻¹ (55-58). This broad band might

mask the presence of the oxygenated carbon species, e.g., acetate, formate, carboxylate, acrolein, observed at 150°C.

Fig. 5.5B shows the infrared spectra collected during NO + O₂ + C₃H₈ adsorption at 150°C and 300°C. At 150°C (Fig. 5.5B, spectrum a), bands at 2967, 1897, 1636, 1601 and 1523 cm⁻¹ were observed. The bands at 1897, 1636, 1601 and 1523 cm⁻¹ can be assigned to mononitrosyl species, surface bridging bidentate nitrate, nitro compounds and monodentate nitrate species. The band at 2967 cm⁻¹ was attributed to the C-H stretching vibrations of C₃H₈.

The introduction of the reaction mixture (NO + O₂ + C₃H₈) at 300°C led to the appearance of bands at 1897 and 1523 cm⁻¹ (Fig. 5.5B, spectrum b). The band at 1897 cm⁻¹ was due to mononitrosyl species and can also be assigned to allene species. Surface monodentate nitrates were detected at 1523 cm⁻¹ during the first minutes of the exposure and were replaced by a broad band at 1535 cm⁻¹. This band can be attributed to overlapping bands at 1550 and 1520 cm⁻¹ caused by organic nitro compounds and monodentate nitrate species. Bands at 2271 and 2200 cm⁻¹, assigned to Al-NCO and Ni-NCO were also visible. The intensity of the bands at 1682 cm⁻¹ assigned to surface acrolein and organic nitrito compound, and at 1636 cm⁻¹ assigned to C=C stretching and bridging bidentate nitrate species increased with exposure time. The weak band at 2967 cm⁻¹ corresponding to C-H stretching vibrations of the C₃H₈ remained stable during the adsorption.

Temperature programmed desorption

Fig. 5.6 shows the spectra of the species adsorbed collected during the temperature programmed desorption up to 450°C after the exposure of NiNaMOR to NO + C₃H₆ + O₂ at 150°C. As the temperature increased a band at 2242 cm⁻¹ due to NCO bound to Ni²⁺ appeared and reached a maximum in intensity at 300°C (46),

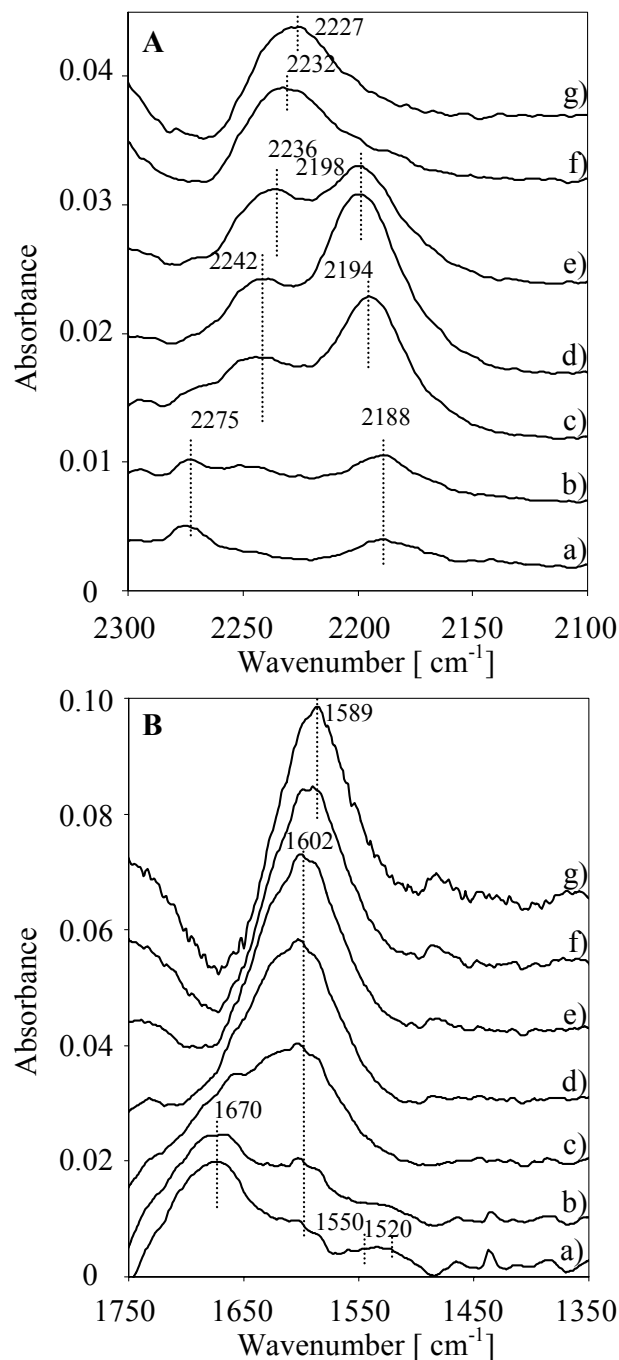


Figure 5.6 Infrared spectra during temperature programmed desorption after exposure at 150°C of NiNaMOR to NO + O₂ + C₃H₆ (a) 150°C, (b) 200°C, (c) 250°C, (d) 300°C, (e) 350°C, (f) 400°C and (g) 450°C in the region (A) 2300-2100 cm^{-1} and (B) 1750-1350 cm^{-1} .

the intensity of the band at 2188 cm^{-1} due to NCO bound to Ni²⁺ increased and the maximum of the peak shifted to higher frequency, reaching 2198 cm^{-1} at 300°C. At temperatures above 300°C the intensity of the band at 2198 cm^{-1} decreased, while the band at 2242 cm^{-1} shifted to 2227 cm^{-1} . In the region 1750-1350 cm^{-1} (Fig.

5.6B), the oxygenated carbon species, e.g., acetate, formate, carboxylate, acrolein, disappeared with increasing temperature giving rise to a broad intense band with a maximum at 1589 cm^{-1} . A very weak band at 3285 cm^{-1} , due to surface amines, was visible.

Fig. 5.7 shows the spectra collected during the temperature programmed desorption of the surface species present in the sample after the He purge of NiNaMOR exposed to $\text{NO} + \text{C}_3\text{H}_6 + \text{O}_2$ at 300°C . As the temperature was increased a broad peak with a shifting maximum from 2245 cm^{-1} at 400°C to 2230 cm^{-1} at 450°C appeared. The intensity of the band at 2190 cm^{-1} increased reaching a maximum at 400°C ; the position of the maximum shifted to 2195 cm^{-1} . Only one band at 1601 cm^{-1} was present in the region $1350\text{-}1750\text{ cm}^{-1}$ (Fig. 5.7B) and attributed to carbonaceous deposits on the sample. As the temperature increased the intensity of this band decreased slightly and shifted to 1590 cm^{-1} at 450°C . A very weak band at 3387 cm^{-1} assigned to surface amines was present.

Fig. 5.8 shows the spectra collected during the temperature programmed desorption carried out after purging the sample exposed to the reaction mixture containing C_3H_8 at 300°C with He. The intensity of the band assigned to Al-NCO (2271 cm^{-1}) decreased with temperature and disappeared at 400°C . The intensity of the band at 2194 cm^{-1} corresponding to Ni-NCO reached a maximum at 400°C , while the presence of the second type of Ni-NCO species at 2227 cm^{-1} , was not evident at temperatures below 400°C . The appearance of two different bands corresponding to Ni-NCO species is probably an indication of the presence of Ni^{2+} ions in different locations inside the zeolite structure. In the region $1750\text{-}1350\text{ cm}^{-1}$ the weak bands at 1684 , assigned to surface acrolein and organic nitrito compound, 1636 cm^{-1} due to C=C stretching and bridging bidentate nitrate species and 1541 cm^{-1} attributed to organic nitro compounds, disappeared giving rise to a broad band at 1591 cm^{-1} .

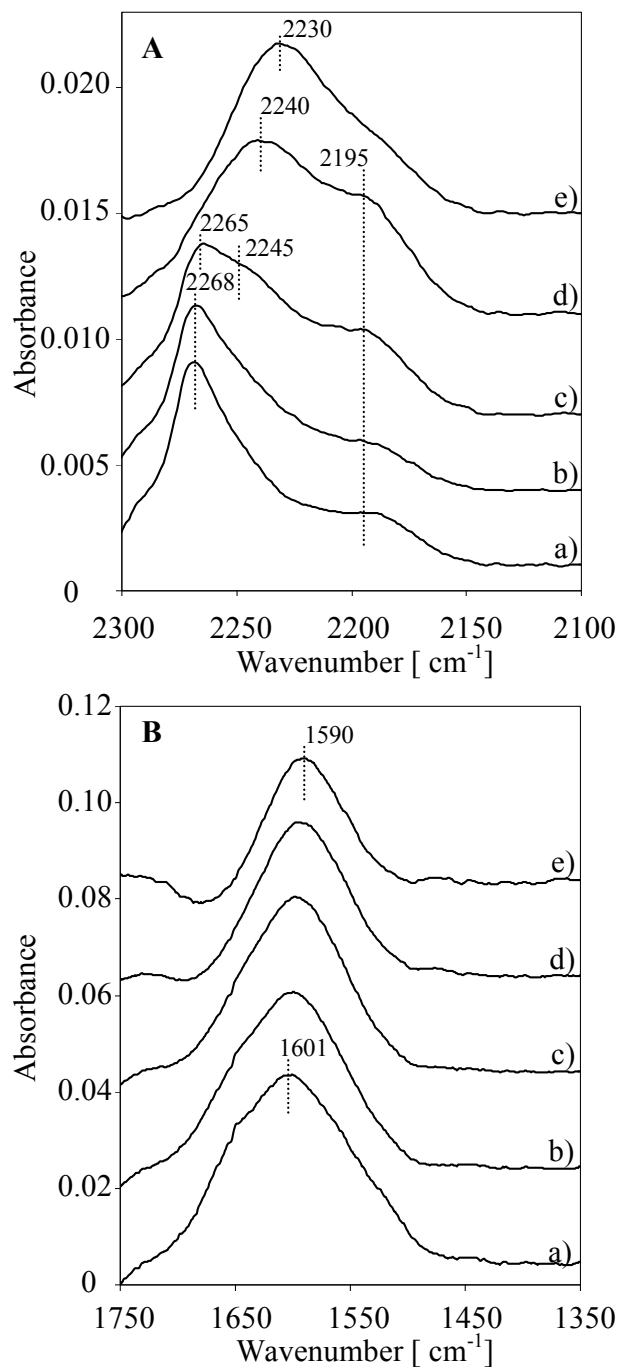


Figure 5.7 Infrared spectra during temperature programmed desorption after exposure at 300°C of NiNaMOR to NO + O₂ + C₃H₆. (a) Before He purge, (b) 300°C, (c) 350°C, (d) 400°C and (e) 450°C.

Temperature programmed reaction

Fig. 5.9 shows the changes in the spectra during exposure of NiNaMOR to the

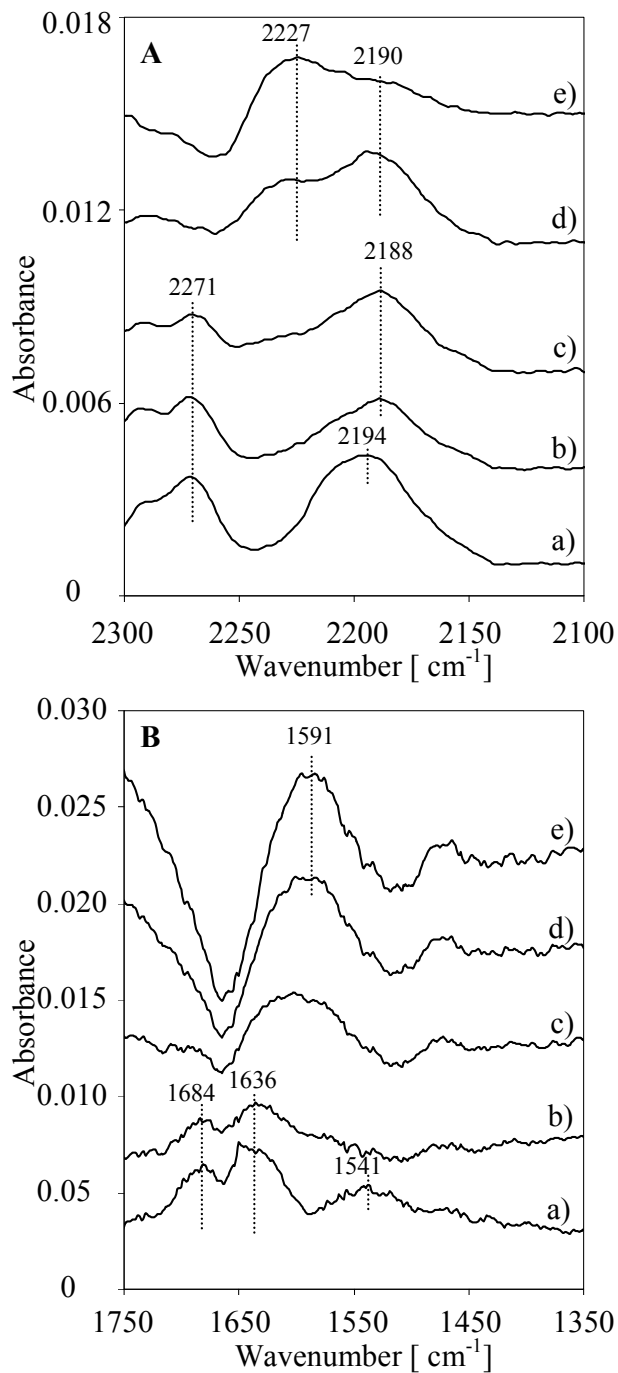


Figure 5.8 Infrared spectra during temperature programmed desorption after exposure at 300°C of NiNaMOR to NO + O₂ + C₃H₈. (a) Before He purge, (b) 300°C, (c) 350°C, (d) 400°C and (e) 450°C.

reaction mixture (NO + O₂ + C₃H₆) between 150 and 450°C. The sample was exposed for first time to the reaction mixture at 50°C. The temperature was then increased to 150°C (Fig. 5.9, spectrum a). The bands were better resolved in

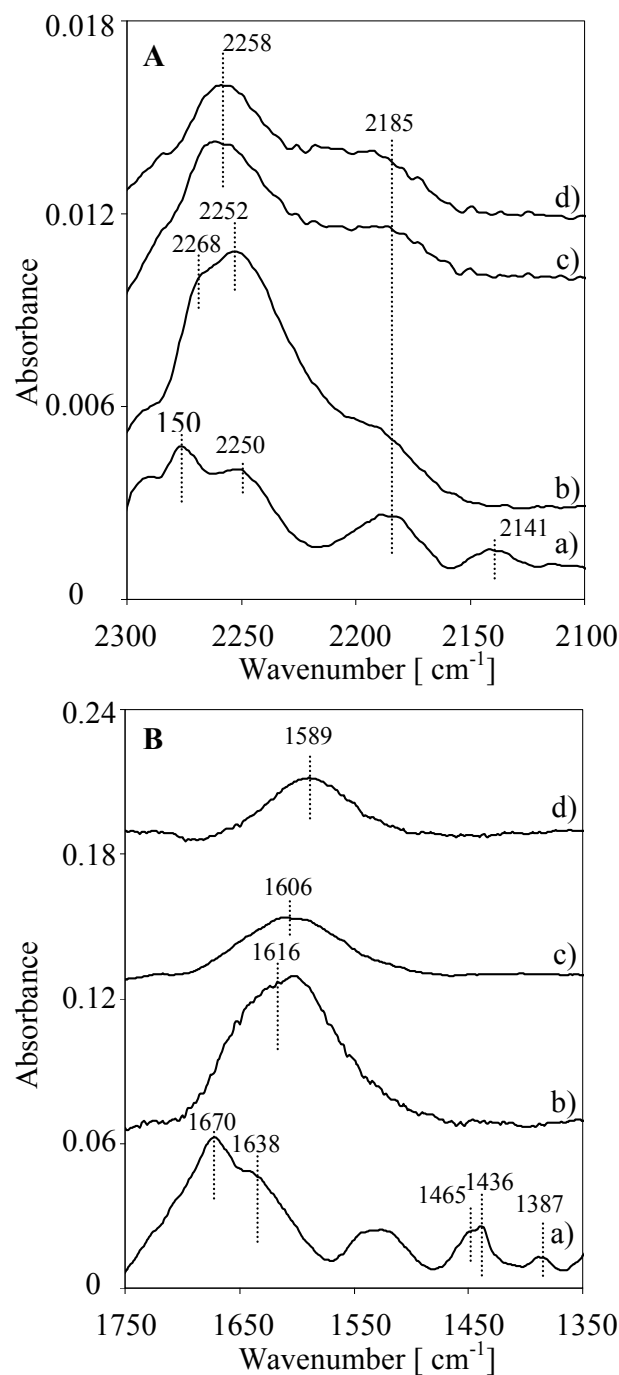


Figure 5.9 Infrared spectra collected during TPR of $\text{NO} + \text{O}_2 + \text{C}_3\text{H}_6$ on NiNaMOR. Spectra at (a) 150°C, (b) 300°C, (c) 400°C and (d) 450°C in the region (A) 2300-2100 cm^{-1} and (B) 1750-1730 cm^{-1} .

comparison with the spectrum during TPD (Fig. 5.6, spectrum a). Bands at 2276, 2250, 2185 and 2141 cm^{-1} assigned to Al-NCO, Ni-NCO and CN species were observed. At 150°C the same position for most of the bands was observed in comparison with the experiment of the adsorption of $\text{NO} + \text{O}_2 + \text{C}_3\text{H}_6$ at 150°C

(Fig. 5.5A, spectrum a). At 300°C bands at 3317, 3125, 2933, 2250, 2198 cm^{-1} and a broad band with a maximum at 1616 cm^{-1} were observed. After the temperature was increased to 400°C, three bands were present at 3116, 2258 and 1606 cm^{-1} . When temperature was increased to 450°C the bands at 3118, 2258 and 1589 cm^{-1} were less intense in comparison to those at 400°C. The intensity of the band at 2258 cm^{-1} decreased considerably, when the sample was purged with He.

Fig. 5.10 shows the spectra collected during the TPR of $\text{NO} + \text{O}_2 + \text{C}_3\text{H}_8$ from 150°C up to 450°C. Fig. 5.10A shows the spectra during the TPR of $\text{NO} + \text{O}_2 + \text{C}_3\text{H}_8$ in the region of isocyanates. At 150°C, isocyanates were not present but a band at 2166 cm^{-1} corresponding to NO^+ . Isocyanates associated to Al (2270 cm^{-1}) and Ni (2200 cm^{-1}) were observed at 300°C. In contrast to the spectra collected during the TPD after $\text{NO} + \text{O}_2 + \text{C}_3\text{H}_8$ where a second Ni-NCO species was observed at 2227 cm^{-1} , during the TPR no band corresponding to such a species was observed. In the region 1750-1350 cm^{-1} (Fig. 5.10B) weak bands ascribed to nitrates and nitro compounds were visible at temperatures up to 400°C.

5.4. Discussion

5.4.1. Importance of the presence of oxygen

The reduction of NO with hydrocarbons on NiNaMOR in the absence of oxygen took place only at temperatures above 450°C. Significant amounts of carbonaceous species containing also nitrogen were found deposited on the catalyst (see Fig. 5.2A). Oxygen was found to be required for the formation of adsorbed NO_x species and oxygenated carbon species observed on the surface of NiNaMOR.

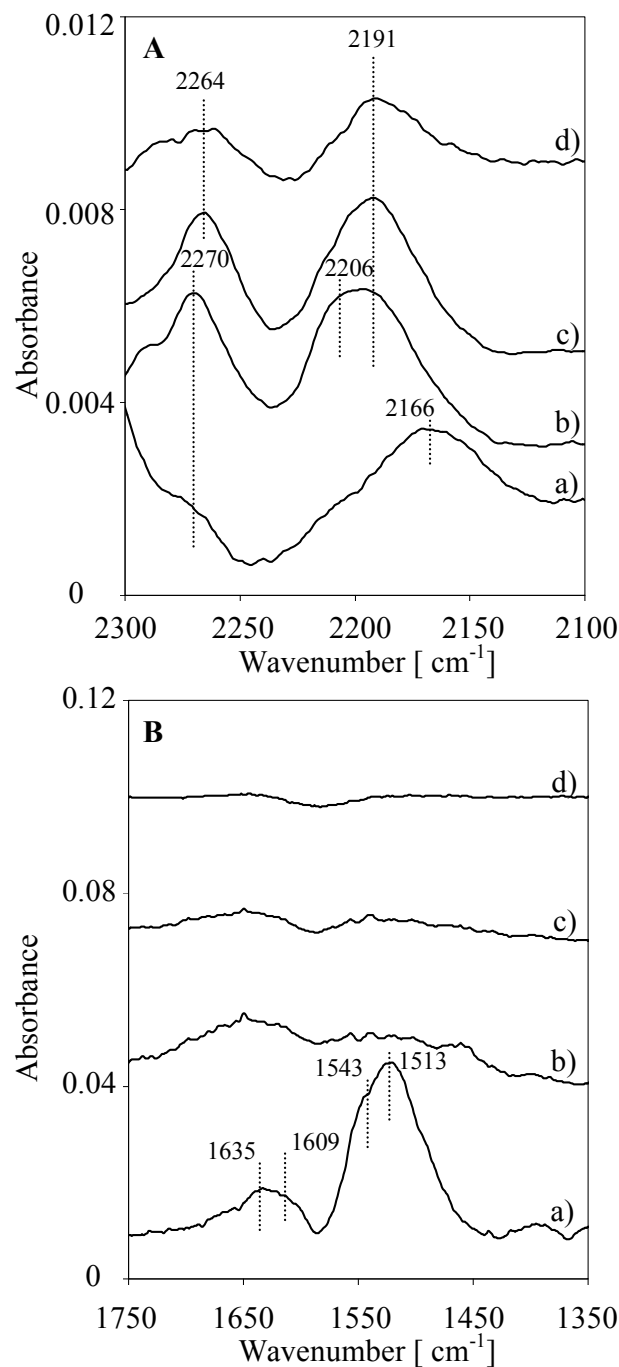


Figure 5.10 Infrared spectra collected during TPR of $\text{NO} + \text{O}_2 + \text{C}_3\text{H}_8$ on NiNaMOR. Spectra at (a) 150°C , (b) 300°C , (c) 400°C and (d) 450°C in the region (A) $2300\text{-}2100\text{ cm}^{-1}$ and (B) $1750\text{-}1730\text{ cm}^{-1}$.

5.4.2. Stability and reactivity of adsorbed NO_x species

At 150°C , monodentate nitrates are the predominant adsorbed NO_x during $\text{NO} + \text{O}_2$ adsorption (see Fig. 5.4A, spectrum a). Small amounts of NO_2^- were also

observed. When the sample containing adsorbed NO_x species was exposed to the flow of C_3H_6 a low extent formation of light aromatic species was observed (see Fig. 5.4A, spectrum b).

At 300°C , monodentate nitrates were observed only during the first minutes of exposure of the sample to $\text{NO} + \text{O}_2$. These species were replaced by low concentrations of bridging bidentate nitrates indicating that the symmetry of NO_3^- changes as exposure time increased. The immediate formation of carbonaceous deposits was observed upon the exposure of the former sample to C_3H_6 . Surface species like isocyanates and cyanides were not observed.

The decrease in intensity of the band assigned to the bridged hydroxyl groups of the zeolite was evident at 150°C and 300°C after the exposure of the sample to C_3H_6 (Fig. 5.4) indicating the blockage of these sites due to presence of the olefin. This was not observed in the case of C_3H_8 .

5.4.3. Reaction intermediates

The IR spectra suggest that oxygenated carbon species, such as acetate, formate, carboxylate, and acrolein are formed on the catalyst, when C_3H_6 and O_2 are admitted at 150°C . Similar species together with species such as allyl oximes, isocyanates, cyanides, organic nitro compounds and organic nitrito compounds were observed when the sample was exposed to the reaction mixture at 150°C (Fig. 5.5A, spectrum a). Depending on the experimental conditions isocyanates were observed associated with different sites of the material, i.e., Al and Ni. Generally, these species were stable to the purge of He and remained, at least partly, adsorbed on the surface of the catalyst. Organic oxygenate species formed on the surface of the catalyst at 150°C , i.e., acrolein, carboxylate, and organic nitrito and nitro compounds species associated to the bands at 1670 and 1550 cm^{-1} (Fig. 5.6B), decomposed at temperatures above 250°C under He flow to give rise to small

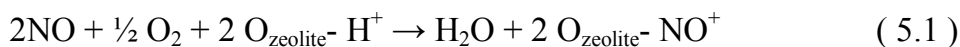
amounts of aromatic coke (band at 1590 cm^{-1}). In parallel with these transformations, the appearance of a second type of Ni-NCO was observed (Fig. 5.6A). The difference in the wavenumber of the two types of Ni-NCO (~ 2200 and $\sim 2230\text{ cm}^{-1}$) is attributed to different coordinations or location in the zeolite lattice of the Ni ions (54). When the adsorption of $\text{NO} + \text{O}_2 + \text{C}_3\text{H}_6$ was carried out at 300°C , a high concentration of isocyanates bound to Al was observed together with a high amount of carbonaceous deposits (Fig. 5.5A, spectrum a). As the temperature was increased in a flow of He (TPD, see Fig. 5.7), the concentration of Ni bound isocyanates also increased, while the amount of carbonaceous deposits decreased. This decrease is related to the combustion of oxygenated species. At temperatures above 250°C the band at $\sim 2230\text{ cm}^{-1}$ suggests the presence of Ni-NCO species. Their presence coincides with the temperatures where NO conversion starts to be significant during the kinetic experiments hinting that these species might act as reaction intermediates.

Cyanides are weak species not stable to the purge with He and are observed only at 150°C when the sample was exposed to the reaction mixture (Fig. 5.5A, spectrum a, and Fig. 5.9A, spectrum a). Reaction between gas phase C_3H_6 or C_3H_8 and the surface species originated from adsorption of $\text{NO} + \text{O}_2$ does not lead to formation of isocyanates or cyanides at 150 and 300°C (Fig. 5.4).

In contrast to C_3H_6 , at low temperatures C_3H_8 does not effectively compete for acid sites. The nitrogen-containing species are adsorbed preferentially. At 300°C , the concentration of surface species is, therefore, much lower with C_3H_8 than with C_3H_6 . Small amounts of organic deposits and nitrates are present on the surface upon the adsorption of the reaction mixture at 300°C (see Fig. 5.5A, spectrum b), which further decrease upon purging the sample with He. However, the species are stable up to 350°C . Also for propane, the disappearance during TPD coincides with the appearance of a second type of Ni-NCO species and with the point of increasing NO conversion during the kinetic experiments (see Fig. 5.2B).

During TPR of $\text{NO} + \text{C}_3\text{H}_6 + \text{O}_2$ the band at 2230 cm^{-1} related to one of the Ni-NCO species is substituted by a band at 2250 cm^{-1} , which shifted to higher wavenumbers with temperature. The absence of the band at 2230 cm^{-1} during the exposure of NiNaMOR to the reaction mixture might indicate that the corresponding species is a reaction intermediate, which reacts with the gas flow O_2 , and/or $\text{NO} + \text{O}_2$ in an Eley Rideal type reaction to give rise to dinitrogen. The absence of the band at $\sim 2230 \text{ cm}^{-1}$ attributed to Ni-NCO under these conditions suggests that similar reaction intermediates may be involved during the NO reduction with propene and with propane.

The scheme of the reaction mechanism proposed for the reduction of NO with C_3H_6 or C_3H_8 is shown in Fig. 5.11. Nitrates and nitro compounds are formed on the surface of the catalyst from the interaction of NO and O_2 . They transform to organic nitrite and nitro compounds in the presence of hydrocarbons. As mentioned above, the partially acidic nature of the catalyst (33) justifies the formation of nitrosonium ion, NO^+ (29) (see Fig. 5.10A, spectrum a),



which reacts with the hydrocarbons to form nitroso compound. The latter has been reported to be unstable and therefore not visible during the reaction (28, 29). Organic nitro, nitrites and nitroso compounds are transformed to surface oximes. These species rearrange subsequently to isocyanates. Finally, isocyanates react with NO_2 in gas phase and give rise to N_2 (15, 19, 31). However, in the presence of water isocyanates can be hydrolyzed readily giving rise to amines (59) and/or ammonia (24, 27), which actually reduce NO_2 to N_2 .

Independently if C_3H_8 or C_3H_6 is used as reducing agent, the same principal reaction mechanism is concluded taking place. However, C_3H_8 is dehydrogenated to C_3H_6 in the first step. This step is concluded to be catalyzed by the transition metal ions at exchange sites and in oxide clusters acting as active sites (60).

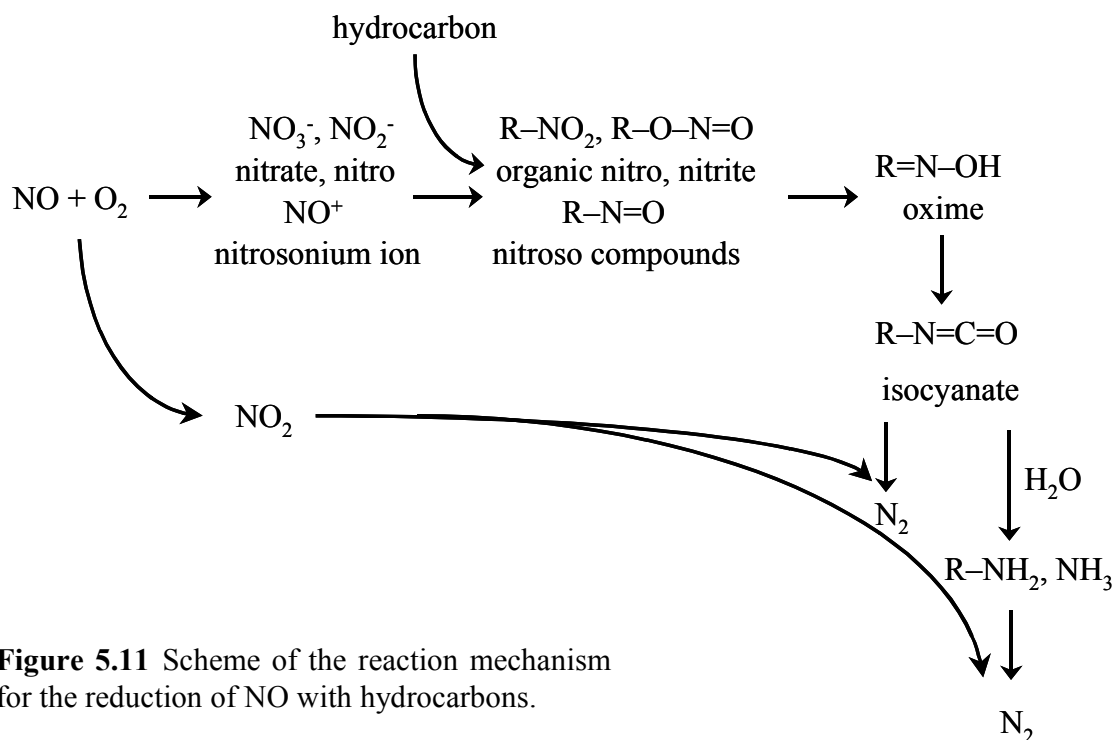


Figure 5.11 Scheme of the reaction mechanism for the reduction of NO with hydrocarbons.

The apparent rate-limiting step is concluded to be related with the formation of a particular isocyanate affiliated with Ni cations (represented by the band at 2230 cm⁻¹). Such bands were observed, when the reaction temperature was increased and alkanes and alkenes were absent from the gas flow. In the presence of reactive gases, e.g., during TPR, its absence is attributed to the immediate formation of N₂, which prevents that these species are observed adsorbed on the surface. Isocyanates adsorbed on Ni (~2195 cm⁻¹), and Al (~2270 cm⁻¹) might be less efficient reaction intermediates in comparison with isocyanates adsorbed on Ni whose N=C=O out-of-phase stretching vibration occurs at ~2230 cm⁻¹.

Oxygenated carbon species, e.g., formaldehyde formate, acetate, acrolein, carboxylate, undergo combustion reaction to form CO₂, and their participation in the formation of isocyanates cannot be ruled out. The concentration of these species on the catalytic surface is considerably larger in the case of the reduction of NO with C₃H₆ in comparison with C₃H₈.

5.5. Conclusions

The presence of oxygen is crucial for the reduction of NO with hydrocarbons on Ni-exchanged zeolites. The reaction mechanism involves the formation of adsorbed NO_x species, e.g., NO₃⁻ and NO₂⁻, which react with the hydrocarbons and form organic nitrito and nitro compounds. The presence of acid sites in the sample explains the formation of nitrosonium ion NO⁺ that might be also involved in the reaction mechanism as a precursor of nitroso compounds. Isocyanates are formed from the rearrangement of the surface species and through a reaction Eley-Rideal type in the presence of gas phase NO₂ dinitrogen is formed. Isocyanates can also be hydrolyzed to amines and ammonia, which reduce NO₂ to N₂. Isocyanates are present associated with Ni and Al, however, it is believed that one type of Ni-NCO is efficient for the formation of N₂. Oxygenated carbon species, e.g., formaldehyde, formate, acetate, carboxylate, acrolein, contribute to the formation of CO₂ and might be involved in the formation of isocyanates.

References

1. Yahiro, H., and Iwamoto, M., *Appl. Catal. A* **222**, 163 (2001).
2. Traa, Y., Burger, B., and Weitkamp, J., *Micropor. Mesopor. Mat.* **30**, 3 (1999).
3. Yan, J. Y., Lei, G.-D., Sachtler, W. M. H., and Kung, H. H., *J. Catal.* **161**, 43 (1996).
4. Wang, X., Chen, H. Y., and Sachtler, W. M. H., *Appl. Catal. B* **26**, L227 (2000).
5. Li, Y., and Armor, J. N., *Appl. Catal. B* **3**, L1 (1993).
6. Li, Y., and Armor, J. N., *Appl. Catal. B* **2**, 239 (1993).

7. Maisuls, S. E., Seshan, K., Feast, S., and Lercher, J. A., *Appl. Catal. B* **29**, 69 (2001).
8. Feng, X., and Hall, W. K., *Catal. Lett.* **41**, 45 (1996).
9. Feng, X., and Hall, W. K., *J. Catal.* **166**, 368 (1997).
10. Voskoboinikov, T. V., Chen, H. Y., and Sachtler, W. M. H., *Appl. Catal. B* **19**, 279 (1998).
11. Chen, H. Y., Voskoboinikov, T., and Sachtler, W. M. H., *J. Catal.* **180**, 171 (1998).
12. Chen, H. Y., Voskoboinikov, T., and Sachtler, W. M. H., *Catal. Today* **54**, 483 (1999).
13. Witzel, F., Sill, G. A., and Hall, W. K., *J. Catal.* **149**, 229 (1994).
14. Shimizu, K. I., Kawabata, H., Maeshima, H., Satsuma, A., and Hattori, T., *J. Phys. Chem. B* **104**, 2885 (2000).
15. Lobree, L. J., Hwang, I. C., Reimer, J. A., and Bell, A. T., *Catal. Lett.* **63**, 233 (1999).
16. Hadjiivanov, K., Klissurski, D., Ramis, G., and Busca, G., *Appl. Catal. B* **7**, 251 (1996).
17. Hwang, I. C., Kim, D. H., and Woo, S. I., *Catal. Today* **44**, 47 (1998).
18. Lobree, L. J., Aylor, A. W., Reimer, J. A., and Bell, A. T., *J. Catal.* **169**, 188 (1997).
19. Hwang, I. C., Kim, D. H., and Woo, S. I., *Catal. Lett.* **42**, 177 (1996).
20. Hadjiivanov, K., Knözinger, H., Tsyntsarski, B., and Dimitrov, L., *Catal. Lett.* **62**, 35 (1999).
21. Campa, M. C., Pietrogiacomini, D., Tuti, S., Ferraris, G., and Indovina, V., *Appl. Catal. B* **18**, 151 (1998).
22. Satsuma, A., Enjoji, T., Shimizu, K. I., Sato, K., Yoshida, H., and Hattori, T., *J. Chem. Soc., Faraday Trans.* **94**, 301 (1998).

23. Ishihara, T., Kagawa, M., Hadama, F., and Takita, Y., *J. Catal.* **169**, 93 (1997).
24. Meunier, F. C., Zuzaniuk, V., Breen, J. P., Olsson, M., and Ross, J. R. H., *Catal. Today* **59**, 287 (2000).
25. Hayes, N. W., Joyner, R. W., and Shpiro, E. S., *Appl. Catal. B* **8**, 343 (1996).
26. Park, S. K., Park, Y. K., Park, S. E., and Kevan, L., *Phys. Chem. Chem. Phys.* **2**, 5500 (2000).
27. Meunier, F. C., Breen, J. P., Zuzaniuk, V., Olsson, M., and Ross, J. R. H., *J. Catal.* **187**, 493 (1999).
28. Pognant, F., Freysz, J. L., Daturi, M., and Saussey, J., *Catal. Today* **70**, 197 (2001).
29. Gerlach, T., Schutze, F.-W., and Baerns, M., *J. Catal.* **185**, 131 (1999).
30. Captain, D. K., and Amiridis, M. D., *J. Catal.* **184**, 377 (1999).
31. Sumiya, S., He, H., Abe, A., Takezawa, N., and Yoshida, K., *J. Chem. Soc.-Faraday Trans.* **94**, 2217 (1998).
32. Bell, A. T., *Catal. Today* **38**, 151 (1997).
33. Chapter 3 of this thesis
34. Chapter 4 of this thesis
35. Mirth, G., Eder, F., and Lercher, J. A., *Appl. Spectroscopy* **48**, 194 (1994).
36. Rudham, R., and Winstanley, A. W., *J. Chem. Soc., Faraday Trans.* **91**, 1689 (1995).
37. Narbeshuber, T. F., Vinek, H., and Lercher, J. A., *J. Catal.* **157**, 388 (1995).
38. Sermon, P. A., Keryou, K. M., and Ahmed, F., *Phys. Chem. Chem. Phys.* **2**, 5723 (2000).
39. Alstrup, I., Petersen, U. E., and Rostrup-Nielsen, J. R., *J. Catal.* **191**, 401 (2000).
40. Jackson, S. D., Kelly, G. J., and Webb, G., *Phys. Chem. Chem. Phys.* **1**, 2581 (1999).

41. Lobree, L. J., Aylor, A. W., Reimer, J. A., and Bell, A. T., *J. Catal.* **181**, 189 (1999).
42. Corma, A., Palomares, A. E., and Fornes, V., *Res. Chem. Intermed.* **24**, 613 (1998).
43. Curtin, T., Grange, P., and Delmon, B., *Catal. Today* **35**, 121 (1997).
44. Hadjiivanov, K., *Catal. Rev. -Sci. Eng* **42**, 71 (2000).
45. Haneda, M., Bion, N., Daturi, M., Saussey, J., Lavalley, J. C., Duprez, D., and Hamada, H., *J. Catal.* **206**, 114 (2002).
46. Chi, Y., and Chuang, S. S. C., *Catal. Today* **62**, 303 (2000).
47. Coltup, N. B., Daly, L. H., and Wiberley, S. E., "Introduction to infrared and raman spectroscopy", (3rd ed.), p. 547. Academic Press, Inc., San Diego, CA, 1990.
48. Miro, E. E., Imoberdorff, G., Vassallo, J., and Petunchi, J. O., *Appl. Catal. B* **22**, 305 (1999).
49. Little, L. H., "Infrared spectra of adsorbed species", p. 428. Academic Press, Inc, London, 1966.
50. Chafik, T., Kameoka, S., Ukisu, Y., and Miyadera, T., *J. Mol. Catal. A-Chem.* **136**, 203 (1998).
51. Djonev, B., Tsyntsarski, B., Klissurski, D., and Hadjiivanov, K., *J. Chem. Soc.-Faraday Trans.* **93**, 4055 (1997).
52. Raskó, J., and Solymosi, F., *J. Chem. Soc., Faraday Trans. 1* **80**, 1841 (1984).
53. Solymosi, F., and Bánsági, T., *J. Catal.* **156**, 75 (1995).
54. Goryashenko, S. S., Park, Y. K., Kim, D. S., and Park, S. E., *Res. Chem. Intermed.* **24**, 933 (1998).
55. Nováková, J., Kubelková, L., Bosáček, V., and Mach, K., *Zeolites* **11**, 135 (1991).

56. Paweewan, B., Barrie, P. J., and Gladden, L. F., *Appl. Catal. A* **185**, 259 (1999).
57. Sarbak, Z., *React. Kinet. Catal. Lett.* **69**, 177 (2000).
58. Yoo, J. W., Lee, C. W., Jeong, H. C., Park, Y. K., and Park, S. E., *Catal. Today* **60**, 255 (2000).
59. Smith, M. B., and March, J., "March's Advanced Organic Chemistry", (5th ed.), p. 2083. John Wiley & Sons, Inc., New York, 2001.
60. Kanazirev, V. I., and Price, G. L., *J. Mol. Catal. A* **96**, 145 (1995).

6. Summary

6.1. Summary

Nitrogen oxides are generated from the combustion of fossil fuels in mobile as well as stationary sources. Adverse effects of nitrogen oxides have been related to the severe environmental problem of the acid rain. Additionally, the presence of nitrogen oxides in gas phase in the low atmosphere causes respiratory problems by affecting the lung function. Worldwide, countries concerned by the quality of the air have established standards for the emissions of noxious gases, nitrogen oxides being among them. The increasingly stricter limits for nitrogen oxides emissions have resulted in activities for the development of technologies for the control of gases from the exhaust of automobiles and power plants. Currently, stationary sources such as power plants use the selective catalytic reduction, commonly known as SCR, for the control of emissions of NO_x . This method uses ammonia as reducing agent. In the case of mobile sources, engines running on gasoline use the three-way catalysts (TWC). These are very efficient when combustion is carried out with stoichiometric air/fuel mixtures. However diesel engines, which work under lean burn conditions, i.e., in the presence of excess of oxygen, represent still a challenge for researchers as NO_x reduction needs to be achieved in the presence of excess oxygen and TWC do not function under these conditions. The reduction of NO with hydrocarbons on transition metal exchanged zeolites has been proposed as an alternative method for the control of NO_x in the presence of excess of oxygen.

In this work, Ni exchanged zeolites were tested for the reduction of NO with propane and propene. For these catalysts, two Brønsted acid sites were formed for each Ni atom incorporated by hydrolysis during the ion exchange of the Na form of the zeolites with Ni. Acid sites associated with Ni^{2+} ions have a weaker acidic character in comparison with the Brønsted OH groups located on the zeolite. In

chapter 2 the influence of the pretreatment, and the effect of the concentration of acid sites, and metal content on the activity of Ni-exchanged mordenite were studied. Non-reduced catalysts showed a high selectivity for the reduction of NO to N₂, while partial reduction of Ni induced the formation of large Ni-oxide clusters and metallic Ni clusters causing the appearance of considerable amounts of NO₂ and N₂O. The activity was enhanced by increasing Ni content, which implies as well the increase of the acid site concentration. The activation of the hydrocarbon molecules is associated to the presence of acidic sites. However, an optimum concentration of acid sites was found to be necessary to maximize the activity for the reduction of NO with propane for samples with a specific Ni loading. Deactivation by formation of carbonaceous deposits was observed for catalysts with Ni loading above the optimum. For reduction with propene, low acid site concentrations favored high NO conversions.

Three zeolites with different channel diameter and pore geometries (ZSM-5, MOR and MCM-22) and exchanged with the same concentration of Ni were used to study the influence of the textural and structural properties on the reduction of NO with propane and propene. Chapter 3 focused on the effect of the acid sites and chapter 4 on the influence of the metal. The activation of hydrocarbons was found to be the rate-limiting step in the reaction and acid sites present in the materials were associated to such a function. Propene is more easily activated due to the presence of the C=C double bond, which facilitates the formation of carbenium ions. During the reduction of NO with propane, propane is transformed into propene by dehydrogenation occurring on the Ni²⁺ ions, which act as Lewis acid sites. The strength of the acid sites is the determining factor and controls the activation of the limited amount of propene formed from propane. Oligomerization of hydrocarbons promoted by the presence of acid sites, occurred in the three Ni-exchanged zeolites causing a partial blocking of the pores. NiNaMOR, which possesses the largest pore diameter, the largest pore volume and the lowest

concentration of acid sites is the most active material from the three studied for the reduction of NO with propene.

The role of Ni on the catalytic properties of Ni-exchanged zeolites for the reduction of NO with propane and propene, and the state of the metal and the zeolite support observed after the reaction were discussed in chapter 4. Ni²⁺ ions are located in ion exchange positions in NiNaMOR, NiNaZSM-5 and NiNaMCM-22. Changes in the activity for the three materials were observed after the reduction of NO with propane and propene. They can be classified into (i) reversible changes resulting from the deposition of carbonaceous deposits and (ii) irreversible changes associated to partial dealumination of the zeolite and migration of Ni. The effects of deposition of carbonaceous deposits were more severe for the materials with higher concentration of acid sites. The effects of the irreversible changes occurring in NiNaMOR were low, since the part of the Ni ions transformed into Ni oxide clusters remained accessible to the reactants. For NiNaZSM-5 the accessibility of the active sites decreased due the formation of Ni oxide species. For NiNaMCM-22, although Ni oxide formation was not observed, metal migrates to positions which are difficult to access. Formation of extraframework alumina was observed in the three cases and might be responsible of the migration of Ni. However the significant decrease in the number of Brønsted acid sites observed by infrared in comparison to the appearance of a weak signal corresponding to extraframework Al observed by ²⁷Al NMR indicates that the aluminum associated to the bridged hydroxyl groups is primarily responsible for the formation of extraframework alumina species, and the aluminum related to the ion exchange positions occupied by Na and Ni are involved only to a lower extent .

In the search for catalysts with potential for commercial application, understanding of the reaction mechanism is crucial. Chapter 5 dealt with an *in situ* infrared study of the surface reactions, which occur during the reduction of NO with propene and propane on Ni-exchanged mordenite. The presence of oxygen

was found to be of crucial importance for the reaction. At temperatures above 150°C the exposure of the sample to a mixture of NO and O₂ gave rise to the formation of nitrate and nitro type compounds. Carbonaceous deposits consisting of oxygenated carbon containing species, aromatic compounds and polyenes were formed on the surface of the catalysts in the presence of propene. The concentration of carbonaceous deposits was significantly lower for propane. A reaction mechanism involving the formation organic nitro and nitrito compounds from the interaction of sorbed NO_x species with activated hydrocarbons was proposed. Two types of isocyanates species associated with Ni in addition to those associated with Al were observed on the surface of the catalyst. It is believed that only one type of Ni-NCO is efficient for the formation of N₂ by the interaction with gas phase NO₂ through an Eley-Rideal type reaction. These isocyanate species are also hydrolyzed forming amines or NH₃, which are efficient reductants of NO.

6.2. Samenvatting

Stikstofoxiden ontstaan bij de verbranding van fossiele brandstoffen uit mobiele danwel stationaire bronnen. Een van gevolgen van stikstofoxiden is de vorming van zure regen welke een uiterst ongewenst probleem vormt. Tevens wordt door de aanwezigheid van stikstofoxiden in the lagere atmosfeer de longfunctie sterk geschaad. Wereldwijd worden door landen welke de kwaliteit van de lucht ernst nemen standaarden opgesteld voor de emissies voor schadelijke gassen waarvan stikstofoxides deel uitmaken. De toenemend strikter wordende limieten voor de emissies van deze schadelijke gassen heeft geleid tot de ontwikkeling van technologieën ter controle en vermindering van deze gassen in de uitlaatgassen van autos en energie centrales. In de huidige situatie maken stationaire bronnen gebruik van de techniek genaamd SCR (selectieve katalytisch reductie) ter controle van de uitstoot van stikstofoxiden (NO_x). Deze methode maakt gebruik van ammonia als reductant. Mobiele bronnen, zoals autos welke op lood vrije benzine lopen, maken gebruik van de ‚drieweg‘ katalysatoren (TWC). De drieweg katalysator is bijzonder werkzaam wanneer de verbranding geschied met en stoichiometrische lucht/brandstof verhouding. De drieweg katalysator werkt uiterst inefficiënt wanneer er een overmaat aan zuurstof aanwezig is. Alhoewel diesel motoren, welke met een functioneren onder arme verbranding condities, nog altijd een uitdaging stellen voor wetenschappers daar de reductie van NO dient te worden voltrokken in de aanwezigheid van een overmaat aan zuurstof waarbij de drie weg katalysator niet meer functioneerd. De reductie van NO met koolwaterstoffen over overgangsmetalen op zeoliet dragers bied een mogelijke oplossing voor de controle van NO_x in de aanwezigheid van een overmaat aan zuurstof.

In deze studie, werden Nikkel uitgewisselde zeolieten getest voor de reductie van NO met propaan en propene. Tijdens de ion-uitwisseling van de Na naar de Ni vorm werden, door middel van hydrolyzering, voor elk Ni atoom ingebracht twee

Bronsted zure groepen gevormd. Bronsted zure groepen, geïnduceerd door de aanwezige Ni^{2+} ionen, zijn van een milder karakter als de Bronsted zure groepen welke oorspronkelijk aanwezig in de zeoliet. In hoofdstuk 2 worden de invloed van de voorbehandeling, effect van de zure posities concentratie en metaal lading op de activiteit van Nikkel uitgewisselde mordeniet bestudeerd. Niet gereduceerde katalysatoren vertoonden aan hoge selectiviteit voor de reductie van NO naar N_2 , terwijl partiële reductie van Nikkel veroorzaakte de vorming van grote Nikkeloxide clusters en Nikkel metaal clusters welke de vorming van aanzienlijke hoeveelheden NO_2 and N_2O tot gevolg hadden. De activiteit werd verbeterd met toenemend Nikkel aandeel, wat tevens impliceert dat de concentratie Bronsted zure groepen werd vergroot. De activering van koolwaterstoffen werd geassocieerd met de concentratie van Bronsted zure groepen. Hoewel, voor de reductie van NO met propaan over mosters met een bepaalde Nikkel lading bleek een optimum aan Bronsted zure groepen nodig om een maximum in de activiteit te verkrijgen. Deactivering door vorming van koolstofhoudende afzettinging werd gevonden voor katalysatoren met een Nikkel lading boven het optimum. Voor de reductie met propaan, een lage zure groepen concentratie begunstigde een hoge NO omzetting.

Drie zeolieten met verschillende kanaal diameters en porie geometrieën (ZSM-5, MOR en MCM-22) en uitgewisseld met gelijke concentraties aan Nikkel werden bestudeerd op de invloed van textuur en structuur eigenschappen op de reductie van NO met propaan en propaan. Hoofdstuk 3 focuste op het effect van de zure groep en hoofdstuk 4 focuste op de invloed van het metaal. De activering van de koolwaterstoffen bleek de snelheids bepalend factor in de reactie en de zure groepen, aanwezig in deze materialen, werd geassocieerd met deze functie. Propaan wordt relatief gemakkelijk geactiveerd vanwege de aanwezigheid van de C=C dubbele binding, welke de vorming van karbo-kationen mogelijk maakt. Bij de reductie van NO met propaan wordt propaan gevormd door middel van dehydrogenering van propaan op Ni^{2+} ionen, welke zich als Lewis zure groepen

gedragen. De sterkte van de zure groepen is de bepalende faktor en controleerd de aktivering van limiterende hoeveelheid uit propaan gevormd propeen. Oligomerisering van koolwaterstoffen vindt plaats op de drie Nikkel uitgewisselde zeolieten, werd bevorderd door de aanwezigheid van zure groepen en veroorzaakte deels een verstopping van de porieen. NiNaMOR, welke de grootste porie diameter, grootste porie volume en de laagste concentratie aan zure groepen bevat bleek het meest aktieve materiaal van de drie bestudeerd voor de reductie van NO met propeen.

De rol van Nikkel op de katalysator eigenschappen van Nikkel uitgewisselde zeolieten voor de reductie van NO met propaan en propeen, en de staat van het metaal en de zeolite drager na de reactie worden bestudeerd in hoofdstuk 4. Ni²⁺ ionen zijn gelocaliseerd in de ion-uitwissel posities in NiNaMOR, NiNaZSM-5 en NiNaMCM-22. Na de reductie van NO met propaan of propeen werden veranderingen in de aktiviteit van de drie materialen geobserveerd. Deze kunnen gekwalificeerd worden als (i) reversiebele veranderingen als gevolg van de vorming van koolstofafzettingen en (ii) niet-reversiebele veranderingen welke worden geassocieerd met gedeeltelijke dealuminering van de zeolite en migratie van Nikkel. Het effect van de afzetting van koolstof was groter voor materialen met hogere concentratie aan zure groepen. De gevolgen van de irreversiebele veranderingen waren gering voor NiNaMOR omdat de deel van de Nikkel ionen die zijn getransformeerd in Nikkel oxides bleven bereikbaar voor de reactanten. Voor NiNaZSM-5 verminderde de bereikbaarheid van de aktieve posities door de vorming van Nikkel oxides. Voor NiNaMCM-22, hoewel geen Nikkel oxides vorming kon worden geobserveerd, het metaal migreert naar moeilijk toegankelijke posities. In all drie gevallen werd de vorming van buiten-structuurlijke alumina geobserveerd en is mogelijk de oorzaak voor de migratie van Nikkel. Alhoewel de aanzienlijke vermindering in het aantal Bronsted zure groepen, geobserveerd d.m.v. infrarood spectroscopy, vergeleken met de ontwikkeling van een zwak

signaal, gemeten met behulp van ^{27}Al NMR en corresponderend met de buiten-structuurlijke alumina, geeft een indicatie dat de alumina geassocieerd met de overbruggende hydroxyl groepen primair verantwoordelijk zijn voor de vorming van buiten-structuurlijk alumina en het alumina, welke in relatie staat tot de door Nikkel en Natrium ingenomen ion uitwissel posities, zijn maar relatief weinig betrokken.

Voor de ontwikkeling van een katalysator met een mogelijke commerciële applicatie is het begrijpen van de onderliggende reactie mechanisme onmisbaar. Hoofdstuk 5 behandelt een *in situ* infrarood studie van de oppervlak reacties, welke optreden tijdens de reductie van NO met propaan en propaan op Nikkel uitgewisseld Mordeniet. De aanwezigheid van zuurstof bleek van cruciaal belang te zijn voor de reactie. Op temperaturen boven 150°C , de blootstelling van het monster aan een mix van NO en O_2 gaf aanleiding tot de vorming van nitraten en nitro houdende componenten. Koolstofafzettingen bestonden uit geoxideerde koolstof houdende componenten, aromatische componenten en meervoudig onverzadigde componenten en werden gevormd op het oppervlak van de katalysator in de aanwezigheid van propaan. De concentratie aan koolstofafzettingen was aanzienlijk lager in het geval van propaan. Een reactiemechanisme welke de vorming van organische nitro en nitrito verbindingen vanuit de interactie tussen de geadsorbeerde NO_x species met de geactiveerde koolwaterstoffen bevat is voorgesteld. Twee types isocyanaten geassocieerd met Nikkel toegevoegd aan die die geassocieerd zijn aan het Al zijn geobserveerd op het oppervlak van de katalysator. Men gelooft dat slechts een type Ni-NCO is efficiënt voor de vorming van N_2 door de interactie van gasvormig NO₂ door middel van een Eley-Rideal type reactie. Deze isocyanaten kunnen ook gehydrolyzeerd worden waarbij amines of ammonia gevormd word, welke efficiënte reductanten zijn voor NO.

6.3. Resumen

Efectos nocivos de los óxidos de nitrógeno han sido relacionados con el grave problema ambiental de la lluvia ácida. La presencia de óxidos de nitrógeno en fase gaseosa en la parte baja de la atmósfera ocasiona problemas en el sistema respiratorio debido a la irritación de los pulmones. Los óxidos de nitrógeno son generados por la quema de combustibles fósiles en fuentes móviles o fijas. A nivel mundial, países preocupados por la calidad del aire han establecido estándares de emisión a la atmósfera de gases nocivos, siendo los óxidos de nitrógeno uno de ellos. Los límites de emisión a lo largo de los años se han vuelto más estrictos, lo cual ha ocasionado el desarrollo de tecnologías para el control de los gases emitidos por los escapes de los automóviles y plantas de generación de electricidad. La reducción catalítica selectiva, comúnmente conocida como SCR, utiliza amoníaco como agente reductor. Este método es amplia y eficientemente aplicado al control de emisiones de NO_x provenientes de fuentes fijas. En el caso de fuentes móviles, los motores que utilizan gasolina como combustible, emplean el catalizador de “tres vías”, TWC, el cual ofrece una alta eficiencia al trabajar en condiciones de composición del gas cercanas a las estequiométricas. Sin embargo, los motores que emplean diesel como combustible, trabajan en condiciones en las que oxígeno se encuentra en exceso, y representan en la actualidad un reto para los investigadores. La reducción de NO con hidrocarburos utilizando catalizadores basados en zeolitas modificadas mediante el intercambio iónico con metales de transición ha sido propuesta como un método alternativo para el control de NO_x en presencia de oxígeno en exceso.

En este trabajo, zeolitas modificadas mediante el intercambio iónico con níquel se han evaluado para su empleo como catalizadores para la reducción de óxido nítrico con propano y propeno. Se encontró que durante el intercambio iónico de la forma sódica de las zeolitas con níquel se generaron por hidrólisis, dos sitios ácidos

de Brønsted por cada átomo de níquel incorporado. Los sitios ácidos asociados con los iones Ni^{2+} tienen un carácter ácido más débil en comparación con los grupos OH localizados en la zeolita. La influencia del pretratamiento del catalizador, y el efecto de la concentración de sitios ácidos y del contenido de metal sobre la actividad de mordenita intercambiada con níquel se han estudiado en el capítulo 2. Los catalizadores no-reducidos mostraron una elevada selectividad para la reducción de NO a N_2 , mientras que la reducción parcial de níquel indujo la formación de aglomeraciones de óxido de níquel y partículas metálicas de níquel causando la aparición de cantidades considerables de NO_2 y N_2O . La actividad de los catalizadores fue mejorada mediante el incremento del contenido de níquel, lo cual implica a su vez, el aumento en la concentración de sitios ácidos. La activación de las moléculas de hidrocarburos está asociada a la presencia de sitios ácidos. Sin embargo, se encontró que para maximizar la actividad catalítica para la reducción de NO con propano de muestras con un determinado contenido de níquel es necesaria una concentración óptima de sitios ácidos. Catalizadores que poseen un contenido de níquel superior al óptimo mostraron desactivación debido a la formación de depósitos carbonáceos. En el caso de la reducción de NO con propeno, una concentración baja de sitios ácidos favoreció elevadas conversiones de NO.

Tres zeolitas con diferente diámetro de canal y geometría de poros (ZSM-5, MOR y MCM-22) intercambiadas con la misma concentración de níquel fueron empleadas en el estudio de la influencia de la geometría de poros en la actividad catalítica para la reducción de NO con propano y propeno. El capítulo 3 se enfocó en el efecto de los sitios ácidos y el capítulo 4 en la influencia del metal. Se encontró que la activación de hidrocarburos constituye la etapa limitante de la velocidad de reacción, y los sitios ácidos se encuentran asociados a dicha función. Propeno es activado más fácilmente debido a la presencia del doble enlace carbono-carbono que facilita la formación de iones carbenio. Durante la reducción

de NO con propano, el alcano es transformado en propeno por la deshidrogenación que tiene lugar sobre los iones Ni^{2+} que actúan como sitios ácidos de Lewis. La fuerza de los sitios ácidos es el factor determinante que controla la activación de la reducida cantidad de propeno formado a partir de propano. La oligomerización de hidrocarburos promovida por la presencia de sitios ácidos tuvo lugar en las tres zeolitas intercambiadas con níquel, ocasionando el bloqueo parcial de los poros. NiNaMOR, que posee el mayor diámetro de poros, el mayor volumen de poros y la más baja concentración de sitios ácidos, es el material más activo de los tres estudiados para la reducción de NO con propano.

En el capítulo 4 se han discutido el papel de Ni en las propiedades catalíticas de zeolites intercambiadas con níquel, empleadas para la reducción de NO con propano y propeno, y los cambios que experimentan el estado del metal y el soporte una vez que los materiales han sido empleados en la reacción. Los iones Ni^{2+} se encuentran localizados en las posiciones de intercambio iónico en NiNaMOR, NiNaZSM-5 y NiNaMCM-22. Variaciones en la actividad catalítica de los tres materiales se han observado después de ser utilizados para la reducción de NO con propano y propeno. Estos cambios pueden ser clasificados en (i) cambios reversibles, que resultan de la formación de depósitos carbonaceos y, (ii) cambios irreversibles asociados a la desaluminización de las zeolitas y a la migración de níquel. Los efectos de la formación de depósitos carbonaceos fueron más severos para aquellos materiales que poseen la mayor concentración de sitios ácidos. Los efectos de los cambios irreversibles que ocurren en NiNaMOR fueron limitados, ya que la porción de iones níquel que fue transformada en aglomeraciones de óxidos de níquel continuó siendo accesible a los reactivos. En el caso de NiNaZSM-5, la accesibilidad de los sitios activos disminuyó debido a la formación de óxidos de níquel. En el caso de NiNaMCM-22, aunque la formación de óxidos de níquel no fue observada, el metal se desplazó para ocupar posiciones de difícil accesibilidad. La formación de óxido de aluminio fuera de la estructura zeolítica fue observada en

los tres casos y es probable que sea responsable de la migración de níquel. Sin embargo, la disminución significativa en el número de sitios ácidos de Brønsted observada mediante espectroscopía de infrarrojo, en comparación con el surgimiento de una señal débil correspondiente a óxido de aluminio fuera de la estructura zeolítica mediante resonancia magnética nuclear de ^{27}Al , indica que el aluminio asociado a los grupos hidroxilo con estructura puente son los principales responsables de la formación de óxido de aluminio fuera de la estructura zeolítica y en menor extensión el aluminio asociado a las posiciones de intercambio iónico ocupadas por sodio y níquel.

La comprensión del mecanismo de reacción es crucial en la búsqueda de catalizadores con potencial para aplicación comercial. En el capítulo 5 se estudió el mecanismo de la reducción de NO con propeno y propano sobre un catalizador de mordenita intercambiada con níquel mediante un estudio *in situ* por espectroscopía de infrarrojo. Se encontró que la presencia de oxígeno es de crucial importancia para la reacción. A temperaturas superiores a 150°C la exposición de la muestra a una mezcla de NO y O_2 , ocasionó la formación de nitratos y compuestos nitro sobre la superficie. Depósitos carbonaceos que consisten de especies carbónicas oxigenadas, compuestos aromáticos y polienos se formaron sobre la superficie del catalizador en presencia de propeno. La concentración de depósitos carbonaceos fue mucho más baja en presencia de propano. Se propuso un mecanismo de reacción que involucra la formación de compuestos orgánicos nitro y nitrito a partir de la interacción de especies NO_x adsorbidas con hidrocarburos activados. Dos tipos de isocianatos asociados con níquel, además de aquéllos asociados con silicio y aluminio fueron observados sobre la superficie del catalizador. Se cree que sólo uno de los tipos de Ni-NCO es eficiente en la formación de N_2 mediante la interacción con NO_2 en fase gaseosa a través de una reacción del tipo Eley-Rideal.

6.4. Zusammenfassung

Die Verbrennung fossiler Brennstoffe in mobilen, wie auch stationären Quellen führt zum Ausstoß von Stickoxiden. Diese Gase stellen eine schwere Belastung für die Umwelt dar und tragen zu saurem Regen, sowie Atemwegsbeschwerden bei. Aufgrund des steigenden Umweltbewusstseins und zur Qualitätssicherung der Atemluft wurden weltweit Emissionsgrenzwerte für gesundheitsschädliche Gase, zu welchen auch Stickoxide zählen, festgelegt. Die Verschärfung der Emissionsrichtlinien für Stickoxide führte zu einer verstärkten Förderung neuer Technologien zur Eindämmung des Gasaustoßes bei Automobilen und Industrieanlagen. Zur Minderung der NO_x Emission stationärer Quellen, wie Kraftwerke, wird derzeit die "Selektive katalytische Reduktion", kurz SCR, unter Verwendung von Ammoniak als Reduktionsmittel, eingesetzt. Bei mobile Quellen, wie Benzinmotoren, wird die Technologie des Drei-Wege-Katalysators (TWC) angewand. Solange die Verbrennung unter einem stöchiometrischen Luft/Brennstoff Verhältnis abläuft, sind beide Methoden sehr effizient. Dies ist jedoch nicht der Fall für Dieselmotoren, die unter Brennstoff-armen (mageren) Bedingungen, d. h. im Sauerstoffüberschuß, arbeiten und dadurch den Einsatz eines Drei-Wege-Katalysatores verwehren. Somit stellt die Entwicklung NO_x -armer Dieselmotoren weiterhin eine Herausforderung für die Forschung dar. Als Alternative wird hierbei die Reduktion von NO unter Anwesenheit von Kohlenwasserstoffen an Übergangsmetallkation getauschten Zeolithen diskutiert.

In der vorliegenden Arbeit wurden Ni-getauschte Zeolithe für die Reduktion von NO mit Propan und Propen getestet. Der Ni-Kationenaustausch in wässriger Lösung führte, ausgehend von der Na-Form des Zeolithen, zur Hydrolyse von Nickel und damit zur Bildung von je zwei Brønsted sauren Hyrdoxyl-Zentren pro Nickelkation. Die Säurestärke der sauren Zentren am Ni^{2+} Ion ist schwächer als die der Brønsted sauren OH-Gruppen des Zeolithgitters. In Kapitel 2 wurden der

Einfluß der Katalysatorvorbehandlung, sowie die Konzentration der sauren Zentren und des Metallgehalts von Ni-getauschtem Mordenit untersucht. Dieses Material zeigte in der nicht-reduzierten Form eine hohe Selektivität für die Reduktion von NO zu N₂, wohingegen die partiell-reduzierte Form, für die eine Bildung großer Nickeloxidcluster und Cluster metallischen Nickels nachgewiesen werden konnte, zu beträchtlichen Mengen an NO₂ und N₂O führte. Die Katalysatoraktivität stieg mit steigendem Nickelgehalt und der damit verbundenen steigenden Zahl an Säurezentren. Die Aktivierung der Kohlenwasserstoffe verhält sich analog zur Zahl der Säurezentren. Um jedoch maximale Katalysatoraktivität für die Reduktion von NO mit Propan zu erreichen, ist bei gegebener Nickelbeladung eine optimale Zentrenkonzentration notwendig. Bei höherer Beladung erfolgt eine Deaktivierung aufgrund der Bildung kohlenstoffhaltiger Ablagerungen. In Anwesenheit von Propen ist die Umwandlung von NO bei einem niedrigeren Nickelgehalt bevorzugt.

Zur Untersuchung des Einflusses der texturalen und strukturellen Katalysatoreigenschaften auf die Reduktion von NO mit Propan und Propen wurden drei Zeolithtypen (ZSM-5, MOR und MCM-22) mit gleicher Nickelbeladung synthetisiert, die sich jedoch in ihrem Porendurchmesser und ihrer Porengeometrie unterscheiden. In Kapitel 3 wurde der Einfluß der sauren Zentren in Kapitel 4 der des Metalls untersucht. Die Aktivierung der Kohlenwasserstoffspezies konnte als der geschwindikeitsbestimmende Schritt der Reaktion nachgewiesen werden, welche wiederum in Zusammenhang zur Konzentration der Säurezentren steht. Aufgrund der vorhandenen C=C Doppelbindung ist die Aktivierung von Propen erleichtert und somit auch die Bildung des Carbeniumions. Die Reduktion von NO mit Propan führt zur Bildung von Propen. Diese Dehydrogenierung von Propan erfolgt am Lewis sauren Ni²⁺ Zentrum, wobei dessen Säurestärke wiederum den begrenzenden Faktor für die Aktivierung des gebildeten Propens darstellt. Eine Oligomerisierung der Kohlenwasserstoffe konnte für alle drei Ni-getauschten Zeolithmaterialien

nachgewiesen werden. Sie wird von den Säurezentren gefördert und führt zur teilweisen Blockierung des Porensystems. Für die Reduktion von NO mit Propen erwies sich unter den drei untersuchten Materialien NiNaMOR, der Zeolith mit dem größten Porendurchmesser und größtem Porenvolumen, sowie der geringsten Zahl an Säurezentren, als aktivster Katalysator.

In Kapitel 4 wurde die Rolle von Ni auf die katalytischen Eigenschaften der getauschten Zeolithe in Bezug auf die Reduktion von NO mit Propan und Propen, sowie der Zustand des Metalls und des Zeolithträgers nach der Reaktion untersucht. Ni²⁺ Ionen konnten auf Ionenaustauschplätzen in NiNaMOR, NiNaZSM-5 und NiNaMCM-22 lokalisiert werden. Eine Aktivitätsänderung der drei untersuchten Materialien nach der Reduktion von NO mit Propan und Propen wurde festgestellt. Es kann zwischen (i) einer reversiblen Änderung, aufgrund der Ablagerung kohlenstoffhaltiger Spezies, und (ii) einer irreversiblen Änderung, verbunden mit einer teilweisen Dealuminierung des Zeolites und einer Wanderung von Nickel, unterschieden werden. Erstere war stärker für Materialien, die eine hohe Zahl saurer Zentren aufwiesen. Die irreversible Änderung war hingegen niedrig für NiNaMOR, da der Teil der Nickelionen, der in Nickeloxid umgewandelt worden ist, weiterhin zugänglich war für die Reaktanten. Für NiNaZSM-5 führte die Bildung von Nickeloxid zu einer verringerten Zugänglichkeit der aktiven Zentren. Wobei in NiNaMCM-22, für das keine Bildung von Nickeloxid festgestellt werden konnte, eine Wanderung des Metalions zu schwer erreichbaren Plätzen erfolgte. Für alle drei Fälle konnte die Entstehung von Extragitter-Alumiumspezies beobachtet werden, welche vermutlich für die Migration von Nickel verantwortlich sind. Über IR Spektroskopie konnte gezeigt werden, daß die Anzahl Brønsted saurer Zentren deutlich sank. ²⁷Al MAS NMR spektroskopische Methoden zeigten lediglich die Entstehung eines schwachen Signals, welches Extragitter-Alumiumspezies zugeordnet werden konnte. Diese Beobachtungen führen zu der Folgerung, daß vermehrt Al-Atom, die in Positionen

neben verbrückten Hydroxylgruppen lokalisiert sind, zur Bildung von Extragitter-Aluminiumspezies führen, wohingegen Aluminiumatome in Ionenaustauschpositionen, die mit den Gegenkationen Natrium und Nickel besetzt sind, nur zu einem geringeren Grad beitragen.

Die Kenntnis des Reaktionsmechanismus ist bei der Suche nach Katalysatoren Potential für eine kommerzielle Anwendung Voraussetzung. In Kapitel 5 wurden Oberflächenreaktionen, die während der Reduktion von NO mit Propan und Propen an Ni-getauschten Mordenit ablaufen mit *in situ* Infrarot Untersuchungen verfolgt. Die Anwesenheit von Sauerstoff wurde als ausschlaggebende Voraussetzung gefunden. Wurde das Material einer Mischung aus NO und O₂ bei Temperaturen über 150°C ausgesetzt, erfolgte die Bildung von Nitrat und Nitro-artigen Verbindungen. Kohlenstoffhaltige Ablagerungen, bestehend aus Carboxyverbindungen, aromatischen Verbindungen und Polyenen, bildeten sich unter Anwesenheit von Propen auf der Katalysatoroberfläche. Für Propan war die Konzentration dieser Ablagerungen deutlich geringer. Ein Reaktionsmechanismus, der die Bildung von organischen Nitro- und Nitrito-Verbindungen, aufgrund von Wechselwirkungen zwischen adsorbierten NO_x-Spezies und aktivierten Kohlenwasserstoffen, zur Folge hat, wurde postuliert. Neben den Isocyanatspezies, die in Zusammenhang mit Aluminium stehen, wurden zusätzlich zwei Spezies für Ni auf der Katalysatoroberfläche gefunden. Es wird angenommen, daß nur ein Typ von Ni-NCO effektiv zur Bildung von N₂ beiträgt und die Wechselwirkung mit Gasphasen NO₂ über einen Eley-Rideal Reaktionstyp erfolgt. Diese Isocyanatspezies werden zusätzlich unter der Bildung von NH₃ hydrolysiert, welches wiederum ein effektives Reduktionsmittel für NO darstellt.

6.5. Résumé

La combustion d'énergies fossiles par des sources mobiles ou stationnaires engendre, entre autre, la formation d'oxydes d'azotes (NO_x). Le rôle néfaste de ces oxydes au niveau environnemental lors de pluies dites « acides » a été clairement mis en évidence. De plus, la présence d'oxyde d'azote dans la basse atmosphère affecte directement les poumons et est à l'origine de graves problèmes respiratoires. Dans le monde, la plupart des pays industrialisés ont adoptés des lois pour améliorer la qualité de l'air en limitant les émissions de gaz azotés, et, entre autre, en limitant l'émission d'oxydes d'azotes. La politique stricte de ces pays sur la diminution des émissions d'oxydes d'azotes a eu pour effet de générer de gros investissements industriels et le développement de nouvelles technologies pour le contrôle des émissions de gaz des automobiles et des industries. A l'heure actuelle, les sources dites "stationnaires" telles que les industries produisant de l'énergie utilisent des méthodes catalytiques dites de réduction sélective (SCR) pour la réduction des NO_x . Ces méthodes utilisent généralement l'ammoniaque comme agent réducteur. Dans le cas de sources mobiles, les moteurs à essence utilisent des catalyseurs dit 3-voies (TWC). Ces catalyseurs sont très efficaces lorsque la combustion se fait avec un mélange stœchiométrique air/essence. Cependant, les moteurs à essence qui sont utilisés dans des milieux "lean burn", c'est à dire dans des milieux riches en oxygène, ne sont pas encore au point. En effet, la réduction des NO_x doit se faire en milieu oxydant, condition dans laquelle les TWC ne sont pas très actifs. Ainsi, la réduction des NO_x par des molécules carbonées en utilisant des métaux de transitions a été proposée comme une alternative possible pour le contrôle des NO_x en présence de mélange riche en oxygène.

Dans ce travail, des catalyseurs de Ni échangé sur des zéolithes ont été testés pour la réduction de NO en utilisant du propane et du propène. Dans le cas de ces

catalyseurs contenant du nickel, deux sites acides de Brønsted sont formés pour chaque atome de Ni incorporé par hydrolyse pendant l'échange cationique de Na par Ni. Les sites acides associés aux ions Ni^{2+} ont un caractère acide plus faible en comparaison au groupe OH de Brønsted de la zéolithe. Dans le chapitre 2, l'activité de catalyseurs zéolithiques contenant du Ni a été étudiée en fonction de l'influence du prétraitement, de la variation de la concentration des sites acides et du changement de la quantité de métal. Les catalyseurs non réduits ont donné une très grande sélectivité pour la formation de N_2 , alors que la réduction partielle du Ni induit la formation de larges particules d'oxyde de Ni et de Ni métallique, causant la formation de grande quantité de NO_2 et de N_2O . L'activité augmente en augmentant la quantité de Ni présent dans le catalyseur ce qui implique aussi une augmentation des sites acides. L'activation des molécules carbonées est associée à ces sites acides. Cependant, une concentration optimale de sites acides est nécessaire pour avec une activité optimale du catalyseur pour la réduction de NO avec du propane pour une quantité de Ni donnée. La désactivation du catalyseur par la formation de dépôts carbonés a été observée pour les catalyseurs ayant une quantité de Ni supérieure à l'optimum concentration de sites acides. Pour la réduction en présence de propène, une faible quantité de sites acides est nécessaire une conversion importante de NO.

Trois zéolithes avec des tailles de pores différentes (ZSM-5, MOR et MCM-22) ayant la même quantité de Ni échanges ont été testées pour une étude de l'influence de la structure des pores sur la réduction de NO par du propane et du propène. Le chapitre 3 montre les effets dus à la variation des sites acides et le chapitre 4 ceux qui sont dus au métal. L'activation des molécules carbonées est l'étape limitante de la réaction et est associée à la fonction acide du catalyseur. La présence d'une double liaison dans la molécule de propène favorise son activation et la formation d'un carbocation. Lors de la réduction avec le propane, les molécules de propane sont transformées en propène par dehydrogenation sur les ions Ni^{2+} , qui agissent

alors en tant que sites acides de Lewis. La force de ces sites est le facteur déterminant et contrôle la formation d'un nombre limité de molécules de propène à partir des molécules de propane. L'oligomérisation des molécules carbonées sur les sites acides provoque un blocage partiel des pores de la zéolithe. NiNaMOR possédant les plus grand diamètre et volume de pores ainsi que la plus petite concentration de sites acides, est le matériau le plus actif pour la réduction de NO par le propène.

Le rôle du Ni sur les propriétés catalytiques du catalyseur pour la réduction de NO avec le propane et le propène, l'état d'oxydation du métal et de la zéolithe après réaction sont discutés dans le chapitre 4. Les ions Ni^{2+} sont localisés aux positions d'échanges d'ioniques dans le cas des trois supports, c'est à dire pour NiNaMOR, NiNaZSM-5 et NiNaMCM-22. Des changements d'activités sur les trois matériaux ont été observés après réduction de NO par le propane et le propène. Ces changements peuvent être classés en deux catégories, (i) des changements réversibles dus au dépôt de produits carbonés à la surface du catalyseur. (ii) des changements irréversibles associés à une désalumination partielle de la zéolithe et à la migration du Ni. Les effets néfastes dus au dépôt de carbone sur les catalyseurs sont plus importants dans le cas des catalyseurs les plus acides. Les effets irréversibles sont moins importants sur NiNaMOR du à l'accessibilité des molécules d'oxyde de Ni formées à partir des ions nickel. Dans le cas de NiNaZSM-5, l'accessibilité aux sites acides diminue à cause de la formation d'espèces d'oxyde de Nickel. Dans le cas de NiNaMCM-22 bien que la formation d'oxyde de nickel ne soit pas observée, le nickel métallique migre dans des endroits difficiles d'accès. La formation d'aluminium extra réseau (EFAL) a été observé sur tous les catalyseurs et est probablement responsable de la migration du nickel. Cependant, la forte diminution du nombre de sites acides de Brønsted observé par infrarouge comparée à la faible apparition d'un signal correspondant à des EFAL observé par la RMN de ^{27}Al indique que l'aluminium associé aux

groupes hydroxyles pontés est le principal responsable de la formation des EFAL alors que l'aluminium relié aux positions d'échanges d'ions ou sont présents le Na et le Ni est beaucoup moins affecté.

Dans la recherche d'un catalyseur potentiel pour une application commerciale, la compréhension du mécanisme de la réaction est primordiale. Le chapitre 5 est consacré à une étude d'infra rouge in situ des réactions de surfaces qui se passent pendant la réduction de NO par le propane et le propène sur des catalyseurs à base de nickel. La présence d'oxygène a été montrée comme étant un facteur crucial de la réaction. A des températures supérieures à 150°C l'exposition des échantillons à un mélange de NO et O₂ provoque la formation de composés de type nitrate et nitro. Des dépôts carbonés composés de molécules contenant de l'oxygène, de molécules aromatiques et de molécules contenant de nombreuses doubles liaisons sont formés à la surface des catalyseurs en présence de propène. La concentration de ces dépôts carbonés est beaucoup moins importante en présence propane. Un mécanisme de réaction impliquant la formation de composés "nitro" et "nitrito" issus de l'interaction entre les molécules de NO_x et les molécules des produits carbonés activés est proposé. Deux espèces d'isocyanates associées aux nickel en plus de celles associées ont été mises en évidence à la surface du catalyseur. Nous croyons que seulement un type de ces espèces Ni-NCO est impliqué dans la formation de l'azote par l'interaction avec du NO₂ présent dans la phase gazeuse et réagissant dans une réaction de type Eley-Rideal. Ces composés "isocyanate" peuvent aussi être hydrolysés pour former des amines ou de l'ammoniaque, qui sont actifs pour la réduction de NO.

Curriculum vitae

Bertha Isabel Mosqueda Jiménez was born on the 16th of August 1973 in Valle de Santiago, Gto., México. In 1990 she finished high school with distinction in the area of Physics and Mathematics at the Instituto Potosino. She studied Chemical Engineering at the Chemistry Department of the University of San Luis Potosí and graduated in 1995 with distinction. At the same university she started her master studies in Chemical Engineering. In 1996, she joined the research group of Dr. Guadalupe Cárdenas and Dr. Brent Handy working on microkinetic studies of the reduction of NO with hydrogen. As part of her master studies she spent a summer period working under the supervision of Prof. dr. James A. Dumesic at the Chemical Engineering Department of the University of Wisconsin. She got the degree of M.Sc. in August 1998. Immediately after she started working as a PhD student at Chemical Technology department of the University of Twente under the supervision of Prof. dr. Johannes A. Lercher. The work carried on the reduction of nitrogen oxides over zeolite-supported nickel catalysts is described in this thesis.

List of publications

Mosqueda Jiménez, B. I., Cárdenas Galindo, M. G., Handy, B. E. "Estudios microcinéticos de la reducción de NO_x con hidrógeno" Avances en Ingeniería Química, **7** 104 (1998)

Hong, Z., Fogash, K.B., Watwe, R.M., Kim, B., Mosqueda-Jimenez, B.I., Natal-Santiago, M.A., Hill, J.M., Dumesic, J.A. "Experimental and DFT studies of initiation processes for butane isomerization over sulfated-zirconia catalysts" Journal of Catalysis, **178**, 489 (1998).

Mosqueda-Jiménez, B.I., Brandmair, M., Jentys, A., Seshan, K. Lercher, J.A. "Reduction of nitric oxide by hydrocarbons on Ni-ion exchanged zeolites" Studies in Surface Science and Catalysis, **135**, 328 (2001).

Mosqueda-Jiménez, B.I., Jentys, A., Seshan, K. Lercher, J.A. "Reduction of nitric oxide by propene and propane on Ni-exchanged mordenite" submitted to Applied Catalysis B, (2002).

Maisuls, S.E., Lefferts, L., Seshan, K., Furusawa, T., Aika, K., Mosqueda-Jiménez, B.I., Smidt, M.L., Lercher, J.A. "Selective reduction of NO_x with propylene in the presence of oxygen over Co-Pt promoted H-MFI and H-Y" submitted to Catalysis Today, (2002).

Mosqueda-Jiménez, B.I., Jentys, A., Seshan, K. Lercher, J.A. "Structure-activity relations for Ni-containing zeolites during NO reduction 1. Influence of acid sites" in preparation.

Mosqueda-Jiménez, B.I., Jentys, A., Seshan, K. Lercher, J.A. "Structure-activity relations for Ni-containing zeolites during NO reduction 1. Influence Ni" in preparation.

Mosqueda-Jiménez, B.I., Jentys, A., Seshan, K. Lercher, J.A. "Mechanistic studies of NO reduction with propene and propane on Ni-exchanged mordenite" in preparation.